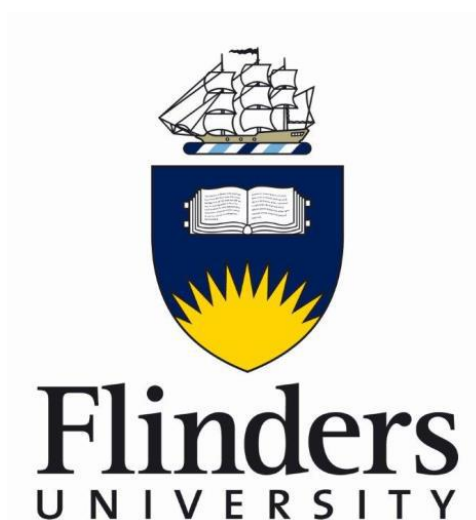


**CHARACTERISATION OF Au₉ –NANOCLUSTERS
DEPOSITED ON TITANIA SURFACES USING
SPECTROSCOPIC AND MICROSCOPIC
TECHNIQUES**



*Thesis Presented to the School of Chemical & Physical Sciences, Faculty of
Science & Engineering of Flinders University in Candidacy for the Degree of*

Doctor of Philosophy (Physics)

June 2016

Hassan Alqahtani

In the Name of Allah, the Most Gracious, the Most Merciful.
Praise be to Allah, the Cherisher and Sustainer of the worlds.

In Loving memory of my beloved

Dad

Mr. Sakar Alqahtani (1940- 2006)

Table of Contents

Abstract	I
Declaration	III
Acknowledgements.....	IV
List of Figures	IX
List of Tables.....	XVI
Contextual Statement.....	XVIII
Chapter 1: Introduction.....	1
REFERENCES.....	10
Chapter 2:Thesis Aims.....	16
2.1 KEY RESEARCH POINTS	17
2.2 THESIS OUTLINE.....	18
Chapter 3:Experimental techniques.....	20
3.1 X-RAY PHOTOELECTRON SPECTROSCOPY (XPS).....	22
3.2 METASTABLE INDUCED ELECTRON SPECTROSCOPY (MIES).....	28
3.3 SCANNING TRANSMISSION ELECTRON MICROSCOPY (STEM).....	31
3.4 SCANNING PROBE MICROSCOPE (SPM)	33
3.4.1 SCANNING TUNNELLING MICROSCOPE (STM).....	33
3.4.1 ATOMIC FORCE MICROSCOPE (AFM).....	36
3.5 MATERIALS.....	38
3.6 REFERENCES:.....	39

Chapter 4:Atomically Resolved Structure of Ligand

Protected Au₉ Clusters on TiO₂ Nanosheets..... 44

4.1 ABSTRACT	45
4.2 INTRODUCTION.....	46
4.3 EXPERIMENTAL	47
4.4 RESULTS AND DISCUSSION.....	51
4.5 CONCLUSION.....	63
4.6 REFERENCES	64

Chapter 5:Grouping and aggregation of ligand protected

Au₉ clusters on TiO₂ nanosheets 70

5.1 ABSTRACT	71
5.2 INTRODUCTION.....	72
5.3 EXPERIMENTAL	74
5.4 RESULTS AND DISCUSSION.....	75
5.4.1 AFM-OBSERVATION AND HEIGHT DISTRIBUTION OF AU₉ CLUSTERS ON TITANIA NANOSHEETS	75
5.4.2 STM-OBSERVATION AND WIDTH DISTRIBUTION OF AU₉ CLUSTERS ON TITANIA NANOSHEETS	83
5.4.3 XPS RESULTS OF AU₉ CLUSTERS ON TITANIA NANOSHEET	91
5.4.4 INTEGRATING AFM, STM AND XPS RESULTS.....	94
5.5 CONCLUSION.....	96
5.6 REFERENCES	97

Chapter 6:Aggregation behaviour of ligands protected Au₉

clusters on sputtered ALD TiO₂ 105

6.1 ABSTRACT	106
6.2 INTRODUCTION.....	107
6.3 EXPERIMENTAL	108
6.4 Results and Discussion	110
6.4.1 AFM-OBSERVATION AND HEIGHT DISTRIBUTION OF AU₉ CLUSTERS ON ALD TITANIA	110

6.4.2 XPS RESULTS OF AU ₉ CLUSTERS ON ALD TITANIA	118
6.4.3 DISCUSSION AFM AND XPS RESULTS	122
6.5 CONCLUSION.....	123
6.6 REFERENCES	125

Chapter 7: Investigation of phosphine-stabilised Au₉

Clusters on Acidic pre-treated ALD TiO₂ 135

7.1 ABSTRACT	136
7.2 INTRODUCTION.....	137
7.3 EXPERIMENTAL	139
7.4 RESULTS AND DISCUSSION.....	140
7.4.1 XPS RESULTS OF AU ₉ CLUSTERS ON ALD TITANIA	140
7.4.2 MIES RESULTS OF AU ₉ CLUSTERS ON ALD TITANIA.....	156
7.5 CONCLUSION.....	165
7.6 REFERENCES	166

Chapter 8: Conclusion 174

Appendix 178

Abstract

In this work chemically made clusters stabilised by organic ligands, $\text{Au}_9(\text{PPh}_3)_8(\text{NO}_3)_3$ (Abbreviated Au_9), deposited on titania surfaces are investigated by using various surface sciences techniques to study gold clusters and the effects of titania surfaces. Supported size specific metallic nano-clusters have emerged as superior catalysts in a few cases but until now fabrication and activation of catalysts using chemically synthesised atomically precise gold (Au) clusters supported on titania has not been well understood.

Titanium oxide (TiO_2) is used widely as support for metal based catalysts compared with other 'inert' supports (e.g. SiO_2 , BN). It was demonstrated in the case of ideal flat TiO_2 surfaces that defects significantly affect adsorption energy, cluster shape, and electronic structure of Au nanoclusters supported on them and influence their unique catalytic properties. Au clusters strongly bind to reduced titania surfaces due to defects, such as oxygen vacancies. Defects can be created by pre-treatment of titania surfaces before Au cluster deposition, such as sputtering with Ar^+ , acidic pre-treatment and annealing in UHV.

Chemical reactivity of metal clusters is determined by three main factors: (a) size of clusters, (b) geometric arrangement of atoms forming clusters and (c) electronic structure. Also, metal oxide supports play an important role in changing the catalytic activity of nanoclusters.

In this study, various surface techniques were used to investigate the above factors using various substrates and various pre-treatment methods. Chemical compositions of clusters deposited on titania surface and removal of ligands after heat treatment were monitored using XPS. The heating process caused the Au clusters to partially agglomerate with the remaining isolated precise Au clusters.

Aberration corrected HAADF-STEM with low electron-beam acceleration voltage was used to resolve the detailed structure of ultra small protected Au₉ clusters deposited on titania nanosheet at atomic resolution for the first time. Such microscopes are capable of directly determining the geometric structure of Au₉ clusters deposited on substrates. We compared experimental Au₉ structures using STEM with DFT calculations of clusters of nine Au atoms in the gas phase. While substrate influence on Au₉ structure is missing in DFT calculations, it is possible to classify structures of Au₉ clusters deposited on titania as found experimentally using STEM. AFM and STM observations show nanoclusters are highly distributed and their average size was measured. STM showed an individual Au₉ deposited on titania nanosheet. In addition, Metastable Induced Electron Spectroscopy (MIES) was applied to quantitatively determine valance electronic structure of supported Au clusters.

Declaration

I certify that this thesis does not incorporate without acknowledgment any material previously submitted for a degree or diploma in any university; and that to the best of my knowledge and belief it does not contain any material previously published or written by another person except where due reference is made in the text.

.....

Hassan Sakar Alqahtani

June 2016

Acknowledgements

This thesis, and the journey of my PhD, would not have been possible without the support of Allah (God) almighty and his blessing in the form of wonderful advisors, colleagues, parents, friends, family and the right opportunities that came my way. Allah will not thank a person who does not thank people. Thus, great thanks go to different people who supported my journey.

Firstly, I would like to deeply thank my supervisor, Prof. Gunther Andersson, for his invaluable guidance throughout my PhD. Having worked in his group for the last five years during my Master and PhD period, I have become enormously grateful for the opportunity to learn from such a dedicated professional, and to work closely with a good person. Gunther showed confidence in me and gave me opportunities, advice, encouragement and enthusiasm.

I owe my deepest gratitude to my supervisor, Prof. Tomonobu Nakayam, from the National Institute of Material Sciences (NIMS) in Japan for his time and guidance, particularly during my fellowship visit. I feel privileged to have had the opportunity to work at NIMS and gain invaluable experience at one of the world's most accomplished research institutes. I would also like to thank his group for their support.

I am also indebted to collaborators on this project, Prof. Greg Metha and Dr. Vladimir Golovko and their group, for providing me with DFT calculations and synthesis materials. I would like to extend my special thanks to Kimoto-san and Sasaki-san from NIMS for their support in STEM and titania nanosheet during my fellowship visit.

I would also like to thank my colleagues in Andersson's group for guidance and assistance throughout my project as well as members of the School of Chemistry and Physics who made this time both informative and enjoyable. I would like to specifically thank my co-supervisor, Prof. Jamie Quinton for his advice. Special thanks go to Dr. Dana Thomsen for support in editing my PhD thesis.

I gratefully acknowledge the funding sources which made my PhD work possible. I am very grateful to King Abdullah program, Saudi Arabia, for giving me the opportunity to continue post graduate study in Australia.

Lastly, a special thanks to my family, especially my Mother for her love and encouragement. Most of all, I really appreciate my loving wife for her love and support during the stressful days of my PhD. I love you!

Hassan Alqahtani

Flinders University

June 2016

List of Publications

Refereed Journal Articles

1. **Al Qahtani, H. S.;** Kimoto, K.; Bennett, T.; Alvino, J. F.; Andersson, G. G.; Metha, G. F.; Golovko, V. B.; Sasaki, T.; Nakayama, T., Atomically resolved structure of ligand-protected Au₉ clusters on TiO₂ nanosheets using aberration-corrected STEM. *The Journal of Chemical Physics* 2016, *144* (11), 114703.
2. **Al Qahtani, H. S.;** Higuchi, R.; Sasaki, T.; Metha, G. F.; Golovko, V. B.; Andersson, G. G.; Nakayama, T., grouping and aggregation of ligand Protected Au₉ Clusters on TiO₂ nanosheet. *Planned submission to Physical Review B* 2016.
3. **Al Qahtani, H. S.;** Metha, G. F.; Golovko, V. B.; Andersson, G. G.; Nakayama, T., Aggregation behavior of Ligands protected Au₉ Clusters on sputtered ALD TiO₂ Using AFM and XPS techniques. *Planned submission to ACS Applied Materials and Interfaces* 2016.
4. Anderson, D. P.; Alvino, J. F.; Gentleman, A.; **Al Qahtani, H.;** Thomsen, L.; Polson, M. I.; Metha, G. F.; Golovko, V. B.; Andersson, G. G., Chemically-synthesised, atomically-precise gold clusters deposited and activated on titania. *Physical Chemistry Chemical Physics* 2013, *15* (11), 3917-3929.
5. Anderson, D. P.; Adnan, R. H.; Alvino, J. F.; Shipper, O.; Donoeva, B.; Ruzicka, J.-Y.; **Al Qahtani, H.;** Harris, H. H.; Cowie, B.; Aitken, J. B.; Golovko, V. B.; Metha, G. F.; Andersson, G. G., Chemically synthesised atomically precise gold clusters deposited and activated on titania. Part II. *Physical Chemistry Chemical Physics* 2013, *15* (35), 14806-14813.

6. Andersson, G. G.; Golovko, V. B.; Alvino, J. F.; Bennett, T.; Wrede, O.; Mejia, S. M.; **Al Qahtani, H. S.**; Adnan, R.; Gunby, N.; Anderson, D. P.; Metha, G. F., Phosphine-stabilised Au₉ clusters interacting with titania and silica surfaces: The first evidence for the density of states signature of the support-immobilised cluster. *The Journal of Chemical Physics* 2014, *141* (1), 014702.

Conference contributions

- 1) Hassan S. AlQahtani, Jason F. Alvino, Gregory F. Metha, Vladimir G. Golovko, Tomonobu Nakayama, Gunther G. Andersson, "Raman Spectra of Chemically-Synthesized, Atomically-Precise Gold Clusters"(contributed, poster), ACSIN-12 & ICSPM21, Tsukuba Int. Conf. Center, Tsukuba, Ibaraki, Japan, 2013/11/04 - 2013/11/08.
- 2) Hassan S. Alqahtani, Gregory F. Metha, Vladimir B. Golovko, Tomonobu Nakayama, Gunther G. Andersson, "TEM images of Chemically-Synthesized, Atomically-Precise Gold Nano—Clusters" (contributed, poster), TNT Japan 2014, Tokyo Big Site, Aomi, Tokyo, Japan, 2014/01/29 -2014/01/31.
- 3) Hassan S. AlQahtani, Gregory F. Metha, Vladimir B. Golovko, Tomonobu Nakayama, Gunther G. Andersson, "STEM images of Chemically-Synthesized, Atomically-Precise Gold Nano-Clusters" (contributed, oral & poster), MANA Internaitonal Symposium, Tsukuba Int. Conf. Center, Tsukuba, Ibaraki, Japan, 2014/03/05 - 2014/03/07.
- 4) Hassan S. Alqahtani, Gregory F. Metha, Vladimir B. Golovko, Tomonobu Nakayama, Gunther G. Andersson, "AFM images of Chemically-Synthesized, Atomically-Precise Gold Nano-Clusters on ALD Titania" (contributed, poster), 17th International Conference on NC-AFM ,Tsukuba Int. Conf. Center ,Tsukuba, Japan, 2014/08/04 -2014/08/08.
- 5) Hassan S. AlQahtani, Jason F. Alvino, Gregory F. Metha, Vladimir G. Golovko, Tomonobu Nakayama, Gunther G. Andersson, "Raman Spectra of Chemically-Synthesized, Atomically-Precise Gold Clusters"(contributed, poster), CNST2015, Flinders Centre for NanoScale Science and Technology 5th Annual Conference. Tonsely building in Flinders University, Adelaide, Australia, 2015/17/06.

Conference attendance

“Structure Control of Atomic/Molecular Thin Films and Their Application”, 2013 NIMS conference, Tsukuba Int. Conf. Center, Tsukuba, Japan, 2013/07/01 - 2013/07/03.

“A strong Future from Soft Materials”, 2014 NIMS conference, Tsukuba Int. Conf. Center, Tsukuba, Japan, 2014/07/01 - 2014/07/03.

List of Figures

Figure 1.1: Publications on ‘gold catalysis’ from 1970 to June 12th, 2011. ²	2
Figure 1.2: Photocatalytic conversion of water using deposited Au clusters on titania surfaces. It should be noted, that the energy levels drawn for Au clusters are a schematic and have been added for illustration. The energy levels are not based on experimental results or calculations.	3
Figure 1.3: Concept for development of cluster-based materials. ¹¹	5
Figure 1.4 : Crystal structures of Au ₈ (left column), Au ₉ (centre column) and Au ₁₁ (right column) clusters showing exact number of Au atoms per cluster core. The top row shows space-filled models, while the centre row shows the ball and stick model positions of all atoms except hydrogen. The bottom row shows geometries of the metal cores. The atomic colour scheme is gold (Au), orange (P), green (Cl), and black (C). ¹⁷	6
Figure 3.1: The working principle of a photoemission spectrometer. Monochromatic photons with energy $h\nu$ are produced by light source hitting the sample surface at a certain angle ψ . ²	23
Figure 3.2: Electron mean free path. ³	24
Figure 3.3: De-excitation mechanisms of a metastable atom via resonance ionisation (a ₁) followed by Auger neutralisation (a ₂) and via Auger de-exciation (b) on an insulator surface. ¹⁵	29
Figure 3.4: Schematic showing the main components of high-resolution STEM. ²¹	33
Figure 3.5: Scanning tunnelling microscope components. ²²	35
Figure 3.6: Schematic illustration of an atomic force microscope connected to a computer. ²⁸	37

Figure 4.1: (a) The large area STEM image shows various groups of Au atoms on a TiO₂ nanosheet. The blue circles show Au₉ clusters, red circles are aggregated clusters, while the green circles indicate single, dimer and trimer gold atoms. (b₁-b₃) STEM images of single, dimer and trimer gold atoms, respectively. The scale bar corresponds to 10 nm in Figure 4.1a, while 0.2nm corresponds to Figure 4.1b.50

Figure 4. 2: STEM images of different structures with 8-10 Au atoms which were infrequently observed in the STEM experiments. The scale bar corresponds to 0.5 nm.51

Figure 4. 3: High-resolution HAADF-STEM images of [Au₉(PPh₃)₈](NO₃)₃ clusters deposited on titania nanosheet under optimised imaging conditions. Panel a shows 3D-like configuration transformed into pseudo 2D configurations shown in panels b and c. The scale bar corresponds to 0.5 nm and images are slightly smoothed. Panels I, III and IV show DFT models for three different isomers of Au₉ clusters. See text for further details of calculations. (Note that structure II was not observed in the STEM images). Cartesian coordinates of Au₉ clusters is shown in Appendix A (i.e. structures (I), (III) and (IV)).52

Figure 4. 4: Schematic illustration of changes occurring when an Au₉ cluster loses some ligands and interacts with the titania nanosheet substrate. In (a) the cluster (i.e. [Au₉(PPh₃)₈]³⁺, without counter-ions) is shown after deposition. The ligands are attached to the cluster core and the core is not in contact with the substrate. In (b) four ligands are removed (i.e. Au₉(PPh₃)₄) and the cluster core is in contact with the substrate. (Note: the exact number of ligands removed is unknown and may be more than shown here. Also, whilst these figures are based upon the crystal structures of the Au₉ cluster and surface separately, relative position and orientation of the cluster–surface interaction does not involve geometric or energy minimisation processes).54

Figure 4. 5: The (gas-phase) calculated structures and relative energies of the three lowest energy Au₉ clusters (II, III and IV) and a possible transition state structure for transferring

between structures III and IV. Structure I is the calculated structure of $[Au_9(PPh_3)_8]^{3+}$ with ligands omitted..... 59

Figure 4. 6: SXPS Peak Position of the $4f_{7/2}$ Au peak of $[Au_9(PPh_3)_8](NO_3)_3$ clusters deposited on titania nanosheets. 61

Figure 5. 1: AFM topographies of (a) large image of pure titania nanosheets showing the size of nanosheet, (b) focusing on one of titania nanosheet to measure thickness. The line profile in (c) Thickness profile of the titania nanosheet (b) which is around 1.2 nm. 76

Figure 5. 2: STEM image of titania nanosheet. (b) Thickness profile reconstructed along the blue line..... 77

Figure 5. 3: AFM 3D images of (a and d) pure titania nanosheet as, (b) after deposition of Au_9 clusters, (c) after annealing of (b), (e) titania nanosheet exposed to MeOH, and (f) after annealing of (c). Image sizes are $200 \times 200 nm^2$ 77

Figure 5.4: AFM topographies of (a and d) pure titania nanosheetas, (b) deposited Au clusters, (c) annealed Au clusters on titania nanosheet, (e) blank sample without Au clusters, which is MeOH titania nanosheet, and (f) annealed MeOH blank sample. Image size is $1.0 \times 1.0 \mu m^2$ 78

Figure 5.5: Schematic illustration of gold clusters deposited on titania nanosheet: a) before annealing and b) after annealing. The green and orange lines represent results obtained from AFM and STM, respectively. The lines indicating emission of electrons represent XPS results. 79

Figure 5.6: Height distribution of features in the AFM images: (a) as deposited Au clusters, and (b) after annealing to 200 °C. Cluster mean height before annealing is 0.75 ± 0.2 nm while after annealing it is 1.0 ± 0.4 nm. 82

Figure 5.7: STM images of annealed Au_9 clusters on titania nanosheets measured at higher gap voltage (20pA, -6V). Scan size is $30 \times 30 nm^2$ 83

Figure 5.8: Energy levels of (a) ligands Au₉ before heating and (b) naked gold clusters after heating. The molecular orbital visualisations of combined molecular orbitals (LUMO, LUMO+1) and (LUMO, LUMO+1, LUMO+2) are also shown in this figure.87

Figure 5.9: STM images of Au₉ clusters deposited on titania nanosheets: (a) as-deposited, (b) after annealing to 200 °C. Images (c) and (d) are magnifications of (a) and (b). Image size is 50 x 50 nm² for a and b and 20 x 20 nm² for c and d. STM operation conditions were (a) +1.5V, 20pA; (b) +2.0V, 18pA; (c) +1.5V, 20pA; (d) +2.5V, 25pA. Heights and widths of clusters surrounded by open blue circles were used for histogram analysis (Fig. 5.11).88

Figure 5.10: STM images of (a) MeOH titania nanosheet, (b) annealed MeOH titania nanosheet, (c) Zommed- MeOH titania nanosheet, and (d) Zommed-annealed MeOH blank sample. Image size is 50 x 50 nm² for a and b, while 20 x 20 nm² for c and d. a: +2.0V, 25pA; b: +2.5V, 20pA; c: +2.5V, 25pA; d: +2.5V, 20pA.89

Figure 5.11: Histogram of features in STM images attributed to Au clusters. Width is shown in (a) for as-deposited samples and (b) after annealing. Height is shown in (c) for as-deposited samples and (d) after annealing.90

Figure 5.12: XPS of [Au₉(PPh₃)₈](NO₃)₃ clusters on titania nanosheet (a) 4f Au spectrum of as-deposited samples, (b) after annealing and (c) the 2p P peak of as-deposited samples.93

Figure 5.13: XPS peak position of [Au₉(PPh₃)₈](NO₃)₃ clusters on titania nanosheet (a) 2p Ti peak as-deposited and (b) 2p Ti peak as-annealed related to titania nanosheet.93

Figure 6.1: AFM topographies of ALD titania (a) exposed to MeOH, (b) sputtered for 30 seconds and exposed to MeOH, (c) exposed to MeOH and subsequently acid treated for 30 seconds, (d) exposed to MeOH and subsequently acid treated for 5 minutes, and (e) exposed to MeOH and subsequently acid treated for 10 minutes. Surface roughness is shown as root mean square (Ra) for each image. Image size is 500 x 500nm². 110

Figure 6.2: AFM 3D images of sputtered ALD titania (a) exposed only to MeOH, (b-d) after deposition of Au₉ clusters with a range of different concentration from MeOH solutions (0.0002mM – 0.02mM), (e) annealed blank sample without deposited Au NCs, and (f-h) annealed after Au NC deposition with the same concentrations as b-d. The size of images are 500 x 500nm². 112

Figure 6.3: AFM topographies of sputtered ALD titania (a) exposed only to MeOH, (b-d) after deposition of Au₉ clusters with a range of different concentrations from MeOH solutions (0.0002mM – 0.02mM), (e) annealed blank sample without deposited Au NCs, and (f-h) annealed after Au NC deposition with the same concentrations as b-d. The size of images are 2.0 x 2.0µm². 113

Figure 6.4: Height distribution of features in AFM images: (a) as deposited Au NCs, and (b) after annealing to 200 °C. The cluster mean height before annealing is 1.7 ± 0.6 nm, while after annealing it is 2.9 ± 1.6 nm. 115

Figure 6.5: NC-AFM Amplitude images of Au₉ nanoclusters deposited on ALD titania pre-treated by Ar⁺ sputtering. (a) amplitude image after a C-AFM scan shown in the white marked subregion. Clusters inside the C-AFM area are swept to the edge of the scanned region. (b) is a magnification image after C-AFM scan. The white arrow points at individual Au NCs. Au NCs have the same features after removal by the contact scan. The black arrow indicates an area with instability in the feedback loop. 117

Figure 6.6: NC-AFM topography and amplitude images of Au₉ nanoclusters deposited on ALD titania pre-treated by Ar⁺ sputtering. The same sample (a) topography and (b) amplitude image after a C-AFM scan (c) in the marked subregion. Clusters inside the C-AFM area are swept to the edge of the scanned zone. 118

Figure 6.7: XP spectra of $[Au_9(PPh_3)_8](NO_3)_3$ clusters on ALD titania (a) Au 4f region of as-deposited samples, (b) after annealing, (c) P 2p spectrum of as-deposited samples and (d) after annealing. Au(0) is the LBP-Au, while Au(I) is the HBP-Au.....	120
Figure 6.8: XP spectra of Ti 2p (a) of pure ALD titania, (b) of Au_9 clusters deposited on sputtered ALD titania and (b) Au_9 clusters on sputtered ALD titania after annealing.	121
Figure 7.1: XPS spectra of carbon (calibration) with fitted peaks including Shirley background.	141
Figure 7.2: Au XP spectra of deposited Au cluster before heating for (a) 0.1 mM and (b) 0.001 mM.	142
Figure 7.3: Au-HBP position and FWHM for all Au_9 concentrations before heating.	143
Figure 7.4: Au XP spectra of deposited Au cluster after heating for (a) 0.01 mM and (b) 0.001 mM loading.	144
Figure 7.5: Au-LBP and Au-HBP position and FWHM for all Au_9 concentrations after heating.	145
Figure 7.6: P XPS spectrum of deposited Au cluster before heating.	147
Figure 7.6: P-LBP position and FWHM for all Au_9 concentrations before heating.	148
Figure 7.8: P-LBP position and FWHM for all Au_9 concentrations after heating. The ligands were removed completely after heating treatment except for these two concentrations.....	149
Figure 7.9: Ratio of the intensities of P-LBP to the sum of respective Au peak intensities (i.e. the sum of Au-LBP and Au-HBP).	151
Figure 7.10: Ti XP spectra of deposited Au cluster sample (a) before and (b) after heating.	152
Figure 7.11: Ratio of the intensities of the sum of Au peak intensities to Ti intensity.	153

Figure 7.12: S XP spectra of deposited Au cluster sample (a) before and (b) after heating.	154
Figure 7.13: Ratio of intensities of the S peak to intensities of Ti peak.	155
Figure 7.14: Relative intensities of the S peak to the sum of intensities of respective Au peaks.	155
Figure 7.15: Reference spectra for fitting the series of Au ₉ /titania MIE spectra including the bare titania resulting from the singular value decomposition (SVD) algorithm.	158
Figure 7.16: MIE experimental spectra of Au ₉ clusters deposited on ALD titania heated to 200°C.	159
Figure 7.17: Fits of the ALD titania sample immersed into the 0.06 mM Au ₉ solution and subsequently heated to 200°C using all three reference spectra.....	159
Figure 7.18: Weighting factors of the reference spectra for fitting the MIE spectra of the Au ₉ /ALD titania heated to 200°C together with Au-HBP intensity measured by XPS.	161
Figure 7.19: Comparison of the reference spectra of Au in our previous study ²⁶ with the current reference spectrum.	161
Figure 7.20: Weighting factors of reference spectra for fitting the MIE spectra of Au ₉ /ALD titania heated to 200°C together with C intensity measured by XPS.	162
Figure 7.21: Comparison of the reference spectra of PPh ₃ in our previous study ²⁶ with the current spectrum.	163
Figure 7.22: Weighting factors of the reference spectra for fitting the MIE spectra of the Au ₉ /ALD titania heated to 200°C together with S intensity measured by XPS.....	164

List of Tables

<i>Table 4.1: All structures resulting from DFT calculations. The structures are shown which have energy less than 1 eV relative to the lowest energy structure.</i>	57
<i>Table 6.1: Fraction of Ti^{3+} and Ti^{4+} in the Ti 2p XP spectrum for various ALD titania samples. Error in the intensities was estimated to be $\pm 1\%$. Au NCs were deposited on sputtered ALD titania.</i>	121
<i>Table 7.1: The values of Au-LBP and Au-HBP position and FWHM for all Au_9 concentrations.</i>	146
<i>Table 7.2: The values of P-LBP position and FWHM for all Au_9 concentrations.</i>	150

Abbreviations

AFM	Atomic Force Microscopy
ADF	Annular Dark Field
ALD	Atomic Layer Deposition
AS	Australian Synchrotron
BF	Bright Field
DFT	Density Functional Theory
DOS	Density Of States
eV	Electron Volt
FWHM	Full Width Half Maximum
HAADF	High Angle Annular Dark Field
HBP	Higher Binding Peak
HSA	Hemispherical Analyser
LBP	Lower Binding Peak
MIES	Metastable Induced Electron Spectroscopy
MS	Mass Spectrometry
NCs	Nanoclusters
NMR	Nuclear Magnetic Resonance
PPh ₃	Triphenylphosphine ligands
SPM	Scanning Probe Microscopy
STEM	Scanning Transmission Electronic Microscopy
STM	Scanning Tunnelling Microscopy
SVD	Single Value Decomposition
TEM	Transmission Electronic Microscopy
UHV	Ultra High Vacuum
UV	Ultra-Violet
XPS	X-ray Photoelectron Spectroscopy

Contextual Statement

This thesis presents investigations of chemically made clusters stabilised by organic ligands deposited on titania surfaces using various surface sciences techniques as part of the author's PhD project.

The introduction chapter (Chapter 1) contains information regarding the project field, while the experimental chapter contains project experimental details, along with parameters of experimental methods used in this study.

Results presented in Chapter 4 are a reformatted version of a published peer-reviewed paper, while Chapters 5 and 6 are reformatted versions of papers planned for submission to peer-reviewed journals.

The author of this thesis was the primary author of the published papers used as the basis of the results chapter. All experimental work was completed by the author. Exceptions are: Prof. Koji Kimoto who carried out STEM measurements; Prof. Greg Metha, Dr. Jason Alvino and Trystan Bennett who undertook DFT calculations. Dr. Valdimir Golovko synthesised Au clusters, while Prof. Takayoshi Sasaki synthesised the titania nanosheet. Dr. Rintaro Higuchi assisted with STM measurements.

The author designed and supervised the measurements of Ms. Gowri Krishnan which are included in Chapter 7.

Prof. Gunther Andersson and Prof. Tomonobu Nakayam have the intellectual contribution of conceptualising experiments, data interpretation and revision of manuscripts.

The author completed all data evaluation and interpretation, prepared the first draft of manuscripts and acknowledges the input of respective co-authors in the final interpretation of results.

CHAPTER 1

Introduction

CHAPTER 1

Over the last centuries, colloidal gold was used to make ruby glass and it was popularly believed that gold has a degree of communication with human eye. Although gold is considered one of the most ancient subjects of investigation in science, its revival now leads to an exponential growth in the number of publications, especially in the fields of nanoscience and nanotechnology with gold catalysis (Figure 1.1).¹⁻²

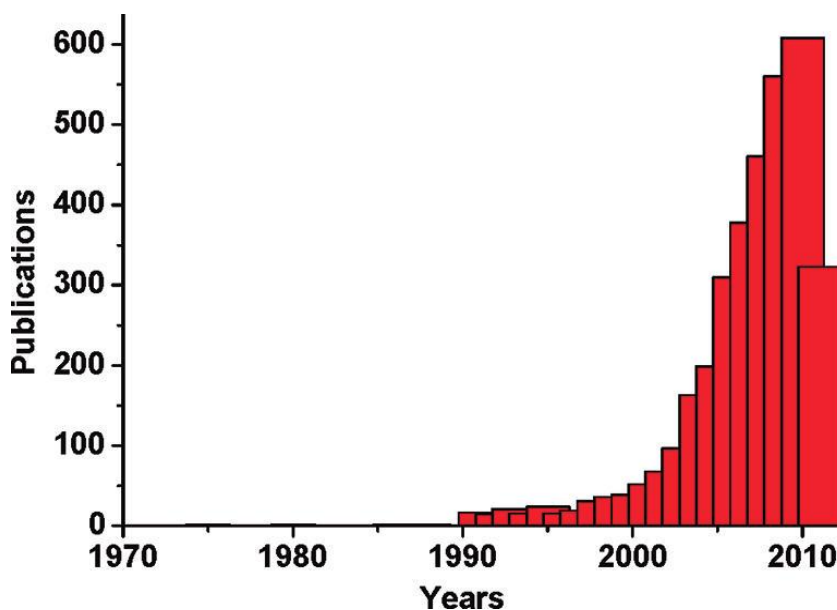


*Figure 1.1: Publications on 'gold catalysis' from 1970 to June 12th, 2011.*²

Heterogeneous catalysis is based on the interaction of molecules of the gas or liquid phases with the surface of solid catalysts. Understanding heterogeneous catalysis requires the methods and tools of surface science.³ Surface science has introduced and exploited many new techniques to study surfaces at the atomic level. This avenue of scientific study may lead to improved or cheaper catalysts as there is already a high demand for catalysts. Indeed, up to 90% of all chemical processes involve catalysts, with 85% of these being solid heterogeneous catalysts.⁴

Growing needs for energy production to meet global demand, along with environmental and economic concern, has resulted in a strong focus on renewable energy sources as the most favourable potential solution.⁵ Most renewable energy sources face challenges in intermitted

energy supply and thus in storage of harvested energy.⁶ Photocatalysis of carbon dioxide and hydrogen from split water molecules provides an efficient and inexpensive way for storing energy harvested from sunlight in chemical energy (hydrocarbons).⁵ The splitting of liquid water (H_2O) into hydrogen and oxygen using semiconductor materials in photocatalysts under UV radiation was first demonstrated by Fujishima and Honda.⁷ In a semiconductor material, such as (TiO_2), light (excitation energy) separates charges into electrons and holes that diffuse to the surface and drive reduction and oxidation processes.⁸ Studies have shown that photocatalytic activity of TiO_2 can be increased by the addition of metal nanoclusters.⁹

Figure 1.2 shows that light excitation energy excites an electron from the valence band to the conduction band leaving a hole behind.¹⁰ The charges drive water splitting processes where the hole causes oxidation and formation of O_2 , the electron responsible for reduction and formation of H_2 .¹⁰ Au clusters help trap electrons and holes and keep charges separate. Therefore, Au clusters on oxide surfaces increase reduction efficiency.⁵

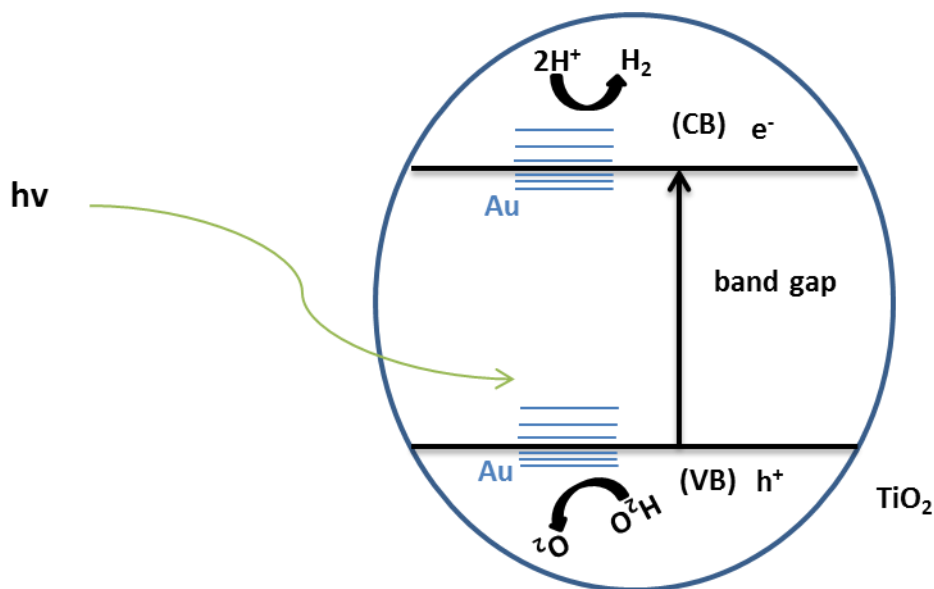


Figure 1.2: Photocatalytic conversion of water using deposited Au clusters on titania surfaces. It should be noted, that the energy levels drawn for Au clusters are a schematic and have been added for illustration. The energy levels are not based on experimental results or calculations.

CHAPTER 1

The following equations represent one option for the reaction:



Metal cluster chemistry is well established and able to deliver large quantities of materials in catalysis processes instead of gas phase cluster. The cluster regime is a transition between two physical states, discrete atom state and solid bulk state. Nanoparticles have a continuous electronic energy band structure similar to bulk Au. Compared to nanoparticles, nanoclusters are molecules which have discrete energy levels and geometric fluxionality. Particles provide edges, kinks and tresses which act as active sites for catalysis. For this reason, the number of atoms forming an Au NC strongly influences the properties of NC modified surfaces. In the case of clusters from 1-100 atoms, a large proportion of atoms lie on the surface, with extremely high surface to volume ratio, compared to the same number of atoms in bulk material (Figure 1.3).

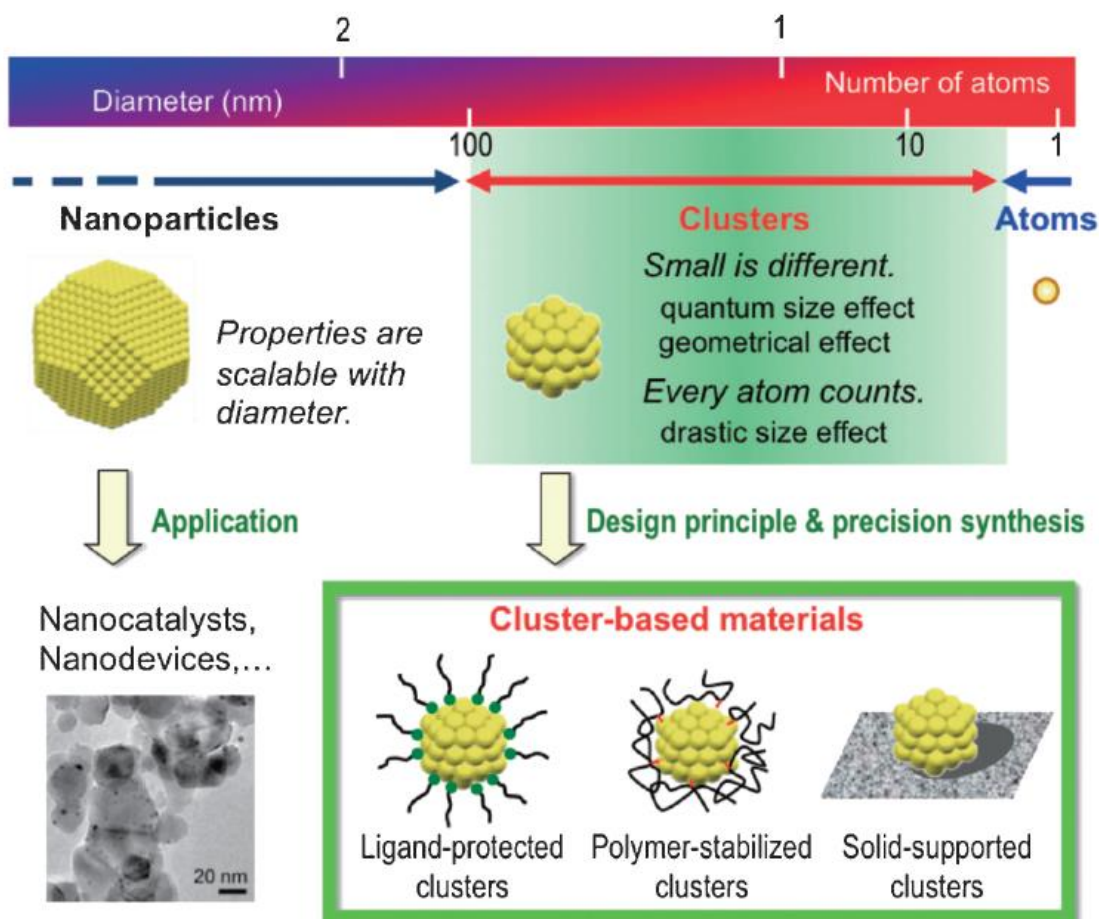


Figure 1.3: Concept for development of cluster-based materials.¹¹

Fabrication of support-immobilised nanoparticles as model systems in heterogeneous catalysis follows two different approaches. The first approach relies on classical surface science which creates metal nanoparticles on flat support, i.e. the gas phase approach.¹²⁻¹³ The second approach involves chemical synthesis of nanoparticles followed by deposition onto support.¹⁴⁻¹⁵ However, chemically synthesised clusters have a number of differences compared with gas phase clusters. Chemically synthesised clusters are stabilised by attaching ligands at the core level (Figure 1.4). For cluster activation, gas molecules access cluster cores to make catalytic reactions occur and ligands are usually removed through heat treatment. Monitoring of heat treatment is a main task as the heating process may not remove all ligands or may change the chemical nature of ligands attached to the metal core.¹⁶ In addition, the presence or absence of ligands influences charge distribution on Au clusters

and interaction with the substrate while the gas phase clusters sit directly onto the substrate. Nevertheless, chemically synthesised clusters offer the huge benefit of easy scale-up production to gram scale and testing of fabricated materials under industrially relevant conditions.

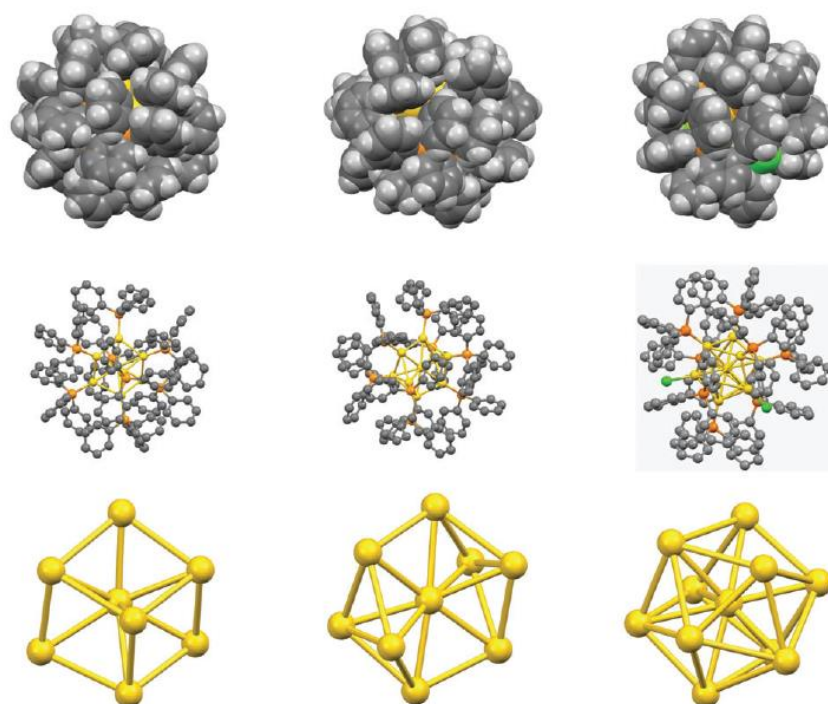


Figure 1.4 : Crystal structures of Au_8 (left column), Au_9 (centre column) and Au_{11} (right column) clusters showing exact number of Au atoms per cluster core. The top row shows space-filled models, while the centre row shows the ball and stick model positions of all atoms except hydrogen. The bottom row shows geometries of the metal cores. The atomic colour scheme is gold (Au), orange (P), green (Cl), and black (C).¹⁷

Chemical reactivity of metal clusters is determined by three main factors: (a) size of clusters¹⁸⁻¹⁹, (b) geometric arrangement of atoms forming clusters and flexibility of geometric changes from one configuration to another which may play an important role as bond length in molecules or lifting energetically adsorbed molecules into states would change²⁰, (c) electronic structure of metal clusters (e.g. oxidation state).¹³ In contrast to nanoparticles, it is not crystal structure, but geometric fluxionality and size dependence of

CHAPTER 1

the electronic structure in nanocluster regime which is important to surface modification.²¹⁻

38

Numerous studies have addressed how catalytic activities are controlled by examining correlations of above key factors and the ability of samples to chemisorb reactants on cluster and substrate sites.³⁹⁻⁴⁰ This relationship cannot be examined by reactivity measurements, structure determination or theoretical calculations alone. For instance, the chemical state of Au clusters with XPS was investigated by Liu et al.⁴¹ who related this to reactivity studies, while the same method has also been used to determine the charge state of clusters.⁴¹⁻⁴³ In addition, scanning tunnelling microscopy (STM) has been used for analysing geometry and electronic structure.⁴⁴

Gold present in very small particles, less than 10 nm in diameter and deposited on metal oxides, is surprisingly catalytically active with many important reactions for chemical industry and environmental protections and has been used in commercial applications.⁴⁵⁻⁴⁶

Gold clusters containing eight or more gold atoms are active, but clusters with less than eight atoms are not active.¹⁸ In the world of nanocatalysis, 'every atom counts!'. Thus, it has been reported that gas phase Au₈ clusters deposited on MgO surfaces show CO oxidation at low-temperature.¹³ Another study by Hutchings and co-workers showed that gold clusters consisting of ~ 10 atoms were used as bilayer clusters for large immobilised gold particles on iron-oxide.⁴⁷ High catalytic activity of CO oxidation was enhanced with presence of Au clusters.

Metal oxide supports play an important role in changing catalytic activity of nanoclusters by charging of nanoclusters through interaction with substrate, e.g. TiO₂ or MgO.⁴⁸ Titania-supported (TiO₂) was observed as a strong support in terms of influence and catalytic activity ability of supported Au clusters compared with other 'inert' supports (e.g. SiO₂, BN). TiO₂

CHAPTER 1

is commonly used as the support material for its ready availability, low cost, low toxicity, sustainability, resistance to photo-corrosion, and versatility.¹⁰ It was demonstrated in the case of ideal flat surfaces of TiO₂ that defects (oxygen vacancies) markedly affect adsorption energy, particle shape, and electronic structure of deposited Au nanoclusters and of unique catalytic properties.⁴⁹ Oxygen vacancy defects result in strong binding between Au and reduced titania surface. Defects can be created by sputtering with Ar⁺ or by annealing in UHV.⁵⁰ Furthermore, active sites are proposed to reside at the interface between Au nanoparticles and oxide support. From a variety of studies, corner and/or edge sites at the perimeter/contact area of the interface between Au nanoparticles and the support are assumed to serve as unique sites for reactant activation.⁵⁰ Therefore, considerable work has focused on characterisation of surface defects of substrate and interaction with clusters.

As mentioned earlier, it is necessary to stabilise metal clusters against aggregation because high surface energies make them extremely unstable.¹¹ Eventually, stabilised ligands must be removed before catalytic reactions occur. Post-fabrication conditions of such catalysts by calcination^{17, 51} or washing¹⁷ afford naked nanoclusters defined by the specific cluster. These conditions, in particular calcination, could increase mobility of clusters to move over the surface and form aggregated clusters. Due to intrinsic properties of Au, interactions between Au and most metal oxides are relatively weak compared to the Au-Au bond. There are two mechanisms responsible for aggregation and coarsening phenomena.⁵² The Ostwald ripening mechanism creates larger aggregated clusters at the expense of smaller ones. The Smoluchowski ripening mechanism occurs when entire clusters diffuse and coalesce. For example, STEM results indicate that Au₁₁ clusters protected by triphenylphosphine and supported on mesoporous silica aggregate into larger particles due to thermal-induced migration of Au₁₁ clusters in longer calcination time (at 200 °C for 8 and 16 h in vacuum). On the other hand, Au₁₁ clusters remaining intact at a shorter time (calcination at 200 °C for

CHAPTER 1

2 h in vacuum) removes all ligands from the Au₁₁ core due to small possibility of aggregation during migration for shorter calcination time.¹¹ Sintering properties can reduce by changing interaction conditions between clusters and substrate to enhance the gold-support interaction and retard clusters sintering.

Comprehensive study of ligand stabilised metal nanocluster processes occurring during catalyst fabrication and post-treatment, such as (1) interaction of the cluster metal core with the support material, (2) presence or absence of ligands, (3) aggregation of cluster metal cores, and (4) changes in geometry and electronic states of metal nanoclusters immobilised on a support, are needed to identify the active site in catalytic reactions. Surprisingly, deposition and fabrication of chemically synthesised atomically precise gold clusters on titania surfaces is not well understood.

REFERENCES

1. Itoh, H.; Naka, K.; Chujo, Y., Synthesis of gold nanoparticles modified with ionic liquid based on the imidazolium cation. *Journal of the American Chemical Society* **2004**, *126* (10), 3026-3027.
2. Zhang, Y.; Cui, X.; Shi, F.; Deng, Y., Nano-Gold Catalysis in Fine Chemical Synthesis. *Chemical Reviews* **2011**.
3. Ertl, G., Heterogeneous catalysis on atomic scale. *Journal of Molecular Catalysis A: Chemical* **2002**, *182-183*, 5-16.
4. Mueller, U.; Schubert, M.; Yaghi, O.; Ertl, G., Handbook of Heterogeneous Catalysis. *Wiley-VCH, Weinheim* **2008**, *1*, 247-262.
5. Izumi, Y., Recent advances in the photocatalytic conversion of carbon dioxide to fuels with water and/or hydrogen using solar energy and beyond. *Coordination Chemistry Reviews* **2013**, *257* (1), 171-186.
6. Sastre, F.; Corma, A.; García, H., Visible-Light Photocatalytic Conversion of Carbon Monoxide to Methane by Nickel (II) Oxide. *Angewandte Chemie* **2013**, *125* (49), 13221-13225.
7. Fujishima, A.; Honda, K., Photolysis-decomposition of water at the surface of an irradiated semiconductor. *Nature* **1972**, *238* (5385), 37-38.
8. Rajalakshmi, K.; Jeyalakshmi, V.; Krishnamurthy, K.; Viswanathan, B., Photocatalytic reduction of carbon dioxide by water on titania: Role of photophysical and structural properties. *Indian Journal of Chemistry-Part A InorganicPhysical Theoretical and Analytical* **2012**, *51* (3), 411.
9. Bernhardt, T.; Heiz, U.; Landman, U., Chemical and catalytic properties of size-selected free and supported clusters. In *Nanocatalysis*, Springer: **2007**, pp 1-191.

CHAPTER 1

10. Jeyalakshmi, V.; Mahalakshmy, R.; Krishnamurthy, K.; Viswanathan, B., Titania based catalysts for photoreduction of carbon dioxide: Role of modifiers. *Indian Journal of Chemistry-Part A Inorganic Physical Theoretical and Analytical* **2012**, *51* (9), 1263.
11. Tsukuda, T., Toward an Atomic-Level Understanding of Size-Specific Properties of Protected and Stabilized Gold Clusters. *Bulletin of the Chemical Society of Japan* **2012**, *85* (2), 151-168.
12. Choudhary, T.; Goodman, D., Catalytically active gold: The role of cluster morphology. *Applied Catalysis A: General* **2005**, *291* (1), 32-36.
13. Yoon, B.; Häkkinen, H.; Landman, U.; Wörz, A. S.; Antonietti, J. M.; Abbet, S.; Judai, K.; Heiz, U., Charging effects on bonding and catalyzed oxidation of CO on Au₈ clusters on MgO. *Science* **2005**, *307* (5708), 403-407.
14. Hungria, A. B.; Raja, R.; Adams, R. D.; Captain, B.; Thomas, J. M.; Midgley, P. A.; Golovko, V.; Johnson, B. F. G., Single-Step Conversion of Dimethyl Terephthalate into Cyclohexanedimethanol with Ru₅PtSn, a Trimetallic Nanoparticle Catalyst. *Angewandte Chemie International Edition* **2006**, *45* (29), 4782-4785.
15. Turner, M.; Golovko, V. B.; Vaughan, O. P. H.; Abdulkin, P.; Berenguer-Murcia, A.; Tikhov, M. S.; Johnson, B. F. G.; Lambert, R. M., Selective oxidation with dioxygen by gold nanoparticle catalysts derived from 55-atom clusters. *Nature* **2008**, *454* (7207), 981-983.
16. Kozlov, A. I.; Kozlova, A. P.; Liu, H.; Iwasawa, Y., A new approach to active supported Au catalysts. *Applied Catalysis A: General* **1999**, *182* (1), 9-28.
17. Anderson, D. P.; Alvino, J. F.; Gentleman, A.; Al Qahtani, H.; Thomsen, L.; Polson, M. I. J.; Metha, G. F.; Golovko, V.; Andersson, G. G., Chemically-Synthesised,

CHAPTER 1

- Atomically-Precise Gold Clusters Deposited and Activated on Titania. *Physical Chemistry Chemical Physics* **2013**.
18. Heiz, U.; Sanchez, A.; Abbet, S.; Schneider, W. D., The reactivity of gold and platinum metals in their cluster phase. *The European Physical Journal D - Atomic, Molecular, Optical and Plasma Physics* **1999**, 9 (1), 35-39.
 19. Lee, S.; Fan, C.; Wu, T.; Anderson, S. L., CO Oxidation on Au/TiO₂ Catalysts Produced by Size-Selected Cluster Deposition. *Journal of the American Chemical Society* **2004**, 126 (18), 5682-5683.
 20. Li, H.; Li, L.; Li, Y., The electronic structure and geometric structure of nanoclusters as catalytic active sites. In *Nanotechnology Reviews*, **2013**; Vol. 2, p 515.
 21. White, R.; Bennett, T.; Golovko, V.; Andersson, G. G.; Metha, G. F., A Systematic Density Functional Theory Study of the Complete De-ligation of Ru₃(CO)₁₂. *accepted for publication in ChemistrySelect* **2016**.
 22. Alvino, J. F.; Bennett, T.; Anderson, D.; Donoeva, B.; Ovoshchnikov, D.; Adnan, R. H.; Appadoo, D.; Golovko, V.; Andersson, G.; Metha, G. F., Far-infrared absorption spectra of synthetically-prepared, ligated metal clusters with Au₆, Au₈, Au₉ and Au₆Pd metal cores. *RSC Advances* **2013**, 3 (44), 22140-22149.
 23. Schmid, G.; Simon, U., Gold nanoparticles: assembly and electrical properties in 1-3 dimensions. *Chemical Communications* **2005**, (6), 697-710.
 24. Schmid, G., Large clusters and colloids. Metals in the embryonic state. *Chemical Reviews* **1992**, 92 (8), 1709-1727.
 25. Della Pina, C.; Falletta, E.; Prati, L.; Rossi, M., Selective oxidation using gold. *Chemical Society Reviews* **2008**, 37 (9), 2077-2095.
 26. Corma, A.; Garcia, H., Supported gold nanoparticles as catalysts for organic reactions. *Chemical Society Reviews* **2008**, 37 (9), 2096-2126.

CHAPTER 1

27. Eustis, S.; El-Sayed, M. A., Why gold nanoparticles are more precious than pretty gold: Noble metal surface plasmon resonance and its enhancement of the radiative and nonradiative properties of nanocrystals of different shapes. *Chemical Society Reviews* **2006**, *35* (3), 209-217.
28. Chen, W.; Chen, S., Oxygen Electroreduction Catalyzed by Gold Nanoclusters: Strong Core Size Effects. *Angewandte Chemie International Edition* **2009**, *48* (24), 4386-4389.
29. Qian, H.; Zhu, M.; Wu, Z.; Jin, R., Quantum Sized Gold Nanoclusters with Atomic Precision. *Accounts of Chemical Research* **2012**, *45* (9), 1470-1479.
30. Chen, M. S.; Goodman, D. W., Structure–activity relationships in supported Au catalysts. *Catalysis Today* **2006**, *111* (1–2), 22-33.
31. Boronat, M.; Corma, A., Molecular approaches to catalysis: Naked gold nanoparticles as quasi-molecular catalysts for green processes. *Journal of Catalysis* **2011**, *284* (2), 138-147.
32. Wilcoxon, J. P.; Abrams, B. L., Synthesis, structure and properties of metal nanoclusters. *Chemical Society Reviews* **2006**, *35* (11), 1162-1194.
33. Yamazoe, S.; Koyasu, K.; Tsukuda, T., Nonscalable Oxidation Catalysis of Gold Clusters. *Accounts of Chemical Research* **2014**, *47* (3), 816-824.
34. Schmid, G., The relevance of shape and size of Au₅₅ clusters. *Chemical Society Reviews* **2008**, *37* (9), 1909-1930.
35. Zeng, C.; Qian, H.; Li, T.; Li, G.; Rosi, N. L.; Yoon, B.; Barnett, R. N.; Whetten, R. L.; Landman, U.; Jin, R., Total Structure and Electronic Properties of the Gold Nanocrystal Au₃₆(SR)₂₄. *Angewandte Chemie* **2012**, *124* (52), 13291-13295.

CHAPTER 1

36. Qin, W.; Lohrman, J.; Ren, S., Magnetic and Optoelectronic Properties of Gold Nanocluster–Thiophene Assembly. *Angewandte Chemie International Edition* **2014**, *53* (28), 7316-7319.
37. Bennett, T.; Falcinella, A. J.; White, R. J.; Adnan, R. H.; Golovko, V.; Andersson, G. G.; Metha, G. F., The effect of counter ions on the far-infrared spectra of tris(triphenylphosphinegold)oxonium dimer salts. *RSC Advances* **2015**, *5* (91), 74499-74505.
38. Bennett, T.; Adnan, R. H.; Alvino, J. F.; Golovko, V.; Andersson, G. G.; Metha, G. F., Identification of the Vibrational Modes in the Far-Infrared Spectra of Ruthenium Carbonyl Clusters and the Effect of Gold Substitution. *Inorganic Chemistry* **2014**, *53* (9), 4340-4349.
39. Lee, S.; Fan, C.; Wu, T.; Anderson, S. L., Cluster size effects on CO oxidation activity, adsorbate affinity, and temporal behavior of model Au/TiO catalysts. *The Journal of chemical physics* **2005**, *123*, 124710.
40. Gong, J., Structure and Surface Chemistry of Gold-Based Model Catalysts. *Chemical Reviews* **2012**, *112* (5), 2987-3054.
41. Liu, L.; Qiao, B.; Ma, Y.; Zhang, J.; Deng, Y., Ferric hydroxide supported gold subnano clusters or quantum dots: enhanced catalytic performance in chemoselective hydrogenation. *Dalton Transactions* **2008**, (19), 2542-2548.
42. Kaden, W. E.; Wu, T.; Kunkel, W. A.; Anderson, S. L., Electronic Structure Controls Reactivity of Size-Selected Pd Clusters Adsorbed on TiO₂ Surfaces. *Science* **2009**, *326* (5954), 826-829.
43. Walther, G.; Mowbray, D. J.; Jiang, T.; Jones, G.; Jensen, S.; Quaade, U. J.; Horch, S., Oxidation of CO and H₂ by O₂ and N₂O on Au/TiO₂ catalysts in microreactors. *Journal of Catalysis* **2008**, *260* (1), 86-92.

CHAPTER 1

44. Lu, J. L.; Gao, H. J.; Shaikhutdinov, S.; Freund, H. J., Gold supported on well-ordered ceria films: nucleation, growth and morphology in CO oxidation reaction. *Catalysis Letters* **2007**, *114* (1), 8-16.
45. Haruta, M., When gold is not noble: catalysis by nanoparticles. *The Chemical Record* **2003**, *3* (2), 75-87.
46. Haruta, M., Size-and support-dependency in the catalysis of gold. *Catalysis Today* **1997**, *36* (1), 153-166.
47. Herzing, A. A.; Kiely, C. J.; Carley, A. F.; Landon, P.; Hutchings, G. J., Identification of Active Gold Nanoclusters on Iron Oxide Supports for CO Oxidation. *Science* **2008**, *321* (5894), 1331-1335.
48. Lim, D.-C.; Hwang, C.-C.; Gantefor, G.; Kim, Y. D., Model catalysts of supported Au nanoparticles and mass-selected clusters. *Physical Chemistry Chemical Physics* **2010**, *12* (46), 15172-15180.
49. Chen, M.; Goodman, D., The structure of catalytically active gold on titania. *Science* **2004**, *306* (5694), 252-255.
50. Chen, M.; Goodman, D. W., Catalytically active gold on ordered titania supports. *Chemical Society Reviews* **2008**, *37* (9), 1860-1870.
51. Liu, Y.; Tsunoyama, H.; Akita, T.; Xie, S.; Tsukuda, T., Aerobic Oxidation of Cyclohexane Catalyzed by Size-Controlled Au Clusters on Hydroxyapatite: Size Effect in the Sub-2 nm Regime. *ACS Catalysis* **2011**, *1*, 2-6.
52. Fukamori, Y.; König, M.; Yoon, B.; Wang, B.; Esch, F.; Heiz, U.; Landman, U., Fundamental Insight into the Substrate-Dependent Ripening of Monodisperse Clusters. *ChemCatChem* **2013**, *5* (11), 3330-3341.

CHAPTER 2

Thesis Aims

CHAPTER 2

This research is part of a larger project which aims to understand the correlation between catalytic activity and structure for the cluster/support system, deposition and activation of clusters and explain key factors affecting activity of atomically precise support immobilised clusters. This current project contributes to achieving the broad research project aim.

2.1 KEY RESEARCH POINTS

In this project, chemically made clusters stabilised by organic ligands were deposited on different TiO₂ surfaces. Chemically synthesised precise gold (Au) clusters used in this work were stabilized by triphenylphosphine ligands. In catalytic reactions, ligands need to be removed to allow reactants to access the active site of Au clusters. Importantly, deposition of clusters and removal of ligands result in non-aggregated clusters, as aggregation would eliminate the ability of clusters to be size specific in catalytic activity. In addition, surface post-treatments are important for addressing aggregations. A combination of surface analytical techniques (XPS and MIES) and high resolution microscopies (STEM, STM and AFM) are used in this study to understand the key properties of chemically produced clusters.

- As the size and geometry of Au clusters control the key properties of the catalyst, size and geometrical structure of clusters deposited on titania before and after annealing need to be determined.
- For a fundamental understanding of cluster-reactant and cluster-surface interaction in the catalytic reaction, the electronic structure and charge state of atomically precise Au clusters before and after annealing must be measured.

CHAPTER 2

- Before performing catalytic reactions, ligands need to be removed for easy access to Au cores. Therefore, monitoring the change in chemical nature of Au cores after ligand removal is an important task.
- Observing cluster distribution over titania after using various pre-treatment surfaces, such as acidic, UV and Ar⁺ sputtering treatment, leads to understanding of the influence of pre-treated surfaces on adsorbed Au clusters.
- DFT calculations help to classify the geometry of experimental Au cluster structures.

An understanding of geometric structures, electronic structure and charge state of Au clusters on titania surface may lead to the development of better catalysts.

2.2 THESIS OUTLINE

Chapter 3 describes experimental methods used in this study, including spectroscopic and microscopic techniques. Additionally, the parameters of techniques are discussed.

Chapters 4 focuses on studies of Au clusters deposited on titania nanosheet in atomic resolution. Geometric structures of adsorbed Au clusters are important for understanding how these clusters are attached on titania nanosheet.

Chapter 5 studies the dispersion of Au clusters on the surface of titania nanosheet. Grouping and aggregations of deposited clusters are discussed in this chapter.

Chapters 6 focuses on studies of Au clusters deposited on ALD titania. In this chapter, we use the sputtering method as the pre-treated condition for titania surfaces. The aggregation behaviour of deposited gold clusters is discussed.

Chapter 7 discusses the effect of sulphuric acid pre-treated ALD titania on Au cluster dispersion. The electronic structure of deposited Au clusters is measured in this chapter.

CHAPTER 2

Comparing between different pre-treated conditions may lead to better Au cluster attachment on titania surfaces.

In the research chapters, the discussion and subsequent conclusions are focused only on that particular study and treated independently of other chapters. Chapter 8 gives a final summary of the work presented in this thesis.

CHAPTER 3

Experimental techniques

CHAPTER 3

Analytical techniques used in this study were chosen to achieve project aims described in Chapter 2. The techniques used were:

- X-ray Photoelectron Spectroscopy (XPS) was used to determine chemical composition of gold (Au) clusters and monitor presence and/or removal of organic ligands. The Australian Synchrotron XPS was used in this study as the number of clusters deposited on the surface is small and difficult to detect by conventional laboratory based XPS systems.
- The size of Au clusters deposited on the metal surface was monitored before and after annealing. XPS allowed determination of cluster size as cluster size influences the peak position through final state effects.
- Meta-Induced Electron Spectroscopy (MIES) was used to quantitatively measure the valence electronic structure of supported Au clusters in the outermost layer.
- Scanning Transmission Electron Spectroscopy (STEM) allowed investigation of the size and geometric structure of Au clusters after deposition at atomic resolution. Density Functional Theory (DFT) calculations helped classify cluster structures observed using the STEM technique.
- Atomic Force Microscopy (AFM) facilitated observation, and determination of size distribution, of Au clusters on titania surfaces before and after heat treatment. The degree of aggregation was also monitored using this technique.
- Scanning Tunneling Microscopy (STM) was used to observe deposited Au clusters on titania in atomic resolution. Individual Au clusters on group Au clusters were observed by STM.

3.1 X-RAY PHOTOELECTRON SPECTROSCOPY (XPS)

Photoelectric effect is based on ejection of electrons by electromagnetic radiation. Photons ionise electrons from a molecule when photon energy is larger than electron binding energy. The difference between these two energies is the kinetic energy of the outgoing electron which is measured via a hemispherical analyser (HSA). Einstein's photoelectric equation describes the relationship between photon energy and kinetic energy of the emitted photoelectron and is illustrated below (Eq.3.1).¹

$$E_{kin} = E_{photon} - \Phi_{spec} - E_{bin} \quad \text{Eq. 3.1}$$

Where E_{kin} is kinetic energy of electrons, E_{photon} is excitation energy, Φ_{spec} is spectrometer work function (constant) and E_{bin} is binding energy of electrons. Spectrometer work function is a constant as it is the same for all measurements.

Depending on incident photon energy, electrons from the valance and core of surface atoms can be detected. Figure 3.1 illustrates the basic elements of an XP instrument, X-ray source, hemispherical electron energy analyser and electron detector. Incident light from the X-ray source emitted the electron from the sample surface at a certain angle and the number of photo-emitted electrons and their kinetic energy of the electron is measured.

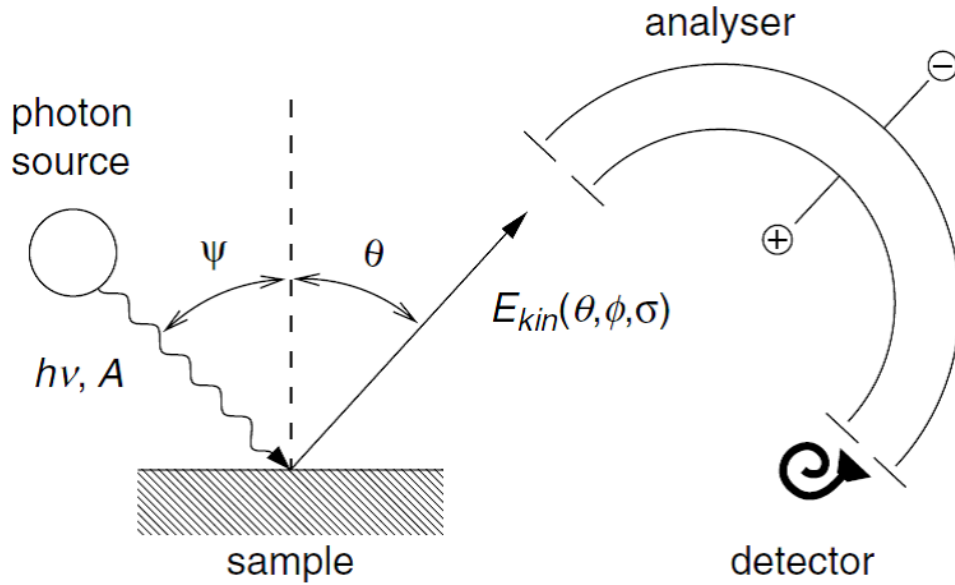


Figure 3.1: The working principle of a photoemission spectrometer. Monochromatic photons with energy $h\nu$ are produced by light source hitting the sample surface at a certain angle ψ .²

Photoelectron spectroscopy is known as a surface sensitive technique due to the mean free path of electrons in matter, that is, the distance that an electron can travel before it interacts with surrounding atoms or electrons. Figure 3.2 shows the electron mean free path in monolayers for a range of electron energies.³ The attenuation of electron intensity is described by

$$I(d, E, \alpha) = I_0 \exp\left(-\frac{d}{\cos(\alpha) \cdot \lambda(E)}\right) \quad \text{Eq.3.2}$$

Where I is intensity measured, I_0 is initial intensity, d is depth from which electrons are emitted, α is angle between the detector and surface normal, $\lambda(E)$ is electron mean free path.

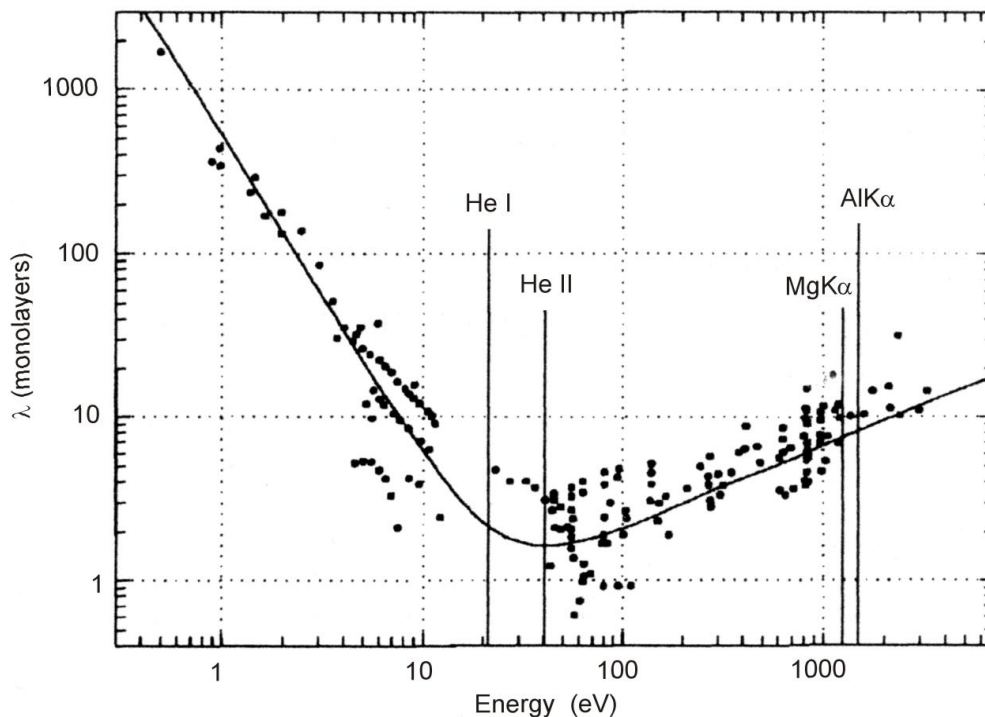


Figure 3.2: Electron mean free path.³

XPS has a depth information of $\sim 3\text{-}5$ nm. XPS has the ability to probe the chemical identity of elements present in a sample.⁴ Two processes lead to emission of electrons from the target. The first process is photo-excitation where photoelectrons are the result of transferring the complete energy of a X-ray photon onto an electron which results in emission of an electron. The second process is Auger excitation which results from relaxation of an electron from a lower binding energy to an orbital with higher binding energy (core electron) of the target atom, i.e. filling the hole left by emission of the photoelectron. Excess energy, as a difference between lower and higher binding energy, is emitted either via a photon or is passed onto another electron which is then emitted. The latter electron is called an Auger electron. Photoelectron peaks are quite sharp (fixed binding energy) compared to Auger electron peaks.

The key information obtained from an XPS spectrum is the peak position of elements, full width half maximum (FWHM) and intensity of a peak. Peak position is characteristic for

CHAPTER 3

each element.⁵ The peak position, FWHM, intensity and background mainly contribute to the uncertainty value. The FWHM of peaks are related to resolution of measurements, while intensity is related to element concentration in the sample.

The binding energy of emitted electrons determined by XPS provides information about the size and chemical state of deposited clusters due to electronic effects.⁶ This concept is essential for interpretation of XPS spectra. In particular, the $4f_{7/2}$ orbital of gold has been chosen in many studies as it provides a sensitive measure of the electronic state of gold. In the following paragraphs, we will explain more about how the binding energy determined by XPS informs about the size and chemical state of the deposited clusters.

Firstly, oxidation state plays a major role in peak position. Higher binding energy was found for Au with the peak shift from Au standard bulk at 84 eV to 85.8-86.2 eV, depending upon interaction with substrates.⁷⁻⁸ Secondly, initial and final effects also determined the peak position and FWHM, which are depending on the elements forming clusters, its size and the interactions with substrate.⁹ Changes in the electronic states resulting from the cluster size or the interaction with substrate contribute to the initial state effect.⁹ The final state effect reflects the de-excitation process of the atom excited by absorption of the X-ray photon. After excitation, the metal nanocluster can remain in a charged state for a certain period of time compared with respective bulk materials.⁹ This shift often depends on cluster size and type of substrate. However, only based on the experimental data it is difficult for gold to interpret the changes of peak positions as an initial or final state effects as the Auger lines are rather weak.⁹⁻¹⁰

Over the last decade, there were many studies of gold films evaporated on various substrates. Kitsudo et al. evaporated gold onto graphite and various oxide surfaces.¹¹ Both the graphite and NiO(001) substrates did not affect the gold peak position where the peak shifts of up to

CHAPTER 3

+0.4 eV on SrTiO₃, Al₂O_x/NiAl(110), TiO₂ and NiO(111). Importantly, the FWHM of the gold peak decreasing slightly with increasing particles size on both SrTiO₃ and graphite. In addition, DiCenzo et al. measured the XPS gold peaks for different size of gas phase Au_n clusters deposited on amorphous carbon. They observed shifts of +0.7, +0.6, +0.5 and +0.5 eV for n = 5, 7, 27 and 33 cluster sizes with slightly broader FWHM for the smaller clusters. In our previous paper, we measured a different Au clusters such as Au₈, Au₉, Au₁₁ and Au₁₀₁ clusters as a reference samples and without substrates (Figure 3 (D)).¹² The peak positions in the gold XPS spectra shift systematically in agreement with the size of the clusters determined by X-ray diffraction immediately after their synthesis. It is noted that we do not have information regarding influence of the ligands on the Au energies, and thus cannot conclude either the Au peak shift from the final state affects or the ligands-Au interact or is it from the combinations of two of them.

Chapter 7 discusses x-ray photoelectron spectroscopy (XPS) conducted in a UHV apparatus using a PHOIBOS-HSA3500 hemispherical analyser at Flinders University Lab. The x-ray used for XPS was the MgK_α line with excitation energy of 1253.6 eV. The analyser was used at pass energy of 10 eV. The survey spectra shows peak of corresponding elements present on the sample surface. XPS was applied in parallel to MIES and provides information about the charge state of the cluster metal core.

Chapters 4, 5 and 6 present the photoelectron spectra of Au₉ clusters recorded using the Soft X-ray Beamline at the Australian Synchrotron (AS). The x-ray technique based on synchrotron radiation is a strong development of recent years for two reasons: it fostered the application of X-ray optics and ‘nanoworld’ is developing rapidly and this technology provides a new and powerful method to characterise nanostructures.¹³ Furthermore, the

CHAPTER 3

brightness for synchrotron measurements is very high with narrow energy resolution which leads to better quality data analysis.

In this work, the AS-XPS technique was conducted using a SPECS Phoibos 150 hemispherical electron analyser. Photon energy used was 690 eV. Spot size of the irradiation beam was adjusted to $\sim 600 \times 600 \mu\text{m}$ with an x-ray photon flux of approximately 10^{12} photon $\text{mm}^{-2} \text{s}^{-1}$. These conditions do not induce damage to samples such as those investigated in this study.¹⁴ The survey spectrum of deposited Au clusters on titania was recorded and high resolution XPS spectra of C, O, Si, P, Ti and Au were recorded at a pass energy of 10 eV with an instrumental resolution of 295 meV.¹⁵ Stability of X-ray energy was monitored using a bulk Au reference and scans were repeated several times to ensure x-ray irradiation did not affect samples.

In this study, all XPS spectra were fitted using the following procedure. A Shirley background was used to remove the electron-scattering background.¹⁶ A pseudo-Voigt function composed of the sum of Gaussian (70%) and Lorentzian (30%) functions was used to fit all peaks.¹⁷ All spectra were fitted with the least number of peaks allowing a variation of FWHM and intensity of corresponding elements. The splitting of 3.67 eV for Au 4f doublets (i.e. between 4f_{7/2} and 4f_{5/2} peak) and 0.84 eV for phosphorus was used. Cross sections were calculated according to Yeh and Lindau using the photo-ionisation cross section and asymmetry parameter.¹⁸ Intensity for each element was then determined. Therefore, quantitative analysis of phosphorous (P), titania and Au intensities is interesting to compare between different Au cluster contributions. The intensity ratio between two species, for example ratio intensity of P to Au, was calculated from the following equation (Eq.3.3).

$$I_{P-Au} = I_P / I_{Au} \quad \text{Eq. 3.3}$$

Where I_{P-Au} is P to Au ratio, I_P is P intensity and I_{Au} is Au intensity.

3.2 METASTABLE INDUCED ELECTRON SPECTROSCOPY (MIES)

MIES the only known method to quantitatively determine electronic structure of the outermost layer within a few Å of the surface. The energy spectrum of emitted electrons were measured using an analyser (HAS). The outermost layer is the important part in samples for heterogeneous catalysis. MIES probes the composition of the outermost layer which is important for interactions and reactions at surfaces. MIES (with excitation energy of 19.8eV) obtains valence band information for just the outermost layer due to metastable helium atoms (denoted He*) exciting molecules with a large cross section. Figure 3.3 shows two de-excitation processes of metastable atoms approaching a surface. He* atoms are de-excited at the surface either via Auger de-excitation or via resonant ionisation with subsequent Auger neutralisation. The Auger de-excitation process was applied for organic materials and semiconductors, while the resonant ionisation process applied metal surfaces with an unoccupied surface orbital in resonance with the 2s orbital of the impinging He* atom.

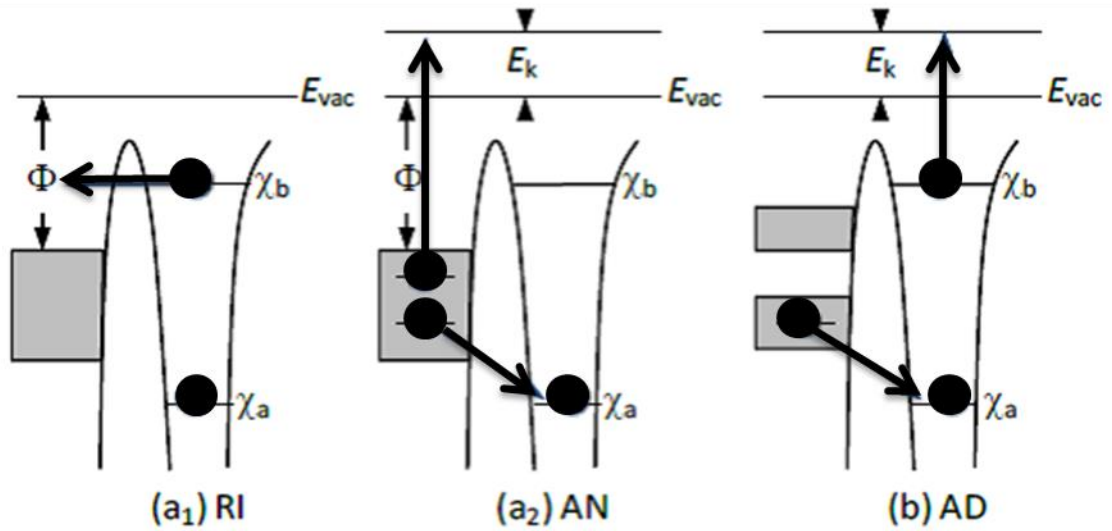


Figure 3.3: De-excitation mechanisms of a metastable atom via resonance ionisation (a₁) followed by Auger neutralisation (a₂) and via Auger de-excitation (b) on an insulator surface.¹⁹

The kinetic energy of the emitted photoelectrons is measured with the help of hemispherical analyser by counting the number the electrons escaped from the surface. The energy relation of Auger de-excitation process is given by:

$$E_{bin} = E_{excitation(He^*)} - \Phi_{spec} - E_{kin} \quad \text{Eq.3.4}$$

where E_{bin} is electron binding energy, $E_{excitation(He^*)}$ is excitation energy of the helium atom, Φ_{spec} is spectrometer work function (constant), E_{kin} is kinetic energy of the electron.

Simultaneously, MIES and UPS measurements were taken in parallel due to the nature of source even though they are separated electronically. The MIES/UPS experiments were performed under a UHV chamber with base pressure of a few 10^{-10} mbar. The source has a two stage cold cathode gas discharge designed and manufactured by MFS, Clausthal-Zellerfeld, Germany. The source simultaneously generates metastable helium (He^*3S_1) and UV light (He I line). Emitted electrons are detected by a hemispherical Phoibos 100 energy analyser from SPECS (Berlin, Germany). Polymer substrate was used as reference sample

CHAPTER 3

to correct the intensity of MIES spectra which has the same spectrum each time we apply MIES measurements. Intensity can change between days and is reflected in the intensity of MIE spectra. All reference spectra were normalised to an arbitrarily chosen reference spectrum and the factors for normalising the intensities of reference spectra were applied to other MIE spectra of the same day. Polymer samples were used here because they do not change over time.

MIE spectra were analysed by the singular value decomposition (SVD) algorithm. Details of the procedure are described elsewhere.²⁰⁻²² The series of measured spectra under similar conditions can be considered a linear combination of reference spectra. In the MIES experiment, reference spectra are well-known in some cases.²⁰ However, in other cases reference spectra are not known. In this case, the SVD algorithm was applied in two steps. In the first step, the numbers of base spectra required to reconstruct a set of measurements was determined. These base spectra are the result of a mathematical procedure and do not necessarily have a physical meaning as base spectra can have negative intensities which are physically meaningless. Linear combinations resulting from SVD should have meaningful physical spectra.

This work follows the procedure of Morgner et al. where the SVD algorithm allows any matrix where row numbers exceed or are equal to column numbers to decompose into the product of three matrices. Therefore, the set of spectra can be considered as a matrix of vectors which result from products of a matrix of orthonormal column vectors, a diagonal with positive or zero elements, and the transpose of an orthogonal matrix.²⁰⁻²² The elements of the diagonal matrix are singular values.

The second step is to determine the reference spectra from base spectra using SVD algorithm. There are two main criterion to follow in defining matrix elements. First, all

reference spectra must be non-negative. Second, all measured MIE spectra must be fitted with a linear combination of reference spectra,

$$S_i = \sum_n a_n S_n^r, \quad \text{Eq.3.5}$$

where S_i are measured spectra, S_n^r are reference spectra, and a_n are weighting coefficients. The sum of weighting factors should be close to unity which confirms that the reference spectrum is physically meaningful. SVD analysis was used in the MIES section in Chapter 7.

3.3 SCANNING TRANSMISSION ELECTRON MICROSCOPY (STEM)

Since the 1930s, Transmission Electron Microscope (TEM) and Scanning Transmission Electron Microscope (STEM) techniques were considered one of the most useful techniques for structure characterisation at the atomic scale.²³⁻²⁴ TEM has a similar optical configuration to an optical microscope. The electrons transmitted through the sample are projected onto a viewing screen or camera for observation after beam bombardment. TEM requires a thin sample of around 100 nm, while the energy beam must be high. Electrons may either transmit the sample without being scattered or be reflected due to interaction with the sample. TEM uses a lens below the sample and electrons of different energies are focused at different focal positions. This affects resolution and contrast of images for having blurring images. In contrast, STEM has no lens below the sample.

Figure 3.4 shows the main components comprising aberration-corrected STEM which are electron source, objective aperture and output detectors.²⁵ STEM combines the principles of

CHAPTER 3

transmission electron microscopy (TEM) and scanning electron microscopy (SEM). STEM has a very high focused beam of electrons with a diameter of about 0.1 nm allowing spatial resolution comparable to interatomic distances. The beam is scanned over a thin specimen and various types of scattering are collected as a function of position. The maximum angle of illumination, including the incident probe which is scanned across the sample by scan coil, are limited by an objective aperture. A variety of output detectors are used to form an image. The bright field (BF) and annular dark field (ADF) detectors give different images of the sample. The STEM BF mode collects transmitted electrons on axis. BF images exhibit crystallographic information as similar to the TEM technique. STEM BF mode can image thicker samples compared to TEM. Also, ADF STEM mode has significant benefits with a unique imaging mode, High Angle Annular Dark Field (HAADF) imaging. Images are based on detection of scattered electrons which/ pass very close to atomic nuclei in samples. HAADF produce high resolution, chemically sensitive, atomic number (Z-) contrast images. HAADF imaging is highly sensitive for atoms with high Z-number, such as Au atoms, due to a large electron scattering. Also, like TEM, backscattered electron and x-rays are produced. Chapter 4 discusses the use of the HAADF-STEM mode to visualise deposited Au clusters on titania nanosheet and HAADF mode is described in detailed. Also, STEM parameters and discussion are provided in Chapter 4.

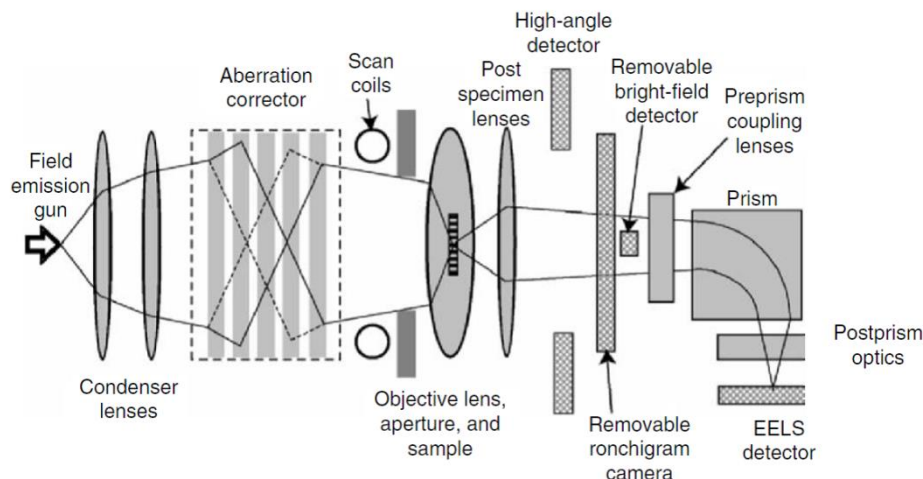


Figure 3.4: Schematic showing the main components of high-resolution STEM.²⁵

3.4 SCANNING PROBE MICROSCOPE (SPM)

The scanning probe microscope (SPM) covers a broad group of instruments used to image and measure properties of materials. By scanning a sharp probe across a surface while monitoring and compiling tip-sample interactions, SPM images are obtained. The two primary forms of SPM are scanning tunneling microscope (STM) and atomic force microscope (AFM).

3.4.1 SCANNING TUNNELLING MICROSCOPE (STM)

The scanning tunnelling microscope (STM) was invented by two physicists at IBM Research Division, Gerd Binnig and Heinrich Rohrer, in 1981 and they shared the Nobel Prize in physics in 1986 for the invention. It was the beginning of scanning probe microscope development and among all scanning probe microscopes STM still provides very high resolution. STM is a novel technique which provides local density of states at surfaces with atomic resolution in real space.²⁶ STM has a number of advantages over scanning electron microscopy (SEM) as STM gives a 3-dimensional (3-D) image of the scanned surface while

CHAPTER 3

SEM does not give information in 3-D. STM employs only bound atoms and no illumination and lenses. STM instruments can be utilised in air, water, liquid, vacuum and ultra-high vacuums. Moreover, STM instruments can also be used in diverse temperature ranges. However, STM has certain disadvantages as it is reliant on highly clean surfaces, sharpness of the tips, vibration control and highly intricate electronics.

STM detects the tunnelling current between conducting tip and sample which are separated by a vacuum gap of typically about 1 nm. This tunnelling current exponentially depends on the gap distance between the tip and the surface, therefore very high resolution in the direction normal to the sample surface is realised. Typically, 0.1 nm variation in tip-sample distance results in one-order of magnitude change in the tunnelling current. Thus, with help of feedback control of gap distance to maintain the current at a certain value, very high resolution well below 0.1 nm is readily obtained in the surface normal direction. By raster scanning the tip over the surface, STM can visualise surface corrugation, such as shape of a molecule, very precisely.²⁷ The lateral (parallel to the sample surface) resolution of STM relies on the locality of the tunnelling current which is strongly dependent on electronic structures of the surface and tip apex.

Usually, STM can be operated in two modes: constant-height and constant-current modes. In constant-height mode, the tip scans a surface and variation of the tunnelling current is recorded as a function of position. In constant-current mode, the tip scans along the surface in x and y directions and the distance between tip and sample (z direction) is controlled by a feedback loop to keep the current constant.²⁸ Displacement of the tip with a piezo actuator corresponds to the cross-section of the sample.

STM usually uses a metallic tip to scan a surface (Figure 3.5). A sharp metal tip (usually tungsten), most likely having one atom at the end, is brought within about 1 nm of the sample

surface. The STM tip can be prepared by electrochemical etching or mechanical cutting of metal wire. By applying a bias voltage typically from 1 mV to 1 V between the tip and sample, a tunnelling current can flow due to the quantum mechanical tunnelling effect.²⁶

For thin vacuum gap of 1 nanometer, wave function of electrons at Fermi level immerse into the gap and appear on the other side, enabling an electron tunnel through the gap. When Fermi levels on the tip and sample are different owing to biased voltage application, tunnelling of electrons results in a unidirectional continuous flow of electrons, called a tunnelling current. When the tunnelling current is produced, the tip is moved over the surface by a piezoelectric driver producing a microscopic image of the surface.²⁸ STM parameters and observation conditions used in this study are outlined in Chapter 5.

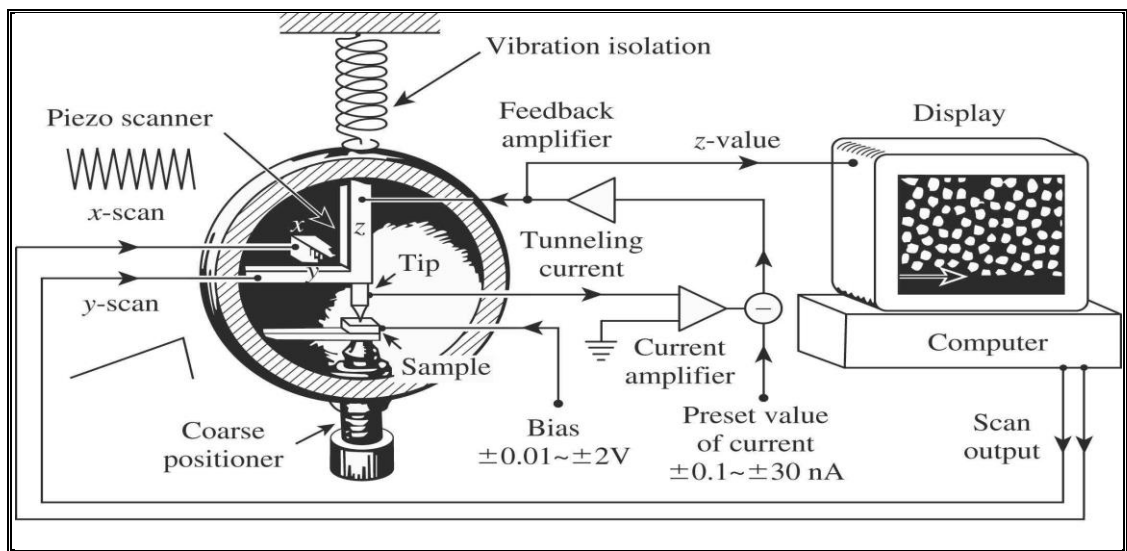


Figure 3.5: Scanning tunnelling microscope components.²⁶

3.4.1 ATOMIC FORCE MICROSCOPE (AFM)

AFM eliminates the restriction of STM in that the sample must be conductive. The invention of AFM in 1986 by Binnig, Quate and Gerber pushed SPM research into biological, geological, and industrial fields²⁹, where many samples investigated are insulators.

Due to exponential dependence of the tunnelling current on distance, the resolution of STM is usually better than AFM. However, AFM is adapted more easily in many cases because, in ambient conditions, metal surfaces are covered with insulating oxide layers or adsorbed layers making it difficult to use STM. In comparison with other forms of scanning probe microscopes, AFM is readily applied to nanometer scale inspection of many different surfaces.³⁰ Therefore, AFM has significantly impacted the fields of materials science, chemistry, biology, physics, and the specialised field of semiconductors. More recent versions of AFM instruments being developed allow the passage of currents between tip and sample. However, the use of such machines is highly challenging and only a few research groups have reported successful use.³⁰⁻³¹

AFM functions by scanning a sharp tip over a surface much the same as a gramophone needle scans a music record (Figure 3.6). The tip is held at the end of a cantilever beam. As the tip is repelled and attracted to the surface because of van der Waals force between atoms of the tip and surface, the cantilever beam is deflected. This detection system uses a laser that reflects onto a position-sensitive photodetector at an oblique angle from the very end of the cantilever. When the tip scans the surface, a feedback system raises and lowers the sample to keep a constant force between the tip and the surface. Without this feedback loop, the tip would 'crash' into a sample with even small topographic features and this phenomenon may occur even with careful AFM operation.

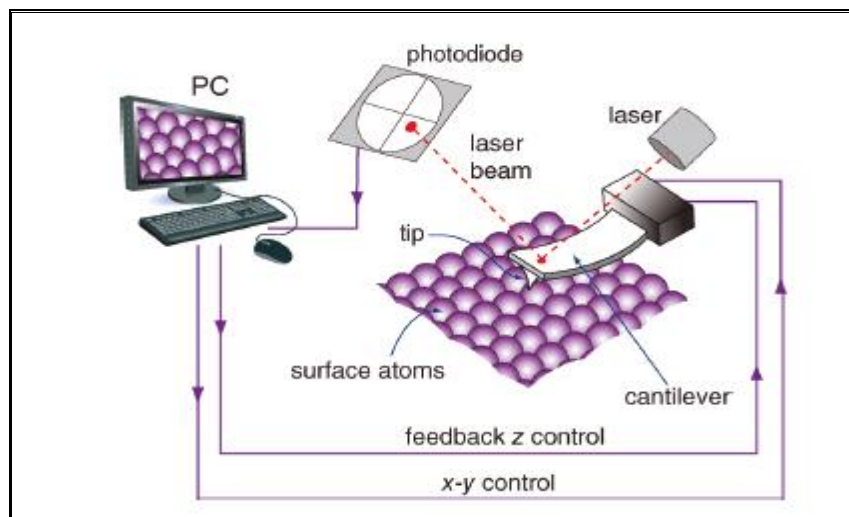


Figure 3.6: Schematic illustration of an atomic force microscope connected to a computer.³²

AFM can provide a high resolution image of surface topography by plotting upward and downward motion as a function of tip position on the sample surface. This mode of operation is called ‘contact mode’. Alternatively, the tip can vibrate rapidly up and down and tap the surface while scanning it. This mode, referred to as ‘tapping’, ‘semi-contact’, or ‘dynamic’ mode, is the most common mode of operation.³²

In this study, AFM images were acquired in AC tapping mode on an Asylum MFP3D SPM (Asylum Research, USA) at room temperature in air. Tapping mode can reduce lateral forces applied to the sample and thus results in a lower degree of damage to samples than contact mode. Au₉ clusters adsorbed from solutions were found to be stable against the tapping AFM mode. AFM cantilevers with a suitable spring constant were chosen to provide stable images under tapping mode, but also such that the tip did not move Au₉ clusters during tip loading and imaging processes. Olympus OMCL-AC160TS-C₃ probes with resonant frequency of 300 kHz (spring constant 26.2 N/m) were used for this purpose. Use of the AFM technique is described in Chapters 5 and 6.

3.5 MATERIALS

Au₉ clusters used in the present work were synthesised according to a well-established method previously reported elsewhere in detail.³³ Each batch of Au₉ clusters was recrystallised at least twice to achieve high purity. Furthermore, the identity of Au₉ was confirmed using nuclear magnetic resonance spectroscopy (NMR), mass spectrometry (MS) and x-ray crystallography.

The titania nanosheets have a thickness of about 1.1 nm³⁴⁻³⁵ and were prepared by delamination of a parent layered K_{0.8}Ti_{1.73}Li_{0.27}O₄ crystal using a soft chemical procedure.³⁶⁻³⁷ For sample preparation, titania nanosheets were deposited on a cleaned 10 mm x 10 mm silicon wafer and exposed to ultraviolet (UV) light irradiation in air to photocatalytically decompose the tetrabutylammonium ions surrounding the nanosheets

Boron doped Si wafers with a resistivity of <0.005 ohm cm from MTI Corporation (USA) were coated with a thin layer of atomic layer deposited (ALD) TiO₂ after removing the oxide layer using SemicoClean solution from Furuuchi Chemical Corporation (Japan). The ALD process produces an amorphous titania surface with a roughness of less than 1 nm rms and is described in detail elsewhere.³⁸ ALD films was produced at 250 °C using 280 deposition cycles. Samples were prepared by cutting the substrates in the dimensions of 10mm x 10mm to be measured using XPS and MIES techniques. This information holds for all ALD titania samples.

3.6 REFERENCES:

1. Arons, A.; Peppard, M., Einstein's Proposal of the Photon Concept—a Translation of the Annalen der Physik Paper of 1905. *American Journal of Physics* **1965**, *33*, 367.
2. Friedrich, R.; Stefan, H., Photoemission spectroscopy—from early days to recent applications. *New Journal of Physics* **2005**, *7* (1), 97.
3. Seah, M.; Dench, W., Surface Interface Analysis 1 (1979). *Full Text via CrossRef/ View Record in Scopus/ Cited By in Scopus (1658)*, 2.
4. Park, E. D.; Lee, J. S., Effects of pretreatment conditions on CO oxidation over supported Au catalysts. *Journal of Catalysis* **1999**, *186* (1), 1-11.
5. Chastain, J.; Moulder, J. F., *Handbook of X-ray photoelectron spectroscopy: a reference book of standard spectra for identification and interpretation of XPS data*. Physical Electronics: **1995**.
6. Porsgaard, S.; Jiang, P.; Borondics, F.; Wendt, S.; Liu, Z.; Bluhm, H.; Besenbacher, F.; Salmeron, M., Charge State of Gold Nanoparticles Supported on Titania under Oxygen Pressure. *Angewandte Chemie International Edition* **2011**, *50* (10), 2266-2269.
7. Juodkazis, K.; Juodkazytė, J.; Jasulaitienė, V.; Lukinskas, A.; Šebeka, B., XPS studies on the gold oxide surface layer formation. *Electrochemistry Communications* **2000**, *2* (7), 503-507.
8. Koslowski, B.; Boyen, H. G.; Wilderotter, C.; Kästle, G.; Ziemann, P.; Wahrenberg, R.; Oelhafen, P., Oxidation of preferentially (1 1 1)-oriented Au films in an oxygen plasma investigated by scanning tunneling microscopy and photoelectron spectroscopy. *Surface Science* **2001**, *475* (1–3), 1-10.

CHAPTER 3

9. Borman, V. D.; Pushkin, M. A.; Tronin, V. N.; Troyan, V. I., Evolution of the electronic properties of transition metal nanoclusters on graphite surface. *Journal of Experimental and Theoretical Physics* **2010**, *110* (6), 1005-1025.
10. Zafeiratos, S.; Kennou, S., A study of gold ultrathin film growth on yttria-stabilized ZrO₂(100). *Surface Science* **1999**, *443* (3), 238-244.
11. Kitsudo, Y.; Iwamoto, A.; Matsumoto, H.; Mitsuhara, K.; Nishimura, T.; Takizawa, M.; Akita, T.; Maeda, Y.; Kido, Y., Final state effect for Au 4f line from gold-nanoparticles grown on oxides and HOPG supports. *Surface science* **2009**, *603* (13), 2108-2114.
12. Anderson, D. P.; Alvino, J. F.; Gentleman, A.; Al Qahtani, H.; Thomsen, L.; Polson, M. I. J.; Metha, G. F.; Golovko, V.; Andersson, G. G., Chemically-Synthesised, Atomically-Precise Gold Clusters Deposited and Activated on Titania. *Physical Chemistry Chemical Physics* **2013**.
13. Lagomarsino, S.; Cedola, A., X-ray microscopy and nanodiffraction. *Encyclopedia of Nanoscience and Nanotechnology* **2004**, *10*, 681-710.
14. Fong, Y.-Y.; Visser, B. R.; Gascooke, J. R.; Cowie, B. C. C.; Thomsen, L.; Metha, G. F.; Buntine, M. A.; Harris, H. H., Photoreduction Kinetics of Sodium Tetrachloroaurate under Synchrotron Soft X-ray Exposure. *Langmuir* **2011**, *27* (13), 8099-8104.
15. Cowie, B. C. C.; Tadich, A.; Thomsen, L., The Current Performance of the Wide Range (90–2500 eV) Soft X-ray Beamline at the Australian Synchrotron. *AIP Conference Proceedings* **2010**, *1234* (1), 307-310.
16. Shirley, D., High-resolution X-ray photoemission spectrum of the valence bands of gold. *Physical Review B* **1972**, *5* (12), 4709.

CHAPTER 3

17. Hughes, H.; Scarfe, J., Lineshapes in core-level photoemission from metals: I. Theory and computational analysis. *Journal of Physics: Condensed Matter* **1996**, *8*, 1421.
18. Yeh, J.; Lindau, I., Atomic subshell photoionization cross sections and asymmetry parameters: 1 Z 103. *Atomic data and nuclear data tables* **1985**, *32* (1), 1-155.
19. Harada, Y.; Masuda, S.; Ozaki, H., Electron Spectroscopy Using Metastable Atoms as Probes for Solid Surfaces. *Chemical Reviews* **1997**, *97* (6), 1897-1952.
20. Berlich, A.; Liu, Y. C.; Morgner, H., Evaporation of Ni and carbon containing species onto NiO/Ni as case study for metal support catalysts investigated by Metastable Induced Electron Spectroscopy (MIES). *Radiation Physics and Chemistry* **2005**, *74* (3), 201-209.
21. Morgner, H., The characterization of liquid and solid surfaces with metastable helium atoms. *Advances in Atomic Molecular and Optical Physics* **2000**, *42*, 387-488.
22. Oberbrodage, J., Determination of a solute electron energy spectrum not accessible experimentally by means of Singular Value Decomposition. *Journal of Electron Spectroscopy and Related Phenomena* **2000**, *107* (3), 231-238.
23. Crewe, A. V.; Wall, J.; Welter, L. M., A High-Resolution Scanning Transmission Electron Microscope. *Journal of Applied Physics* **1968**, *39* (13), 5861-5868.
24. Pennycook, S.; Lupini, A.; Varela, M.; Borisevich, A.; Peng, Y.; Oxley, M.; Van Benthem, K.; Chisholm, M., Scanning transmission electron microscopy for nanostructure characterization. In *Scanning Microscopy for Nanotechnology*, Springer: **2006**, pp 152-191.
25. Varela, M.; Lupini, A. R.; Benthem, K. v.; Borisevich, A. Y.; Chisholm, M. F.; Shibata, N.; Abe, E.; Pennycook, S. J., MATERIALS CHARACTERIZATION IN

- THE ABERRATION-CORRECTED SCANNING TRANSMISSION ELECTRON MICROSCOPE. *Annual Review of Materials Research* **2005**, 35 (1), 539-569.
26. Chen, C. J., *Introduction to scanning tunneling microscopy*. Oxford University Press, USA: **1993**; Vol. 4.
27. Shapter, J. G., *NANO8711 Advanced Nanotechnology GE, Lecture Notes* Flinders University Adelaide, South Australia **2011**.
28. Wiesendanger, R., *Scanning probe microscopy and spectroscopy: methods and applications*. Cambridge Univ Pr: **1994**.
29. Blanchard, C. R., Atomic force microscopy. In *The chemical educator*, **1996**; Vol. 1, pp 1-8.
30. Galloway, G. Atomic Force Microscopy: A Guide to Understanding and Using the AFM. <http://uweb.txstate.edu/~ab35/manuals/AFMmanuals/AFMLabManual.pdf> (accessed 04/10/2011).
31. King, W.; Goodson, K., Thermomechanical formation and thermal detection of polymer nanostructures. In *DEVELOPMENTS IN HEAT TRANSFER*, **2004**; Vol. 13, pp 131-172.
32. Blonder, R.; Joselevich, E.; Cohen, S. R., Atomic Force Microscopy: Opening the Teaching Laboratory to the Nanoworld. In *Journal of Chemical Education*, **2010**.
33. Wen, F.; Englert, U.; Gutrath, B.; Simon, U., Crystal Structure, Electrochemical and Optical Properties of [Au₉(PPh₃)₈](NO₃)₃. *European Journal of Inorganic Chemistry* **2008**, 2008 (1), 106-111.
34. Shibata, T.; Sakai, N.; Fukuda, K.; Ebina, Y.; Sasaki, T., Photocatalytic properties of titania nanostructured films fabricated from titania nanosheets. *Physical Chemistry Chemical Physics* **2007**, 9 (19), 2413-2420.

CHAPTER 3

35. Sasaki, T.; Watanabe, M.; Hashizume, H.; Yamada, H.; Nakazawa, H., Macromolecule-like Aspects for a Colloidal Suspension of an Exfoliated Titanate. Pairwise Association of Nanosheets and Dynamic Reassembling Process Initiated from It. *Journal of the American Chemical Society* **1996**, *118* (35), 8329-8335.
36. Sasaki, T.; Watanabe, M., Osmotic Swelling to Exfoliation. Exceptionally High Degrees of Hydration of a Layered Titanate. *Journal of the American Chemical Society* **1998**, *120* (19), 4682-4689.
37. Sasaki, T.; Nakano, S.; Yamauchi, S.; Watanabe, M., Fabrication of Titanium Dioxide Thin Flakes and Their Porous Aggregate. *Chemistry of Materials* **1997**, *9* (2), 602-608.
38. Walsh, R. B.; Nelson, A.; Skinner, W. M.; Parsons, D.; Craig, V. S. J., Direct Measurement of van der Waals and Diffuse Double-Layer Forces between Titanium Dioxide Surfaces Produced by Atomic Layer Deposition. *The Journal of Physical Chemistry C* **2012**, *116* (14), 7838-7847.

CHAPTER 4

Atomically Resolved Structure of Ligand Protected Au₉ Clusters on TiO₂ Nanosheets

This chapter is a reformatted version of the paper published in *The Journal of Chemical Physics*, 2016, Vol. 144, Issue 11, Page 114703.

4.1 ABSTRACT

Triphenylphosphine ligand-protected Au₉ clusters deposited onto titania nanosheets showed three different atomic configurations, as observed using scanning transmission electron microscopy. The configurations were a 3-dimensional (3D) structure, corresponding to the previously proposed Au₉ core of clusters and two pseudo-2-dimensional (pseudo-2D) structures, newly found in this work. With the help of DFT calculations, observed pseudo-2D structures were attributed to low energy, de-ligated structures formed through interaction with the substrate. The combination of scanning transmission electron microscopy with DFT calculations allowed identification of whether deposited Au₉ clusters were de-ligated in the deposition process.

4.2 INTRODUCTION

Ultra-small metal clusters have attracted much research attention as their physical and chemical properties are between those of single atoms and bulk material.¹⁻² Gold nanoclusters (Au NCs) deposited on metal oxides are catalytically active depending on the number of atoms forming the cluster.³⁻⁶ Catalytic properties are proposed to depend on Au-Au distance, coordination of Au atoms, and electronic structure of Au clusters.⁷⁻⁸ The first two properties describe the geometric structure of Au clusters, while the latter define the density of states (DOS). Clusters deposited onto the surface may show structural transitions between various alternative structures due to intrinsic fluxionality⁹ provided sufficient energy is available for overcoming transition barriers. Structural transitions play an important role in catalytic activity because they can affect the valence electron structure of clusters.^{3, 10-11} When clusters adsorb onto a surface they start interacting with the substrate, which may lead to a change in geometry of cluster structure. Thus, determining the geometrical structure of Au NCs deposited on substrates is of vital importance for understanding NC properties. However, experimentally determining the geometrical structure of individual small clusters deposited onto a solid surface is still a major challenge even with electron microscopy technology currently available.¹²⁻¹⁴

Atomically precise metal clusters can be deposited onto surfaces from the gas phase of size-selected clusters made under UHV conditions^{7, 15} or from solution in size-specific, chemically synthesized clusters.¹⁶⁻¹⁷ The latter route offers the benefit of easy scale-up of production and testing of fabricated materials under industrially relevant conditions. Chemically made clusters, sometimes referred to as “superatoms”, are typically protected by ligands.¹⁸ Our earlier X-ray photoelectron spectroscopy (XPS) studies of [Au₉(PPh₃)₈(NO₃)₃] clusters (from now on abbreviated as Au₉) on titania show that after

deposition at least a fraction of phosphine ligands remain attached to the cluster core.^{17, 19} The term cluster core is used to describe the structure formed only by Au atoms, i.e. the Au₉ cluster without ligands. If desired, subsequent to deposition of clusters onto the support, ligands can be removed from the cluster core through various post-treatments (calcination *etc.*).¹⁷ We have previously investigated the shift in binding energy of Au in relation to the size of Au_n clusters based on the final state effect in XPS.^{17, 19} The XPS data shows that ligands are partially lost in the deposition process and that a fraction of clusters agglomerate to larger particles, while another fraction remains virtually unchanged.^{17, 19} Whether or not agglomeration occurs depends on treatment of the titania support before deposition of Au clusters.^{17, 19}

The aim of this work was to determine the geometrical structure of Au₉ clusters deposited on titania nanosheets at atomic resolution using high-angle annular dark field scanning transmission electron microscopy (HAADF STEM). The structures observed experimentally using STEM were correlated to structures obtained from density functional theory (DFT) calculations of Au₉ clusters without ligands in the gas phase. While the influence of substrate on the Au₉ structure is missing in DFT calculations and direct comparison is not possible, the structures derived from DFT calculations were used to classify STEM-observed structures of Au₉ clusters deposited on the titania nanosheet, although it was expected that the structure and dynamics of clusters were influenced by the substrate.

4.3 EXPERIMENTAL

SAMPLE PREPARATION

For sample preparation, titania nanosheets²⁰ were immersed into a 0.02 mM Au₉ methanol (HPLC grade) solution for 30 minutes, followed by brief rinse in methanol and drying in a stream of dry N₂. The Au₉ clusters were deposited onto titania nanosheets (Ti_{0.87}O₂). The

colloidal suspension of nanosheets was mounted onto a holey carbon film on a TEM grid, followed by ultraviolet (UV) light irradiation in air to photocatalytically decompose tetrabutylammonium ions surrounding the nanosheets.²¹ Based on our previous XPS studies of the same Au₉ clusters deposited on titania nanoparticles, we found that the clusters lose some PPh₃ ligands during the deposition process and that the cluster core comes into contact with the TiO₂ nanoparticle.

SCANNING TRANSMISSION ELECTRON MICROSCOPY

STEM is widely used for characterising structural properties of nanomaterials.²² This technique is used to visualise three-dimensional atomic structures of ultra-small clusters using a well-focused electron beam with a diameter of about 0.1 nm allowing spatial resolution comparable to interatomic distances.

In the present work, a Titan (FEI) STEM was used to investigate Au₉ clusters deposited onto titania nanosheets. Experimental details of Titan STEM are described elsewhere.²³ Here we briefly summarise experimental details. The instrument is equipped with a high-brightness Schottky emission gun (X-FEG) and tandem spherical aberration correctors (DCOR and CETCOR, CEOS). A HAADF detector collects electrons incoherently and elastically scattered from individual atoms to form images with high spatial-resolution.²⁴ HAADF imaging is highly sensitive for atoms with high Z-number; the ligand atoms P, C, O, and H, are difficult to image by STEM because their Z-number is much smaller than that of Au. Such Z-sensitivity offers a huge advantage to HAADF imaging of nanostructures made of heavy atoms in contrast to imaging using conventional transmission electron microscopy (TEM). Recently, Au₉ clusters on a sulfur-functionalised graphene surface were visualised using TEM.²⁵ It is important to note that in electron microscopy electron irradiation can affect samples due to energy transfer from the electron beam to the sample, even at low

CHAPTER 4

electron currents and low electron energies.^{14, 26} In the present study, such energy transfer can lead to partial or full removal of ligands through interaction of the electron beam²⁷ with an Au₉ cluster and movement or rotation of clusters on the surface.^{14, 26} Energy transfer can also be used to study the transformation between alternative cluster morphologies²⁸ and could include morphologies higher in energy than the global energy minimum provided that the barrier for transition between alternative structures is low enough.

Figure 4.1 shows an example of a lower magnification STEM image. Higher magnification images of Au₉ clusters were selected and are shown in Figure 4.3 of the result and discussion section. In Figure 4.1a three different classes of Au atom aggregations can be identified. The first class is marked by red circles and corresponds to aggregated Au₉ clusters. The number of atoms forming these groups is clearly much larger than nine. The second class is marked by blue and shows Au₉ clusters. The third class are single Au atoms and clusters of Au atoms with a number clearly smaller than nine. A few examples of these clusters are indicated with green circles. Atoms indicated by (b₁) are very small Au clusters (dimer and trimer indicated by (b₂) and (b₃), respectively) and are considered fragments of Au₉ clusters. Fragmentation could be caused by electron beam irradiation during the STEM experiment or potentially by cluster/nanosheet interaction during the cluster deposition process. The reason for fragmentation cannot yet be unambiguously clarified as agglomeration of clusters could be induced by electron beam irradiation.

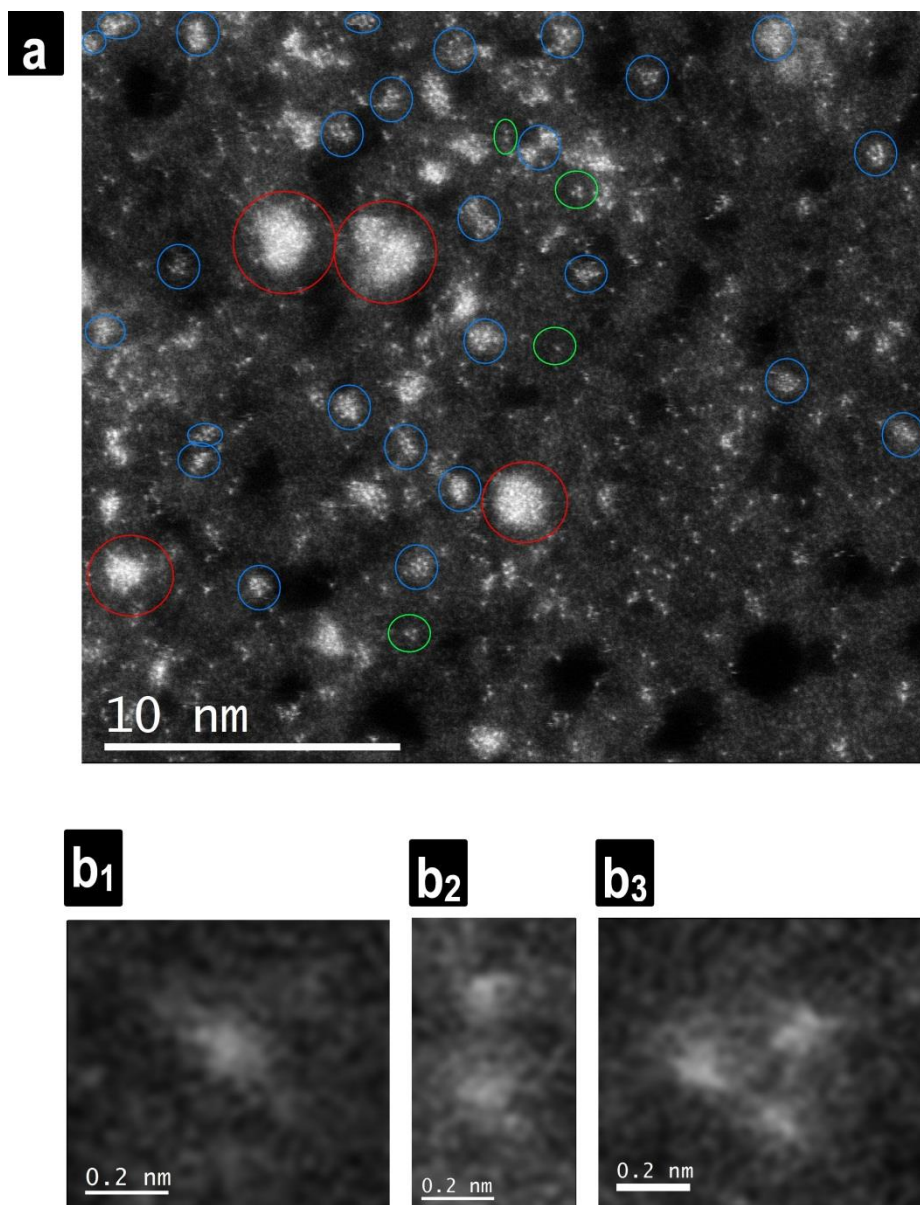


Figure 4.1: (a) The large area STEM image shows various groups of Au atoms on a TiO₂ nanosheet. The blue circles show Au₉ clusters, red circles are aggregated clusters, while the green circles indicate single, dimer and trimer gold atoms. (b₁-b₃) STEM images of single, dimer and trimer gold atoms, respectively. The scale bar corresponds to 10 nm in Figure 4.1a, while 0.2nm corresponds to Figure 4.1b.

A few structures likely to comprise 8-10 Au atoms were identified in STEM images. Figure 4.2 shows several structures not discussed in the paper. We note that the structures in Figure 4.2 were rarely observed, but the structures in Figure 4.3 were often found in our experiments. The DFT calculations did not show a good match with structures shown in

Figure 4.2. This could indicate that these structures do not correspond to single clusters, but to two clusters in close proximity, e.g. $\text{Au}_5 + \text{Au}_2$, $\text{Au}_6 + \text{Au}_3$, or similar combinations. Further investigation is needed to fully understand these structures.

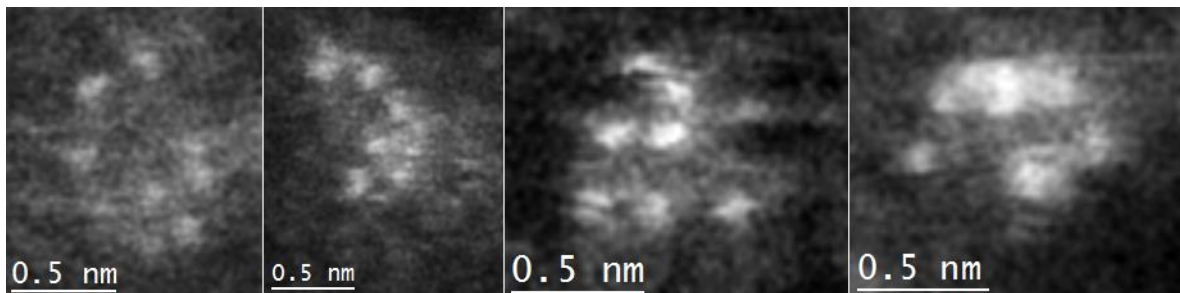


Figure 4.2: STEM images of different structures with 8-10 Au atoms which were infrequently observed in the STEM experiments. The scale bar corresponds to 0.5 nm.

The STEM experiments were conducted at an electron energy of 80 kV and beam current around 25 pA to minimise the effect of electron beam irradiation. Images recorded with the HAADF detector were acquired with DigiScan II and DigitalMicrograph (Gatan) software. The recorded images were processed with DigitalMicrograph (Gatan) and ImageJ software.

4.4 RESULTS AND DISCUSSION

Figure 4.3 (a_1-c_1 , a_2-c_2) shows HAADF-STEM images of Au_9 clusters deposited on titania nanosheets. In these images, the position of individual Au atoms (bright spots in the images) forming Au_9 clusters are resolved. In contrast, atoms forming the substrate were not clearly observed due to a smaller Z-number. Parameters of the STEM experiment were chosen such that imaging was conducted at the mildest possible condition while allowing imaging Au_9 clusters with atomic resolution. In this way, the rate of change for individual clusters and damage of the Au_9 clusters was reduced to the point that the shape of clusters was almost constant and transitions between alternative structures was observed only occasionally.

Observed clusters with around nine gold atoms (Figure 4.3) were selected from STEM images scanning a large area as shown in the experimental section (Figure 4.1).

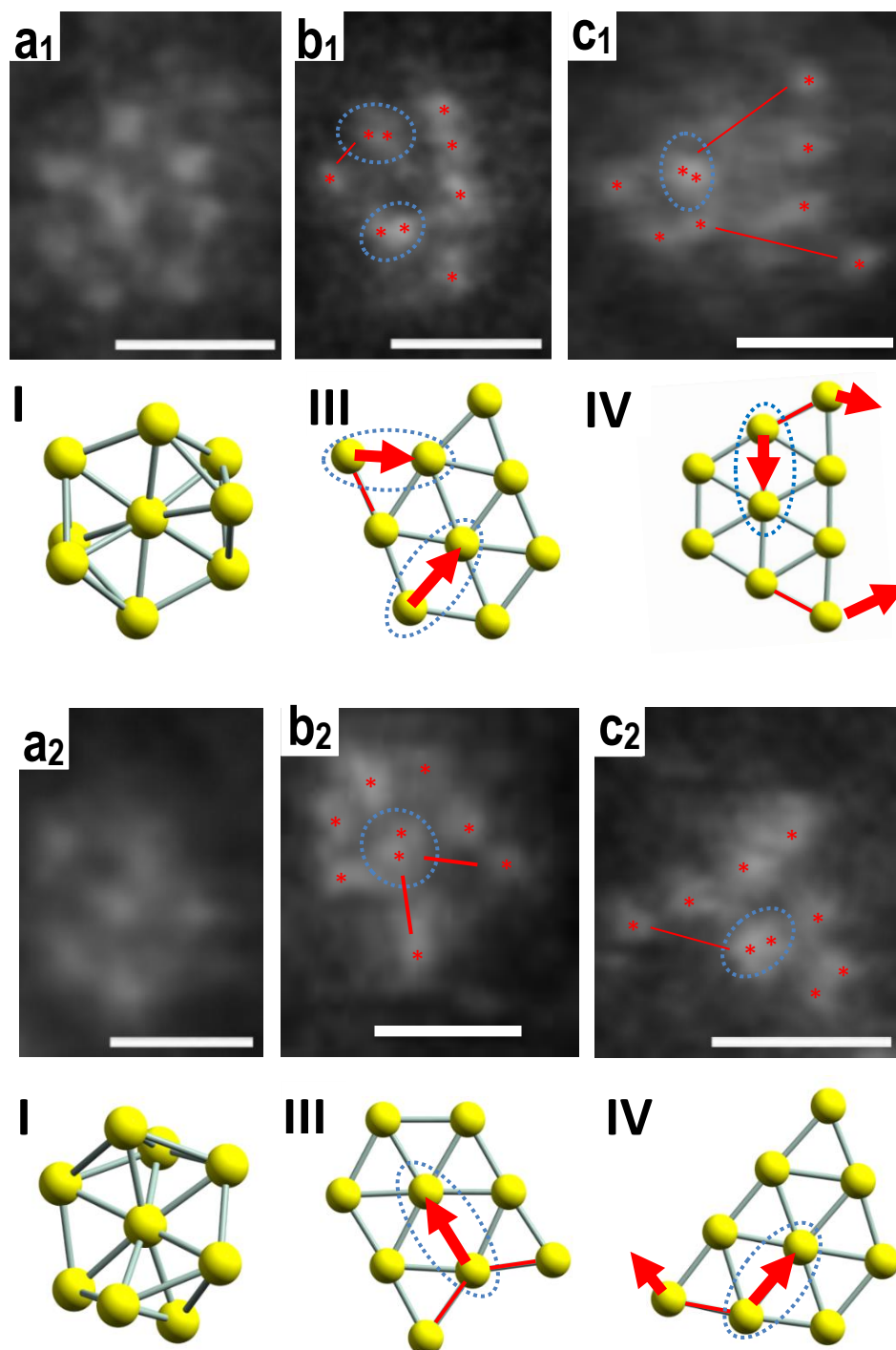


Figure 4.3: High-resolution HAADF-STEM images of $[Au_9(PPh_3)_8](NO_3)_3$ clusters deposited on titania nanosheet under optimised imaging conditions. Panel a shows 3D-like configuration transformed into pseudo 2D configurations shown in panels b and c. The scale

bar corresponds to 0.5 nm and images are slightly smoothed. Panels I, III and IV show DFT models for three different isomers of Au₉ clusters. See text for further details of calculations. (Note that structure II was not observed in the STEM images). Cartesian coordinates of Au₉ clusters is shown in Appendix A (i.e. structures (I), (III) and (IV)).

Three different morphologies of Au₉ cluster cores were identified in the STEM images, as shown in Figure 4.3. The Au core of all Au₉ clusters is approximately 5 Å in diameter. Based on experimentally measured distances between each pair of Au atoms in the clusters, the mean value of interatomic distance is 2.51 ± 0.27 Å, which agrees with previously reported distance in Au₉ crystal structure examined with X-ray crystallography.²⁹ The cluster core morphology shown in Figure 4.3(a) has a structure where Au atoms at the core periphery form a heptagon. Experimentally, very short distances between two adjacent Au atoms are sometimes found in a cluster (upper panel of Figure 4.3(a)), meaning that the axis between such two atoms is not parallel but tilted to the image plane. Configurations of such a cluster are classified as 3-dimensional (3D). The cluster structure in Figure 4.3(b) has three parallel rows of spots and the configuration in Figure 4.3(c) can be approximated as an incomplete triangle. Distances between bright spots in these images appear to be equal and close to the average Au–Au distance. Thus, cluster core morphology in Figures 4.3(b) and 4.3(c) indicates 2-dimensional structures (2D). The presence of these 2D structures, rather than 3D geometry, is expected when cluster structure is influenced by interaction between cluster atoms and metal oxide substrate. Such an interaction becomes stronger through the titania thin-film effect, that is, enhancement of electrical polarisation when the metal oxide film is very thin.³⁰ Previous studies have reported that thin metal oxide films with a thickness of around 1 nm show stronger interaction with Au clusters compared with thick substrates of the same materials.³⁰ Thus, it is reasonable to assume that the use of titania nanosheets with a thickness of 1.1 nm also results in preferential conversion of clusters from 3D heptagon structures to 2D structures owing to cluster-substrate interaction. The prerequisite that the

substrate could influence Au cluster core structure is that the protecting ligands are at least partially removed leading to a direct interaction between cluster and substrate making the clusters less stable (Figure 4.4(b)). Otherwise, the ligands of a fully ligated Au₉ cluster would prevent interaction between cluster core and substrate, as shown in Figure 4.4(a).

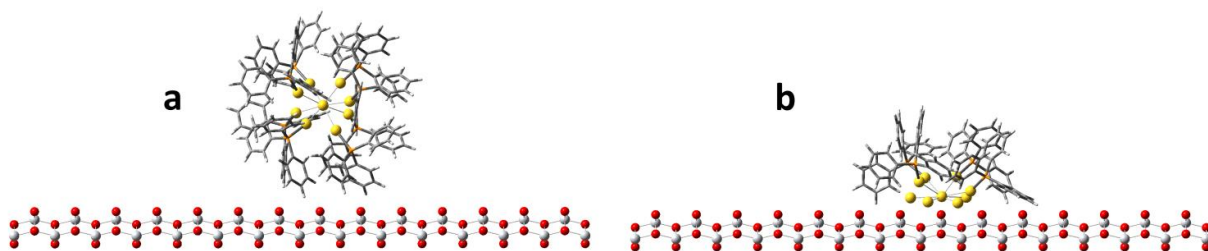


Figure 4.4: Schematic illustration of changes occurring when an Au₉ cluster loses some ligands and interacts with the titania nanosheet substrate. In (a) the cluster (i.e. [Au₉(PPh₃)₈]³⁺, without counter-ions) is shown after deposition. The ligands are attached to the cluster core and the core is not in contact with the substrate. In (b) four ligands are removed (i.e. Au₉(PPh₃)₄) and the cluster core is in contact with the substrate. (Note: the exact number of ligands removed is unknown and may be more than shown here. Also, whilst these figures are based upon the crystal structures of the Au₉ cluster and surface separately, relative position and orientation of the cluster–surface interaction does not involve geometric or energy minimisation processes).

The observed cluster morphologies in Figure 4.3(b) and 4.3(c) do not perfectly match the 2D DFT calculated structures shown with STEM images due to substrate influence and absence of ligands. The outer atoms of the Au core have fewer neighboring atoms than Au atoms in the cluster center. Consequently, compared to center atoms, outer atoms are weakly bound to other Au atoms which allows them to more easily to change position. For example, the Au₉ cluster shown in Figure 4.3(c₁) has two atoms exceptionally far away from the central part of the cluster which reduces the number of bonds to adjacent Au atoms. This suggests that at least one bond is missing (as indicated by red lines in the STEM image) explaining the displacement of these atoms (in directions shown by red arrows on the 2D

structure model). Another peripheral Au atom can then be displaced, while retaining the original bonding to adjacent atoms. This other peripheral Au atom is then positioned either on top or below a further Au atom, resulting in a brighter or broader feature (as highlighted by blue circles in the STEM image and 2D models). Figures 4.3(b) and 4.3(c) are presented in the same manner as Figure 4.3(c₁). We interpret the observed structures in Figure 4.3(b) and 4.3(c) as pseudo-2D structures, that is, under environmental influence, such as the substrate, missing and remaining ligands, these structures are further stabilised by displacing atoms from original positions in stable 2D structures, as shown in the respective figures. More details are provided next based on our theoretical calculations.

The occurrence of a range of different cluster structures indicates the structures have similar relative energies. Consequently, there is a transition occurring between different observed cluster structures. To investigate the transformation between cluster structures, we correlated experimentally determined Au₉ structures with structures (and their energies) obtained from DFT calculations of isolated (i.e. gas-phase) Au₉ clusters. Geometry optimisations for Au₉ clusters was undertaken using the M06 density functional³¹ with the LanL2DZ basis set and corresponding effective core potentials³²⁻³⁵ in the Gaussian 09 (Revision D.01) suite of programs.³⁶ The calculations were carried out using a larger than default grid (Gaussian keyword int=ultrafine) for numerical integral evaluation, with all other cut-offs left at default values. All calculations were undertaken in the C₁ point group. Each geometry optimisation was followed by a harmonic frequency calculation to confirm the geometry was a true minimum with no imaginary frequencies, except for transition states which were optimised to a saddle point with one imaginary frequency. Geometrical structures found through DFT calculations are in agreement with previous calculations³⁷⁻³⁸ and are shown in Table 4.1 (structures found within 1 eV of the lowest energy structure are shown); two of these structures are shown in Figure 4.3 (structures III and IV). It is interesting to note that

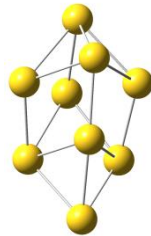
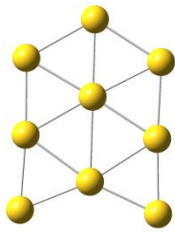
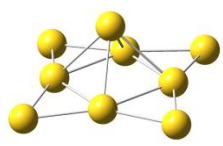
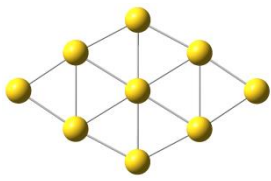
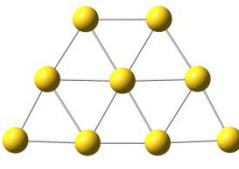
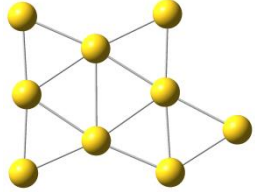
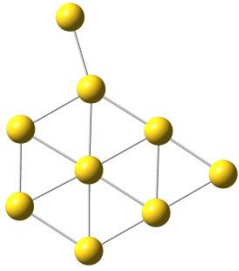
CHAPTER 4

structures (III) and (IV) bear similarities to STEM images despite that DFT calculations were performed for isolated clusters in the gas-phase and did not include cluster–substrate interaction. Figure 4.3 shows only the Au₉ cluster core atoms of the fully ligated cluster (i.e. Au₉(PPh₃)₈]³⁺), which we have previously calculated and shown to be very similar to the structure determined using single crystal X-ray crystallography.³⁸ This structure is very similar to the spherical structure shown in Figures 4.3(a₁) and 4.3(a₂). This supports assigning these observed structures to clusters stabilised by ligands that do not directly interact with the substrate.

Figures 4.3(III) and 4.3(IV) show clusters without ligands which are the starting configuration for the structures in Figures 4.3(b₁), 4.3(b₂), 4.3(c₁) and 4.3(c₂). This supports assignment of these structures to clusters without ligands, or at least a reduced number of ligands, which have a direct interaction with the substrate. It is important to note that it is not possible from these observations to provide information on the strength of this interaction.

It is also important to note several other geometrical structures found through DFT calculations (Table 4.1) were not observed experimentally. A 3D structure (I) and two 2D structures ((V) and (VI)) had no similar structures amongst STEM images and it is not clear why this is the case. The fact that structure (II) was not observed in STEM images may be explained by the hypothesis that clusters without ligands directly interact with the substrate, leading to transformations into pseudo 2D structures, and for this reason the 3D structure (II) could be unstable for deposited clusters.

Table 4.1: All structures resulting from DFT calculations. The structures are shown which have energy less than 1 eV relative to the lowest energy structure.

Isomer	Relative Energy (eV)	Imaginary Frequencies	Geometry
II	0.000	0	
III	0.181	0	
TS	0.250	1	
V	0.345	0	
IV	0.360	0	
VI	0.405	0	
TS (III to IV)	0.971	1	

CHAPTER 4

Relative energies of structures shown in Table 4.1 differ by up to 1 eV (Figure 4.5), which is small compared to the energy that can be deposited through the electron beam. The energy loss of electrons with an energy as used here (80 keV) is in the order of 1 eV/nm, thus 1 – 2 eV per titania nanosheet.³⁹ Therefore, energy deposited locally in the cluster vicinity through the electron beam is certainly sufficient to induce transitions between various cluster structures, including overcoming the activation barrier for transition, even if potential energy differs by 1 eV. Figure 4.5 shows relative energies of several calculated structures, including a possible transition pathway (with an energy barrier of ~0.8 eV from III) for conversion between structures III and IV. The geometry of this transition state could be stable as ligands would have been partially removed from the cluster, so the cluster core would interact with the substrate. This is in line with reasoning for the appearance of 2D pseudo STEM experimental images.

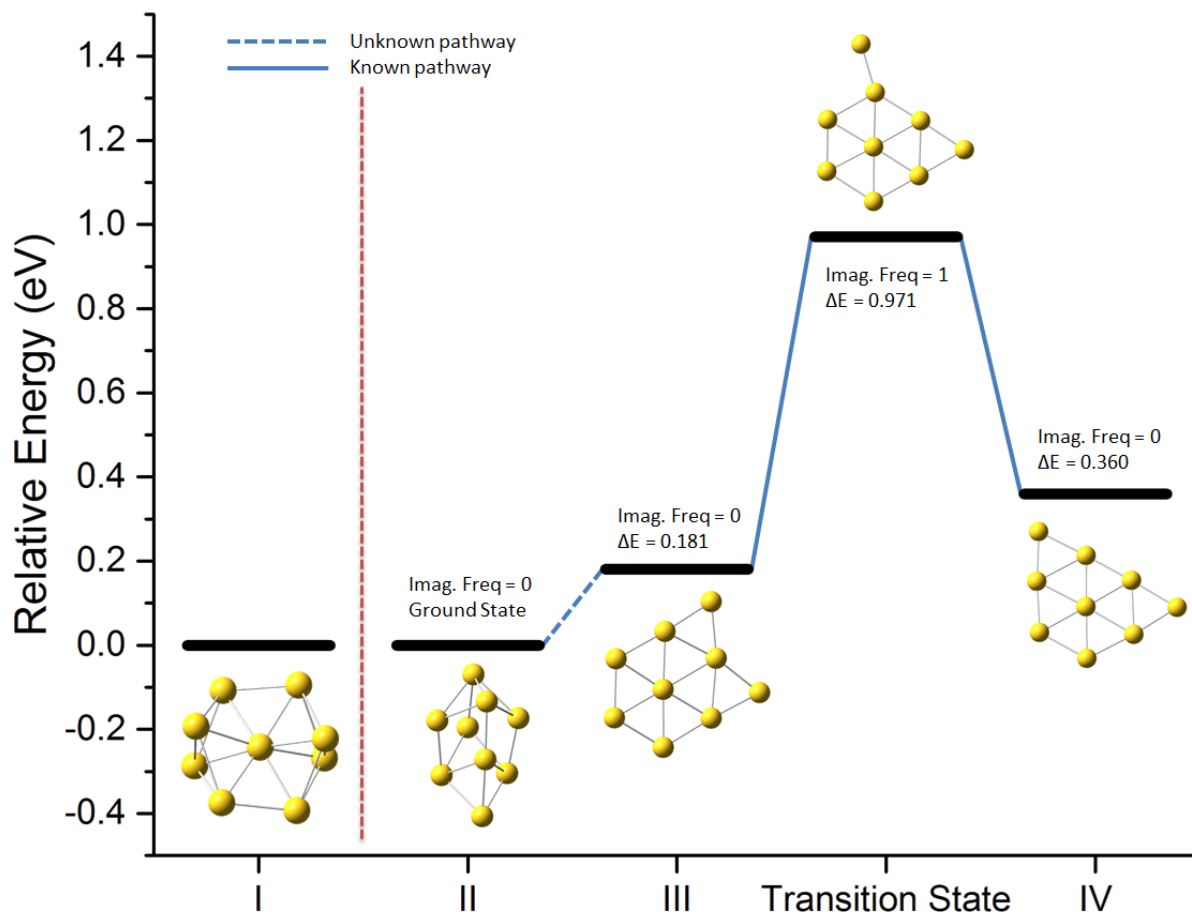


Figure 4.5: The (gas-phase) calculated structures and relative energies of the three lowest energy Au_9 clusters (II, III and IV) and a possible transition state structure for transferring between structures III and IV. Structure I is the calculated structure of $[Au_9(PPh_3)_8]^{3+}$ with ligands omitted.

In previous studies, we used XPS measurements to correlate binding energy of Au for Au_9 clusters to cluster size.^{17, 19} In Figure 4.6, the photoelectron spectrum of Au_9 clusters as deposited on the titania nanosheet is shown. The binding energy of bulk Au for the $4f_{7/2}$ peak is found at a binding energy of 84 eV within a range of ± 0.2 eV, while the corresponding peak for the Au_9 cluster can be fitted with a single peak at 84.8 ± 0.1 eV. This binding energy is very close to the peak position of Au assigned to non-agglomerated supported Au clusters and that of pure, unsupported clusters in microcrystalline form.^{17, 19} The shift in peak position of Au $4f_{7/2}$ peak compared to the bulk Au signal is attributed to final state effect due to the

CHAPTER 4

small size of isolated Au₉ clusters. Through STEM measurements, we found a large number of small Au clusters similar to those shown in Figure 4.3. This strongly supports the conclusion in our previous studies that Au binding energy in an XPS experiment is correlated to cluster size and that the binding energy shift can be explained by final state effect.^{17, 19} STEM images show that clusters other than isolated and ligand-protected clusters are also present on the titania nanosheet. The presence of de-ligated Au clusters and agglomerated clusters makes discussion of XPS results more complex. For full consideration, the possibility of Au clusters interacting with the substrate, e.g. of de-ligated clusters, must be taken into account which could lead to an increase in Au 4f_{7/2} binding energy but was not found here. Further, as discussed above, damage can be induced through the electron beam and lead to a change in cluster structure. Electron beam damage was certainly not occurring during XPS measurements and was thus not considered regarding electron spectroscopy results. A detailed discussion of the Au 4f_{7/2} peak position and correlation of XPS results and STEM measurements are detailed in the next paragraph. The phosphorous spectra can also be fitted with a single, low binding energy peak (P-LBP) at 131.5 eV attributed to phosphorous of ligands bound to Au.¹⁷ This allows for the conclusion that some P-ligands were still attached to the Au cluster core after deposition on the titania nanosheet.

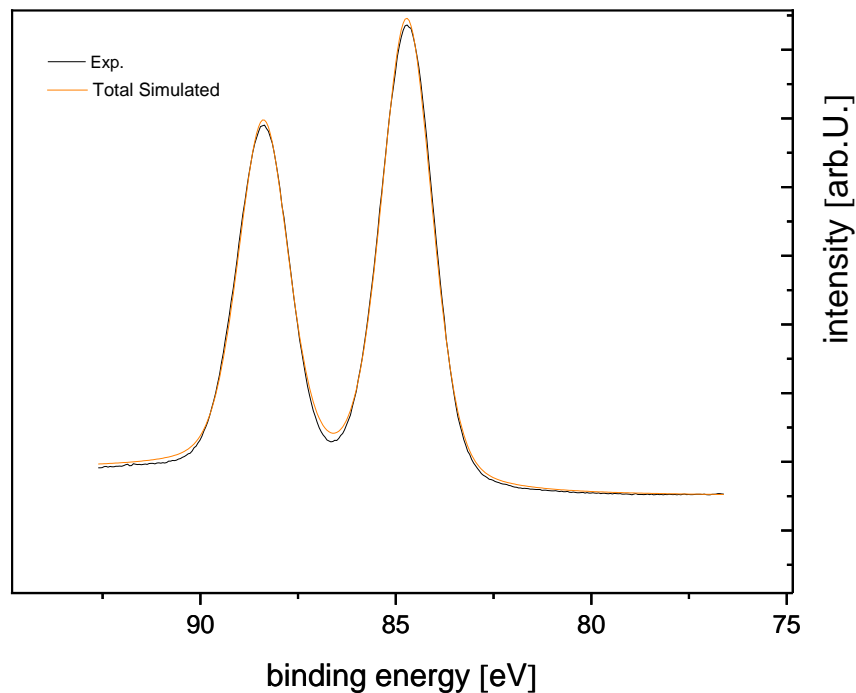


Figure 4.6: SXPS Peak Position of the $4f_{7/2}$ Au peak of $[Au_9(PPh_3)_8](NO_3)_3$ clusters deposited on titania nanosheets.

The XPS measurements of Au_9 deposited on the titania nanosheet show the $4f_{7/2}$ Au peak at 84.8 ± 0.1 eV. The same cluster deposited on untreated anatase nanoparticles was found at 83.7 ± 0.1 eV and at 85.3 ± 0.2 eV.¹⁹ The peak at 85.3 eV was interpreted as being due to isolated Au clusters partially protected by ligands. The peak at 83.7 eV was interpreted as agglomerated Au clusters. Au_9 deposited on sulphuric acid treated P25 at 85.1 ± 0.1 eV¹⁷ was interpreted as isolated and ligand protected Au clusters. The shift of binding energy of small clusters relative to Au binding energy of bulk material was interpreted as final state effect.¹⁷ Treatments for achieving partial or full removal of ligands resulted in the occurrence of a $4f_{7/2}$ Au peak at 85.9 ± 0.1 eV and another peak at 84.8 ± 0.1 eV. The first peak was interpreted as Au_9 cluster cores interacting with the titania substrate and the second peak as ligand protected Au_9 clusters which had not been altered. The $4f_{7/2}$ Au binding energy in the

CHAPTER 4

case of a larger cluster Au₁₀₁ deposited on untreated anatase nanoparticles was found at 83.7 ± 0.1 eV and deposited on sulphuric acid treated P25 at 83.9 ± 0.1 eV. Thus, the peak position of Au₉ cluster found in the present work at 84.8 ± 0.1 eV is close to the ligand protected Au₉ clusters found on anatase nanoparticles and on P25 and based on XPS measurement were interpreted as non-agglomerated Au₉ clusters. Furthermore, we suggest that the Au HBP signals observed in XPS correspond to the population of 3D Au₉ clusters found in STEM images, *i.e.* species that show a 3D structure and are interpreted as ligand protected Au₉ clusters based on match with DFT calculations. However, in the STEM images we also identified Au₉ cluster cores with a pseudo 2D structure and interpreted these as Au₉ cluster cores showing direct interaction with the substrate. According to our previous work, the 4f_{7/2} Au peak in XPS would be expected at a position > 85 eV. However, such a peak was not seen in XPS results. It is noted that we do not have information regarding strength of the interaction between Au clusters and titania substrates, and thus cannot take differences in strength of direct interaction between Au cluster cores and specific substrates (titania nanosheets, anatase or acid treated P25 *etc.*) into account in our discussion. Further, we also found in the STEM images some agglomerated clusters. The 4f_{7/2} Au peak for these agglomerated clusters should be found in a XP spectrum close to 84 eV. Such a peak was also not seen in PS results. We could not investigate to what extent and how quickly exposure of samples to the e-beam during STEM experiments leads to removal of ligands and agglomeration of Au cluster cores. Thus, it cannot be discussed whether not observing 4f_{7/2} Au binding energies at around 84 eV (due to agglomerated clusters) and > 85 eV (due to cluster cores interacting with the substrate) before applying STEM contradict our previous interpretation of XPS results or whether removal of ligands and subsequent direct interaction of Au₉ cluster cores with the substrate and agglomeration of Au₉ clusters is due to e-beam damage during STEM experiments. We assume that e-beam damage is the more likely

reason for the discrepancy between Au cluster structures found in STEM experiments and the previous interpretation of Au₉ XPS results.

4.5 CONCLUSION

In conclusion, this chapter has demonstrated that aberration corrected HAADF-STEM with low electron-beam acceleration voltages can be successfully applied, with atomic resolution, to image the structure of ultra-small Au₉ clusters resulting from deposition of ligand-protected Au₉ clusters onto titania nanosheets. Clusters with both 3D and pseudo 2D structures were correlated to cluster structures determined *via* DFT calculations to rationalise various Au₉ geometrical structures and the possibility of transition between those structures. In particular, the 3D structure was assigned to ligand-protected clusters, indicating that the metal cores of these clusters do not directly interact with the substrate. The pseudo 2D structures were assigned to clusters which had at least partially lost their ligands and interacted directly with the substrate. A transition state between two observed 2D structures was identified from DFT calculations. STEM images support our previous interpretation of XPS studies of Au₉ clusters on titania that concluded clusters that do not agglomerate after depositing onto a TiO₂ surface show shifts in binding energy due to the final state effect.

4.6 REFERENCES

1. Binns, C., Nanoclusters deposited on surfaces. *Surface Science Reports* **2001**, *44* (1–2), 1-49.
2. Qian, M.; Reber, A. C.; Ugrinov, A.; Chaki, N. K.; Mandal, S.; Saavedra, H. M.; Khanna, S. N.; Sen, A.; Weiss, P. S., Cluster-Assembled Materials: Toward Nanomaterials with Precise Control over Properties. *ACS Nano* **2009**, *4* (1), 235-240.
3. Li, H.; Li, L.; Li, Y., The electronic structure and geometric structure of nanoclusters as catalytic active sites. In *Nanotechnology Reviews*, **2013**; Vol. 2, p 515.
4. Lim, D.-C.; Hwang, C.-C.; Gantefor, G.; Kim, Y. D., Model catalysts of supported Au nanoparticles and mass-selected clusters. *Physical Chemistry Chemical Physics* **2010**, *12* (46), 15172-15180.
5. Fu, Q.; Wagner, T., Interaction of nanostructured metal overlayers with oxide surfaces. *Surface Science Reports* **2007**, *62* (11), 431-498.
6. Landman, U.; Yoon, B.; Zhang, C.; Heiz, U.; Arenz, M., Factors in gold nanocatalysis: oxidation of CO in the non-scalable size regime. *Top Catal* **2007**, *44* (1-2), 145-158.
7. Lee, S.; Fan, C.; Wu, T.; Anderson, S. L., CO Oxidation on Aun/TiO₂ Catalysts Produced by Size-Selected Cluster Deposition. *Journal of the American Chemical Society* **2004**, *126* (18), 5682-5683.
8. Kartouzian, A.; Thamer, M.; Soini, T.; Peter, J.; Pitschi, P.; Gilb, S.; Heiz, U., Cavity ring-down spectrometer for measuring the optical response of supported size-selected clusters and surface defects in ultrahigh vacuum. *J. Appl. Phys.* **2008**, *104* (12), 124313-8.

CHAPTER 4

9. Wang, Z. W.; Toikkanen, O.; Quinn, B. M.; Palmer, R. E., Real-Space Observation of Prolate Monolayer-Protected Au₃₈ Clusters Using Aberration-Corrected Scanning Transmission Electron Microscopy. *Small* **2011**, *7* (11), 1542-1545.
10. Wang, L. S.; Cheng, H. S.; Fan, J., Photoelectron spectroscopy of size-selected transition metal clusters: Fe-*n*, *n*=3–24. *The Journal of Chemical Physics* **1995**, *102* (24), 9480-9493.
11. Gates, B. C., Supported Metal Clusters: Synthesis, Structure, and Catalysis. *Chemical Reviews* **1995**, *95* (3), 511-522.
12. Azubel, M.; Koivisto, J.; Malola, S.; Bushnell, D.; Hura, G. L.; Koh, A. L.; Tsunoyama, H.; Tsukuda, T.; Pettersson, M.; Häkkinen, H., Electron microscopy of gold nanoparticles at atomic resolution. *Science* **2014**, *345* (6199), 909-912.
13. Jadzinsky, P. D.; Calero, G.; Ackerson, C. J.; Bushnell, D. A.; Kornberg, R. D., Structure of a thiol monolayer-protected gold nanoparticle at 1.1 Å resolution. *Science* **2007**, *318* (5849), 430-433.
14. Li, Z. Y.; Young, N. P.; Di Vece, M.; Palomba, S.; Palmer, R. E.; Bleloch, A. L.; Curley, B. C.; Johnston, R. L.; Jiang, J.; Yuan, J., Three-dimensional atomic-scale structure of size-selected gold nanoclusters. *Nature* **2008**, *451* (7174), 46-48.
15. Yoon, B.; Häkkinen, H.; Landman, U.; Wörz, A. S.; Antonietti, J.-M.; Abbet, S.; Judai, K.; Heiz, U., Charging Effects on Bonding and Catalyzed Oxidation of CO on Au₈ Clusters on MgO. *Science* **2005**, *307* (5708), 403-407.
16. Chusuei, C. C.; Lai, X.; Davis, K. A.; Bowers, E. K.; Fackler, J. P.; Goodman, D. W., A Nanoscale Model Catalyst Preparation: Solution Deposition of Phosphine-Stabilized Gold Clusters onto a Planar TiO₂(110) Support. *Langmuir* **2001**, *17* (13), 4113-4117.

CHAPTER 4

17. Anderson, D. P.; Alvino, J. F.; Gentleman, A.; Qahtani, H. A.; Thomsen, L.; Polson, M. I. J.; Metha, G. F.; Golovko, V. B.; Andersson, G. G., Chemically-synthesised, atomically-precise gold clusters deposited and activated on titania. *Physical Chemistry Chemical Physics* **2013**, *15* (11), 3917-3929.
18. Walter, M.; Akola, J.; Lopez-Acevedo, O.; Jadzinsky, P. D.; Calero, G.; Ackerson, C. J.; Whetten, R. L.; Grönbeck, H.; Häkkinen, H., A unified view of ligand-protected gold clusters as superatom complexes. *Proceedings of the National Academy of Sciences* **2008**, *105* (27), 9157-9162.
19. Anderson, D. P.; Adnan, R. H.; Alvino, J. F.; Shipper, O.; Donoeva, B.; Ruzicka, J.-Y.; Al Qahtani, H.; Harris, H. H.; Cowie, B.; Aitken, J. B.; Golovko, V. B.; Metha, G. F.; Andersson, G. G., Chemically synthesised atomically precise gold clusters deposited and activated on titania. Part II. *Physical Chemistry Chemical Physics* **2013**, *15* (35), 14806-14813.
20. Sasaki, T.; Nakano, S.; Yamauchi, S.; Watanabe, M., Fabrication of Titanium Dioxide Thin Flakes and Their Porous Aggregate. *Chemistry of Materials* **1997**, *9* (2), 602-608.
21. Sasaki, T.; Ebina, Y.; Fukuda, K.; Tanaka, T.; Harada, M.; Watanabe, M., Titania Nanostructured Films Derived from a Titania Nanosheet/Polycation Multilayer Assembly via Heat Treatment and UV Irradiation. *Chemistry of Materials* **2002**, *14* (8), 3524-3530.
22. Kimoto, K.; Asaka, T.; Nagai, T.; Saito, M.; Matsui, Y.; Ishizuka, K., Element-selective imaging of atomic columns in a crystal using STEM and EELS. *Nature* **2007**, *450* (7170), 702-704.

CHAPTER 4

23. Yamashita, S.; Koshiya, S.; Nagai, T.; Kikkawa, J.; Ishizuka, K.; Kimoto, K., Quantitative annular dark-field imaging of single-layer graphene—II: atomic-resolution image contrast. *Microscopy* **2015**, *64* (6), 409-418.
24. Batson, P. E.; Dellby, N.; Krivanek, O. L., Sub-angstrom resolution using aberration corrected electron optics. *Nature* **2002**, *418* (6898), 617-620.
25. Bosch-Navarro, C.; Laker, Z. P. L.; Thomas, H. R.; Marsden, A. J.; Sloan, J.; Wilson, N. R.; Rourke, J. P., Covalently Binding Atomically Designed Au₉ Clusters to Chemically Modified Graphene. *Angewandte Chemie International Edition* **2015**, *54* (33), 9560-9563.
26. Batson, P. E., Motion of Gold Atoms on Carbon in the Aberration-Corrected STEM. *Microscopy and Microanalysis* **2008**, *14* (01), 89-97.
27. Egerton, R. F.; Li, P.; Malac, M., Radiation damage in the TEM and SEM. *Micron* **2004**, *35* (6), 399-409.
28. Wang, Z. W.; Palmer, R. E., Experimental Evidence for Fluctuating, Chiral-Type Au₅₅ Clusters by Direct Atomic Imaging. *Nano Lett.* **2012**, *12* (11), 5510-5514.
29. Wen, F.; Englert, U.; Gutrath, B.; Simon, U., Crystal Structure, Electrochemical and Optical Properties of [Au₉(PPh₃)₈](NO₃)₃. *European Journal of Inorganic Chemistry* **2008**, *2008* (1), 106-111.
30. Freund, H.-J.; Pacchioni, G., Oxide ultra-thin films on metals: new materials for the design of supported metal catalysts. *Chemical Society Reviews* **2008**, *37* (10), 2224-2242.
31. Zhao, Y.; Truhlar, D., The M06 suite of density functionals for main group thermochemistry, thermochemical kinetics, noncovalent interactions, excited states, and transition elements: two new functionals and systematic testing of four M06-

CHAPTER 4

- class functionals and 12 other functionals. *Theor Chem Account* **2008**, *120* (1-3), 215-241.
32. Hay, P. J.; Wadt, W. R., Ab initio effective core potentials for molecular calculations. Potentials for the transition metal atoms Sc to Hg. *The Journal of Chemical Physics* **1985**, *82* (1), 270-283.
33. Hay, P. J.; Wadt, W. R., Ab initio effective core potentials for molecular calculations. Potentials for K to Au including the outermost core orbitals. *The Journal of Chemical Physics* **1985**, *82* (1), 299-310.
34. Schwerdtfeger, P.; Dolg, M.; Schwarz, W. H. E.; Bowmaker, G. A.; Boyd, P. D. W., Relativistic effects in gold chemistry. I. Diatomic gold compounds. *The Journal of Chemical Physics* **1989**, *91* (3), 1762-1774.
35. Wadt, W. R.; Hay, P. J., Ab initio effective core potentials for molecular calculations. Potentials for main group elements Na to Bi. *The Journal of Chemical Physics* **1985**, *82* (1), 284-298.
36. Frisch, M.; Trucks, G.; Schlegel, H.; Scuseria, G.; Robb, M.; Cheeseman, J.; Scalmani, G.; Barone, V.; Mennucci, B.; Petersson, G., Gaussian 09, revision A. 1. *Gaussian Inc., Wallingford, CT* **2009**.
37. Wang, J.; Wang, G.; Zhao, J., Density-functional study of $Au_n(n=2-20)$ clusters: Lowest-energy structures and electronic properties. *Physical Review B* **2002**, *66* (3), 035418.
38. Alvino, J. F.; Bennett, T.; Anderson, D.; Donoeva, B.; Ovoshchnikov, D.; Adnan, R. H.; Appadoo, D.; Golovko, V.; Andersson, G.; Metha, G. F., Far-infrared absorption spectra of synthetically-prepared, ligated metal clusters with Au₆, Au₈, Au₉ and Au₆Pd metal cores. *RSC Advances* **2013**, *3* (44), 22140-22149.

CHAPTER 4

39. Seltzer, S. M.; Berger, M. J., Evaluation of the collision stopping power of elements and compounds for electrons and positrons. *The International Journal of Applied Radiation and Isotopes* **1982**, 33 (11), 1189-1218.

CHAPTER 5

Grouping and aggregation of ligand protected Au₉ clusters on TiO₂ nanosheets

This chapter is a reformatted version of the manuscript planned to submit to *Physical Review*

B.

5.1 ABSTRACT

Nine-atom Au clusters in the form of $[\text{Au}_9(\text{PPh}_3)_8(\text{NO}_3)_3]$ were deposited onto titania nanosheets after UV pre-treatment of the substrate and examined with scanning tunnelling microscopy (STM), atomic force microscopy (AFM) and synchrotron x-ray photoelectron spectroscopy (XPS) before and after heat treatment. Au clusters attach to the surface as individual clusters or in groups. AFM was performed to determine the height of deposited species and dispersion on titania nanosheets. STM revealed that groups at least partially consisted of individual clusters before and after annealing. XPS showed that before annealing Au clusters were attached to the titania surface as individual clusters and after annealing individual and agglomerated clusters were found on the surface. The combination of AFM, STM and XPS showed that groups formed by clusters consist of individual and agglomerated clusters.

5.2 INTRODUCTION

Nanoclusters (NCs) are of particular interest because of their unique physical and chemical properties which are different to properties of the respective bulk material.¹⁻¹¹ Small clusters containing only a few metal atoms show fluxionality leading to a change in conformation of clusters at room temperature.¹² This is known to decrease with increasing cluster size.¹³⁻¹⁵ Small clusters show discrete energy levels for valence electrons. With increasing cluster size energy levels move closer together. At a size in the order of a few hundred atoms, metal NCs start to exhibit metallic characteristics.¹⁶⁻¹⁹

Metal NCs deposited on surfaces modify the electronic structure of surfaces. For understanding metal NCs properties deposited on surfaces it is important to study their size and dispersion on surfaces and electronic properties.²⁰⁻²¹ Subsequent to deposition on a surface, clusters can agglomerate and lose properties of small clusters. Thus, it is of interest to investigate cluster size after application of post-treatments, such as heating and chemical washing, in an attempt to remove ligands. Metal NCs can be generated either in the gas-phase and subsequently deposited onto surfaces^{15, 22} or fabricated chemically as size specific clusters and be deposited on surfaces from solutions.²³⁻²⁴ Deposited clusters can be used in different technical processes, such as sensors and catalysis. Among all metal NCs available today, Au NCs currently attract interest in catalysis, such as CO oxidation, because Au NCs have unique electronic properties.²⁵⁻²⁶ Catalytic activity of Au clusters deposited onto surfaces has been shown to depend strongly on the size and the number of atoms forming the cluster.^{23-24, 27-33}

The geometric and electronic structure of clusters depends on size of Au NCs. Thus, geometric and electronic structures are affected by cluster distribution on the surface, e.g. whether or not clusters agglomerated to form larger clusters or nanoparticles (NPs).

CHAPTER 5

Microscopic techniques, such as atomic force microscopy (AFM)³⁴ and STM^{19, 35-39}, are important tools for determining geometric and electronic properties of clusters on surfaces, especially size and distribution. Scanning probe microscopic techniques (SPM), such as AFM and STM, are mild techniques compared to electron microscopy, such as transmission electron microscopy (TEM). Recently, we determined the geometrical structure of Au₉ clusters deposited on titania nanosheets with atomic resolution using high-angle annular dark field scanning transmission electron microscopy (HAADF STEM).¹² In electronic microscopy, electron irradiation can easily affect samples due to energy transferred from the electron beam to the sample which can cause serious damage to samples⁴⁰⁻⁴¹ by breaking up clusters or inducing agglomeration. In contrast, SPMs are in principle capable of acquiring high resolution images without affecting size and distribution of clusters across surfaces. Chemical compositions of samples can be identified by high intensity electronic spectroscopy, such as synchrotron x-ray photoelectron spectroscopy (XPS).^{23-24, 42} In previous work we characterised [Au₉(PPh₃)₈(NO₃)₃] clusters (hereafter abbreviated as Au₉) with XPS subsequent to deposition of clusters on titania.²³⁻²⁴ The final state effect of protected Au NCs in XPS offers the possibility to investigate cluster size. XPS data can also be used to determine whether or not ligands are removed from the metallic cluster core and whether or not Au NCs agglomerate.²³⁻²⁴ However, XPS measures a bulk property and is not able to determine distribution of clusters on a surface.

Titania is a particularly interesting support for Au NP-based heterogeneous catalysis.⁴³ On reducible transition metal oxides, such as TiO₂, the presence of an O vacancy associated with extra electrons results in a stronger bond with a metal cluster.⁴⁴⁻⁴⁶ Titania nanosheets were used in the present work as support for Au₉ clusters as they have a higher-dielectric constant than TiO₂ rutile or anatase.⁴⁷ Ultrathin oxide films with a thickness of 20 Å or less are considered an interesting support material because their properties differ from the respective

thicker bulk material.⁴⁸ Thus, it can be expected that the interaction of Au NCs with titania nanosheets is different to other titania substrates.

In the present work, we applied STM and AFM to determine the size and distribution of chemically-synthesised, atomically precise Au₉ clusters deposited onto titania nanosheets. XPS was used to monitor change in size of Au₉ clusters before and after annealing.

5.3 EXPERIMENTAL

Detailed information about the procedure of DFT calculations can be found elsewhere.¹²

SAMPLE PREPARATION

Silicon/titania nanosheet samples were immersed into a 0.02 mM Au₉ methanol (ultrapure grade) solution for 30 minutes, followed by brief rinsing in ultrapure methanol (Methanol Infinity Pure, Wako company-Japan) with subsequent drying in a room temperature stream of pure N₂ extracted from liquid N₂. Annealing of samples presented in this chapter was carried out at 200°C for 20 minutes under high vacuum. Annealing was applied to remove PPh₃ ligands and was performed in a similar way to our previous work.²³⁻²⁴

SCANNING TUNNELING MICROSCOPY

We performed STM measurements on the same samples already investigated with AFM. STM observations were carried out with a constant current mode at room temperature under UHV conditions ($\sim 10^{-9}$ Pa) with electrochemically etched tungsten tips. STM stably imaged the sample surface with conditions of a tunneling current of 25 pA and sample bias voltages (Vs) of 1.5-6 V. Samples were also investigated with STM after heating to 200 °C for 20 minutes after at least 3 to 4 hours under UHV.

5.4 RESULTS AND DISCUSSION

5.4.1 AFM-OBSERVATION AND HEIGHT DISTRIBUTION OF Au₉ CLUSTERS ON TITANIA NANOSHEETS

Profiles obtained from AFM image and STEM images demonstrated a direct correlation between sample height measured with an AFM tip and signal intensity obtained via STEM using an HAADF detector.⁴⁹ In Figures 5.1a and b AFM images of nanosheets are shown and in Figure 5.1c an AFM line scan is shown. Thickness of nanosheets based on the line scan was 1.2 nm. In Figure 5.2 the STEM image of the same samples is shown. Variation of the STEM along the line indicated in Figure 5.2a is shown in Figure 5.2b. Variation in STEM intensity of 1200 units corresponds in the present case to a thickness variation of 1.2 nm.

Figures 5.3a-5.3c show AFM 3D images of the titania nanosheet before and after adsorption of Au₉ clusters and also after annealing, respectively. These 3D images are a magnified area from topographical images shown in Figure 5.4. Figures 5.3d-5.3f show AFM 3D images of titania nanosheets before and after exposure to methanol only, and after annealing, respectively. Methanol was used as solvent in the adsorption process of Au₉ clusters and so these images provide a solvent only reference of processing conditions in the absence of Au₉ clusters. It shows that surface roughness increases only marginally due to solvent exposure. It can be observed that the random distribution of spikes in Figures 5.3b and 5.3c are not seen in the image exposed only to the solvent (Figures 5.3e and 5.3f). Therefore, the spikes in Figures 5.3b and 5.3c must be attributed to Au₉ clusters.

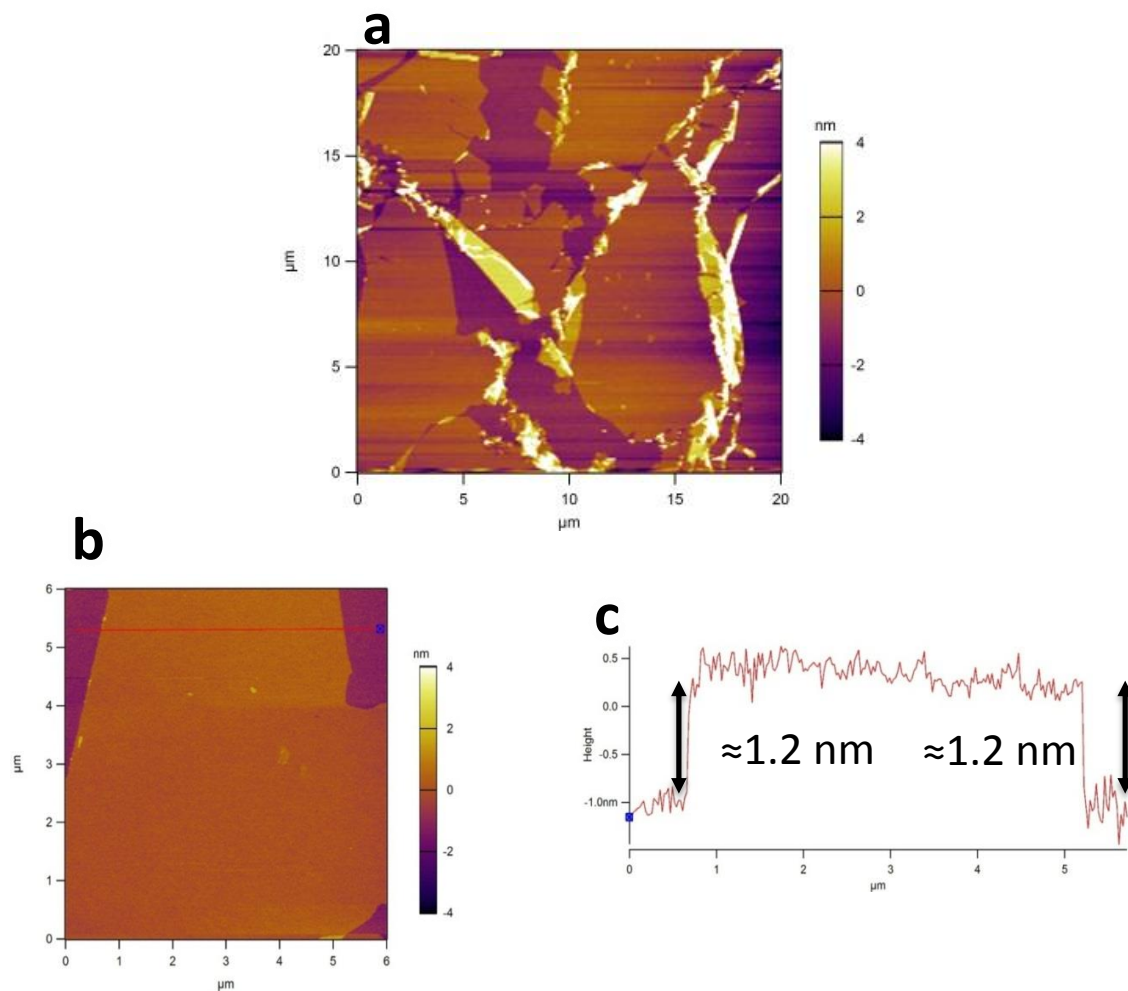


Figure 5.1: AFM topographies of (a) large image of pure titania nanosheets showing the size of nanosheet, (b) focusing on one of titania nanosheet to measure thickness. The line profile in (c) Thickness profile of the titania nanosheet (b) which is around 1.2 nm.

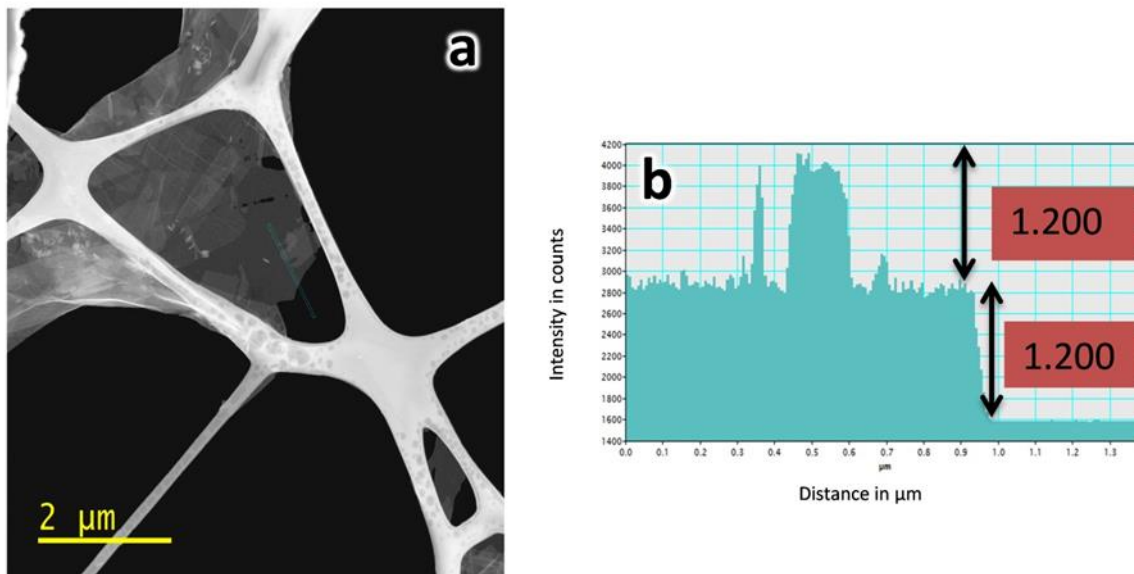


Figure 5.2: STEM image of titania nanosheet. (b) Thickness profile reconstructed along the blue line.

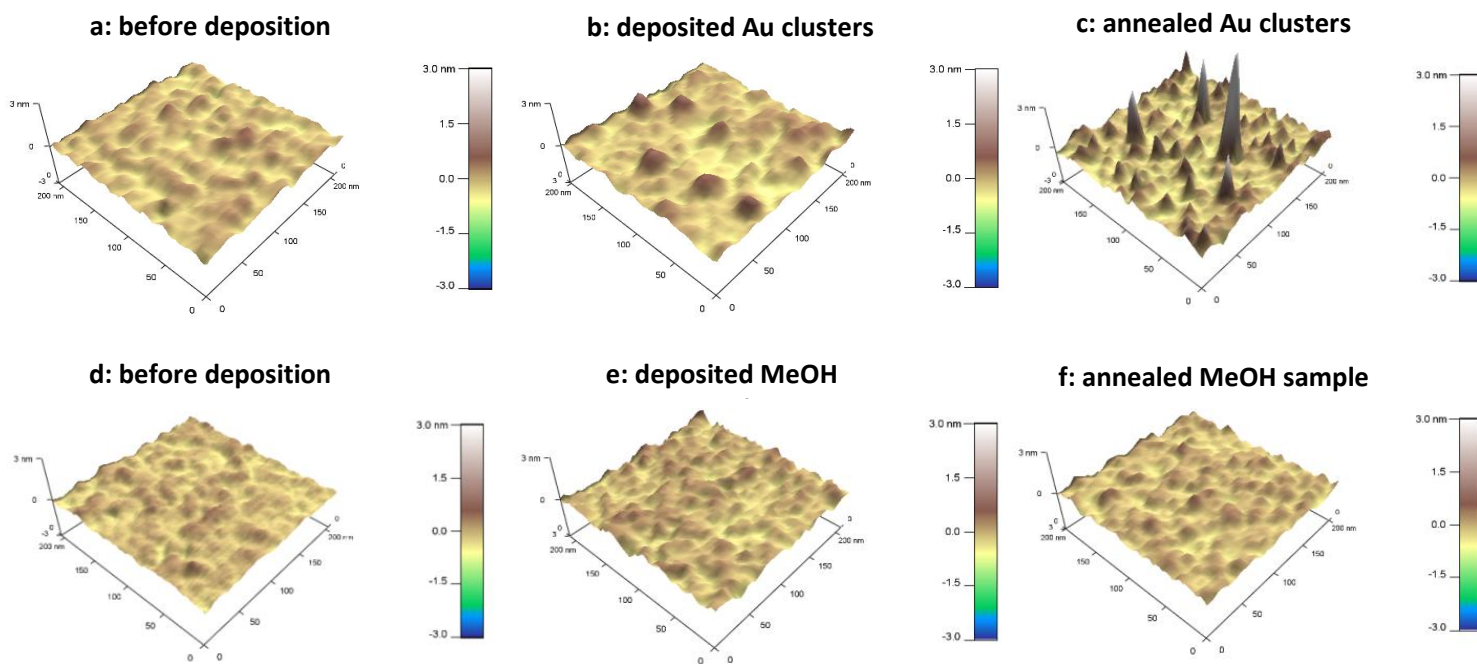


Figure 5.3: AFM 3D images of (a and d) pure titania nanosheet as, (b) after deposition of Au₉ clusters, (c) after annealing of (b), (e) titania nanosheet exposed to MeOH, and (f) after annealing of (c). Image sizes are 200 x 200nm².

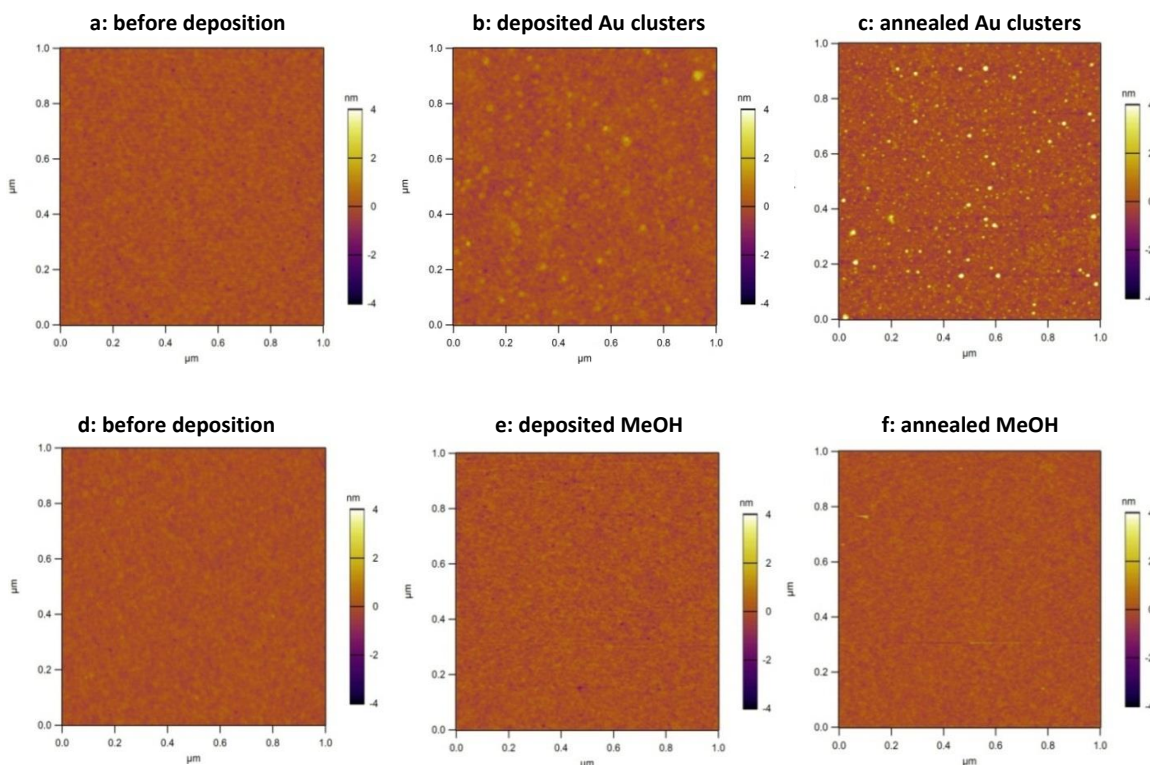


Figure 5.4: AFM topographies of (a and d) pure titania nanosheets, (b) deposited Au clusters, (c) annealed Au clusters on titania nanosheet, (e) blank sample without Au clusters, which is MeOH titania nanosheet, and (f) annealed MeOH blank sample. Image size is $1.0 \times 1.0 \mu\text{m}^2$.

AFM imaging allows for height analysis of Au NCs. Lateral resolution of features in AFM is greater than the size of one individual Au₉ cluster due to the size of AFM tip curvature and range of the interaction force between the surface and tip. Thus, AFM images cannot resolve individual clusters. Height measurement of Au₉ clusters, however, is not affected by tip curvature and can be evaluated. The resulting course of the AFM tip is illustrated in Figure 5.5. In Figure 5.5a, various possible configurations of Au₉ clusters on the titania surface are sketched. On the left a group of Au₉ clusters in close proximity are shown to form a monolayer of clusters. In the centre image a group of Au₉ clusters in close proximity are shown forming a double layer of clusters. Such layering is certainly not limited to mono- or double layers. On the right a single cluster on the titania surface is illustrated. AFM tip scanning over each of the three groups is indicated by the green line. Only the height of

groups or single cluster can be identified. Thus, the left and right case appears similar in the AFM image. The possible scenarios after annealing are sketched in Figure 5.5b. Au₉ clusters have lost ligands and formed groups or individual clusters formed by the cluster core only. The same as before heating, the AFM tip can only identify groups and not individual clusters.

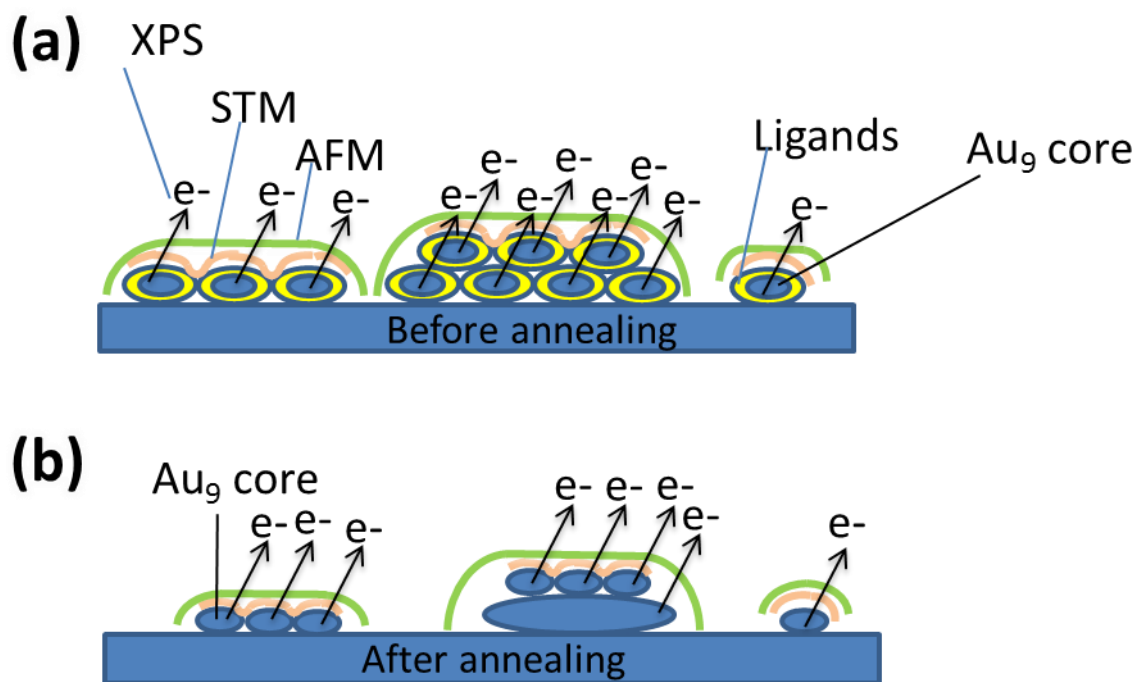


Figure 5.5: Schematic illustration of gold clusters deposited on titania nanosheet: a) before annealing and b) after annealing. The green and orange lines represent results obtained from AFM and STM, respectively. The lines indicating emission of electrons represent XPS results.

Cluster heights were evaluated from AFM images using the particle analysis tool of Asylum software. For evaluating AFM images, a large number of features in AFM images were analysed and height of features shown as statistical distribution. Substrate roughness was taken into account for this procedure to differentiate features related to Au₉ clusters. It was found that the vast majority of features in AFM images of bare titania nanosheets with and without exposure to the solvent were less than 0.5 nm in height. Thus, all features in AFM images of titania nanosheets with adsorbed Au₉ clusters less than 0.5 nm in height were not

considered in statistical analysis. Au₉ clusters are larger than 0.5 nm in diameter⁵⁰ and thus discrimination of 0.5 nm in height analysis did not exclude Au₉ clusters in the evaluation procedure. In Figures 5.6a and 5.6b, height distributions of features identified as Au₉ clusters on titania nanosheets before and after annealing are shown. The fraction of features found for a given height interval were calculated by:

$$fraction_i = \frac{N_i}{\sum_i N_i} ,$$

where $fraction_i$ is the percentage of features found in a given height interval and N_i is the number of features found in a given height interval.

Both graphs (Figures 5.6a and 5.6b) show one clear peak in height distribution. Both distributions are fitted with lognormal distributions using the Levenberg–Marquardt algorithm. Previous studies have shown that particle size distributions can be well approximated by lognormal distribution.⁵¹⁻⁵³ Fitted distributions show a mean height of 0.75 ± 0.2 nm for non-annealed samples and 1.0 ± 0.4 nm for samples subjected to annealing. The distribution of features on annealed samples become broader and the maximum shifted to a larger value. For interpretation of these results, a few aspects must first be considered. Based on DFT calculation of isolated Au₉ clusters, the longest distance across the cluster including PPh₃ ligands was 1.75 nm.¹¹ However, overall shape of the Au₉ cluster is best described as oblate spheroid and mean cluster axes have lengths of 1.75, 1.66 and 1.47 nm. It is likely that clusters orient on the surface such that the longest mean axis (1.75 nm) orients parallel to the surface because this would lead to closest contact and strongest interaction between cluster and substrate. Experimentally, the average height of Au₉ clusters of non-annealed samples is smaller than calculated height. The reason for this discrepancy could be due to the deformation of the Au₉ clusters when adsorbing onto the surface due to the

CHAPTER 5

interaction between the clusters and the surface. Such interaction would lead to a closer contact which could reduce the height of the adsorbed cluster. A second reason could be that Au₉ clusters lose some ligands during the deposition process decreasing their average size. Au₉ clusters after ligand removal show a calculated size of about 0.5 nm which is twice the average distance between two Au atoms forming a cluster.⁵⁴ These calculations of Au cluster size do not take into account that clusters could change shape after deposition. In addition, the peak-to-peak lateral distance in the titania surface roughness is much smaller than the height of clusters. Therefore, we took the top line of the surface roughness as the baseline for determining the heights used for the histogram evaluation. If there are concavities, which are closer to the cluster size, then Au clusters could hide on these cavities. Subsequently, the height of the clusters would be reduced and the respective feature appear at a lower height or even be left out in the evaluation. This has to be considered as an uncertainty in the data evaluation.

After annealing, AFM images show that small clusters are still present on the surface but their number has decreased. The percentage of small clusters dropped to about half of the fraction of the non-annealed sample and the fraction of features with a larger height increased. The change in distribution was interpreted as agglomeration of smaller clusters to form larger clusters or particles. The reason for this result is likely that cluster cores aggregated or Ostwald ripening occurred.⁵⁵ In addition, there is a possibility of diffusion or tip-induced motion of clusters, which will be discussed, in the next main chapter.

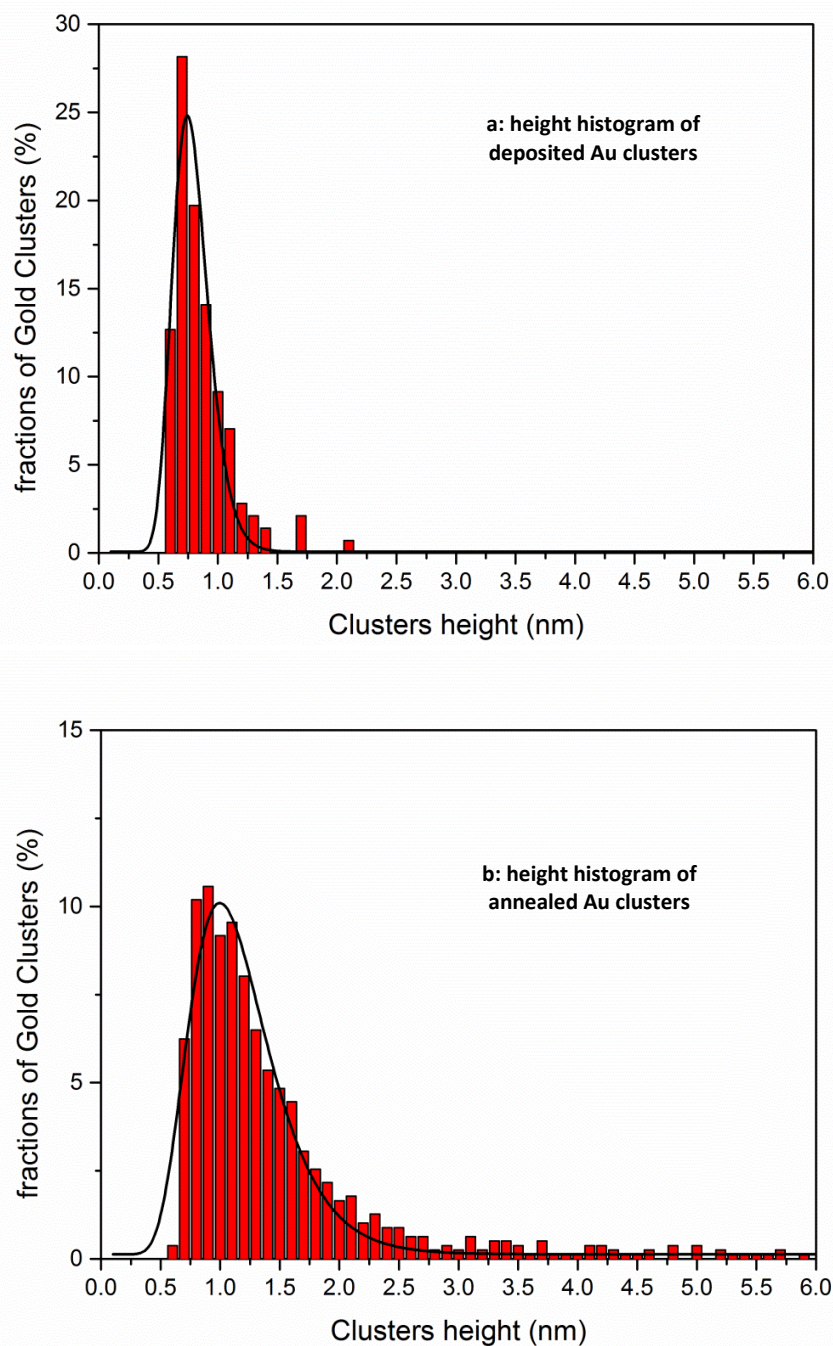


Figure 5.6: Height distribution of features in the AFM images: (a) as deposited Au clusters, and (b) after annealing to 200 °C. Cluster mean height before annealing is 0.75 ± 0.2 nm while after annealing it is 1.0 ± 0.4 nm.

5.4.2 STM-OBSERVATION AND WIDTH DISTRIBUTION OF Au₉ CLUSTERS ON TITANIA NANOSHEETS

STM imaging of samples was performed at different bias voltages from ± 1.5 V to ± 6 V. Small Au NCs deposited on titania surfaces are known to be weakly bound to TiO₂ and are therefore easily moved by the STM tip.⁵⁶ Consequently, individual clusters may not be observed in STM as they may have been swept away in the scanning process. At the expense of resolution, images for this study were typically acquired at very low tunnelling current (\sim pA) to ensure adequate tip-surface separation. We measured STM images of annealed samples at a large bias voltage (i.e. -6.0V) to show a clear image of Au NCs sited next to each other as a group (Figure 5.7).

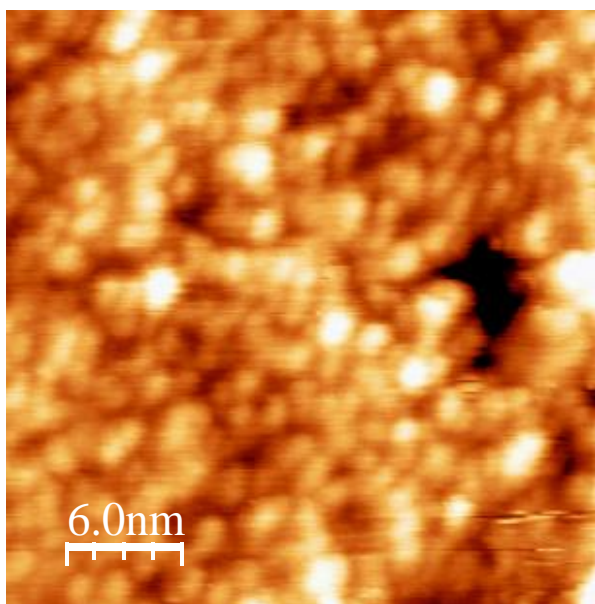


Figure 5.7: STM images of annealed Au₉ clusters on titania nanosheets measured at higher gap voltage (20pA, -6V). Scan size is 30 x 30 nm².

CHAPTER 5

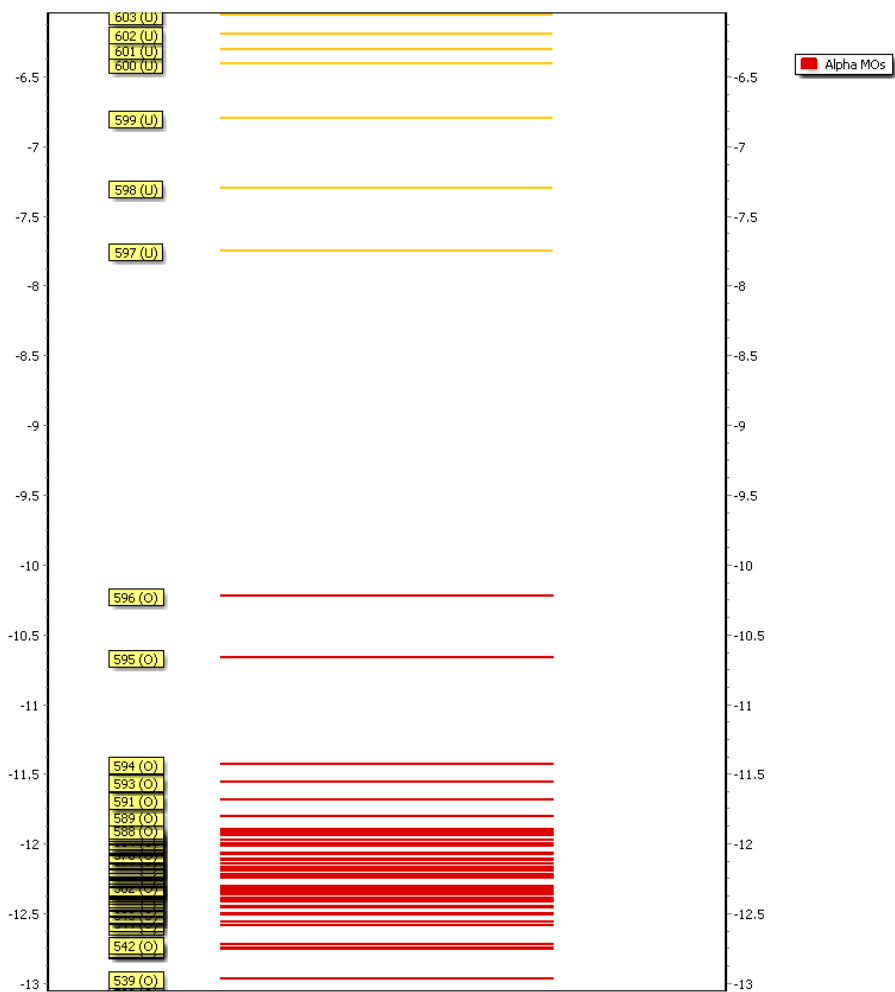
Figure 5.8a shows energy levels of ligated Au₉ before heating, while Figure 5.8b shows the Au₉ cluster core without ligands (corresponding to Au₉ clusters after removing ligands through heating). These isomers have been observed as preferable configurations for deposited Au₉ clusters on titania nanosheet.¹² Molecular orbital visualisations in Figure 5.8a show that the ligands were not electronically transparent to STM at the chosen bias voltages, thus electrons could tunnel into the respective energy levels. In estimating whether electrons could tunnel into specific orbitals of clusters it is important to note that energy of molecular orbitals of a cluster are broadened owing to interaction with the adjacent cluster or substrate. At room temperature, molecular orbitals within an energy range of 0.5 to 1 eV overlap due to energetic broadening of each orbital. Therefore, we consider in Figure 5.8 that, along with a single molecular orbital (i.e. the LUMO), combinations of orbitals can be accessed (i.e. LUMO, LUMO+1 and LUMO+2). It is shown below that in all STM images Au clusters appear approximately hemispherically shaped before and after heating. This implies that electrons tunnel into a range of orbitals and not one specific orbital.

Figures 5.9a and 5.9c show STM images of titania nanosheets with deposited Au₉ clusters before heating. STM images of blank samples, i.e. UV-irradiated nanosheets and MeOH-treated nanosheets on the Si wafer, before and after annealing process are shown in Figure 5.10. A black arrow in Figure 5.9c indicates an example of hemispherically shaped features not observed in the blank sample before heating (Figure 5.10c). Statistical distribution of height and width of features in STM images are shown in Figure 5.11. In statistical analysis we only considered features which were approximately symmetric spots (typical examples are shown as open blue circles in Figure 5.9) to measure width and height, and excluded asymmetric spots as these could be drifting clusters. Width distribution of Au NCs before heating varied from 2 nm to 3 nm with an average of 2.4 ± 0.4 nm (Figure 5.11a). Height distribution varied from 0.2 nm to 0.7 nm with an average of 0.5 ± 0.2 nm (Figure 5.11c).

CHAPTER 5

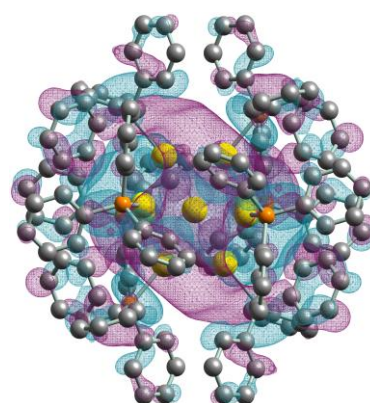
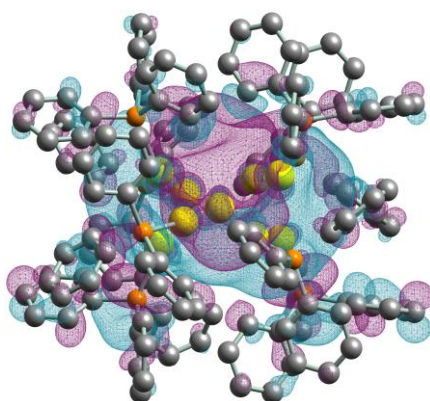
Based on the width of bright hemispherical features, these were considered individual Au₉ clusters (Figure 5.9c). However, the average height of features was smaller than the theoretical height of Au₉ clusters. We assume that the reason for this finding is that during the scanning process the STM tip did not make contact with the layer underlying Au₉ clusters, thus the height variation found in STM images was less than the height of individual clusters. The interpretation of STM images in Figure 5.5a shows an orange line to illustrate that the STM tip did not reach the titania substrate. However, lateral resolution was better than in AFM and individual Au₉ clusters were identified.

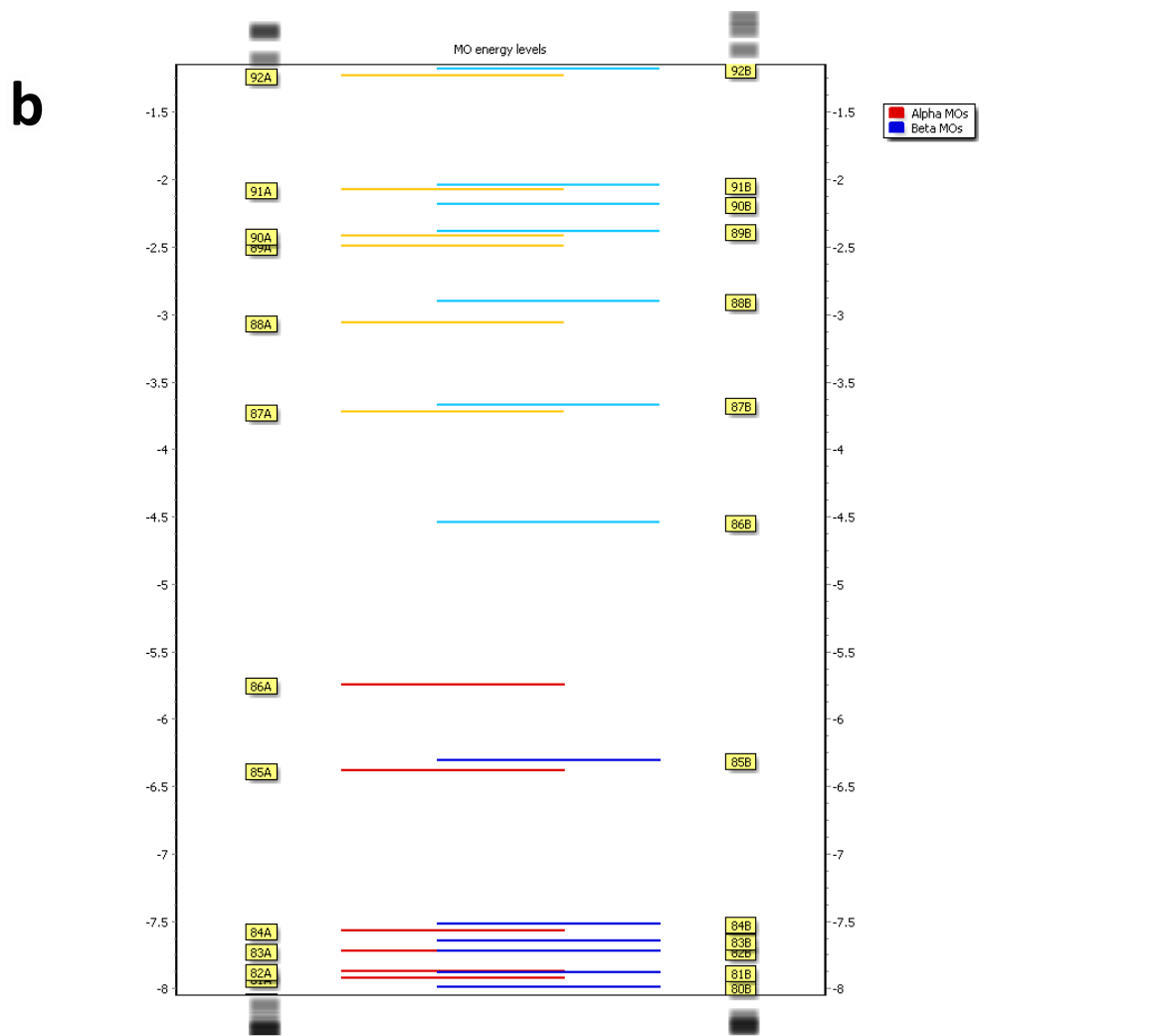
a



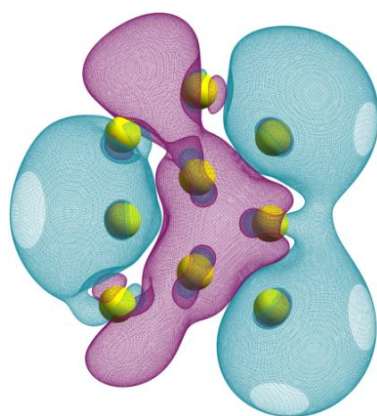
LUMO + (LUMO+1), Contour Value 0.01

LUMO + (LUMO+1) + (LUMO + 2), Contour Value





[(Alpha LUMO 87 + Beta LUMO 87) + (Alpha LUMO 88 + Beta LUMO 88)]/2, Contour Value 0.01



[(Alpha LUMO 87 + Beta LUMO 87) + (Alpha LUMO 88 + Beta LUMO 88) + (Alpha LUMO 89 + Beta LUMO 90)]/2, Contour Value 0.02

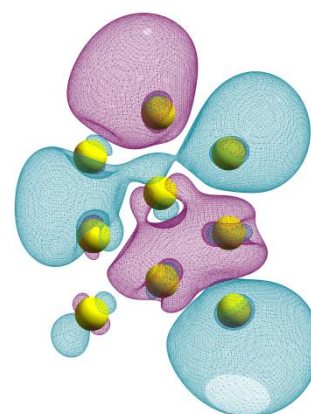


Figure 5.8: Energy levels of (a) ligands Au₉ before heating and (b) naked gold clusters after heating. The molecular orbital visualisations of combined molecular orbitals (LUMO, LUMO+1) and (LUMO, LUMO+1, LUMO+2) are also shown in this figure.

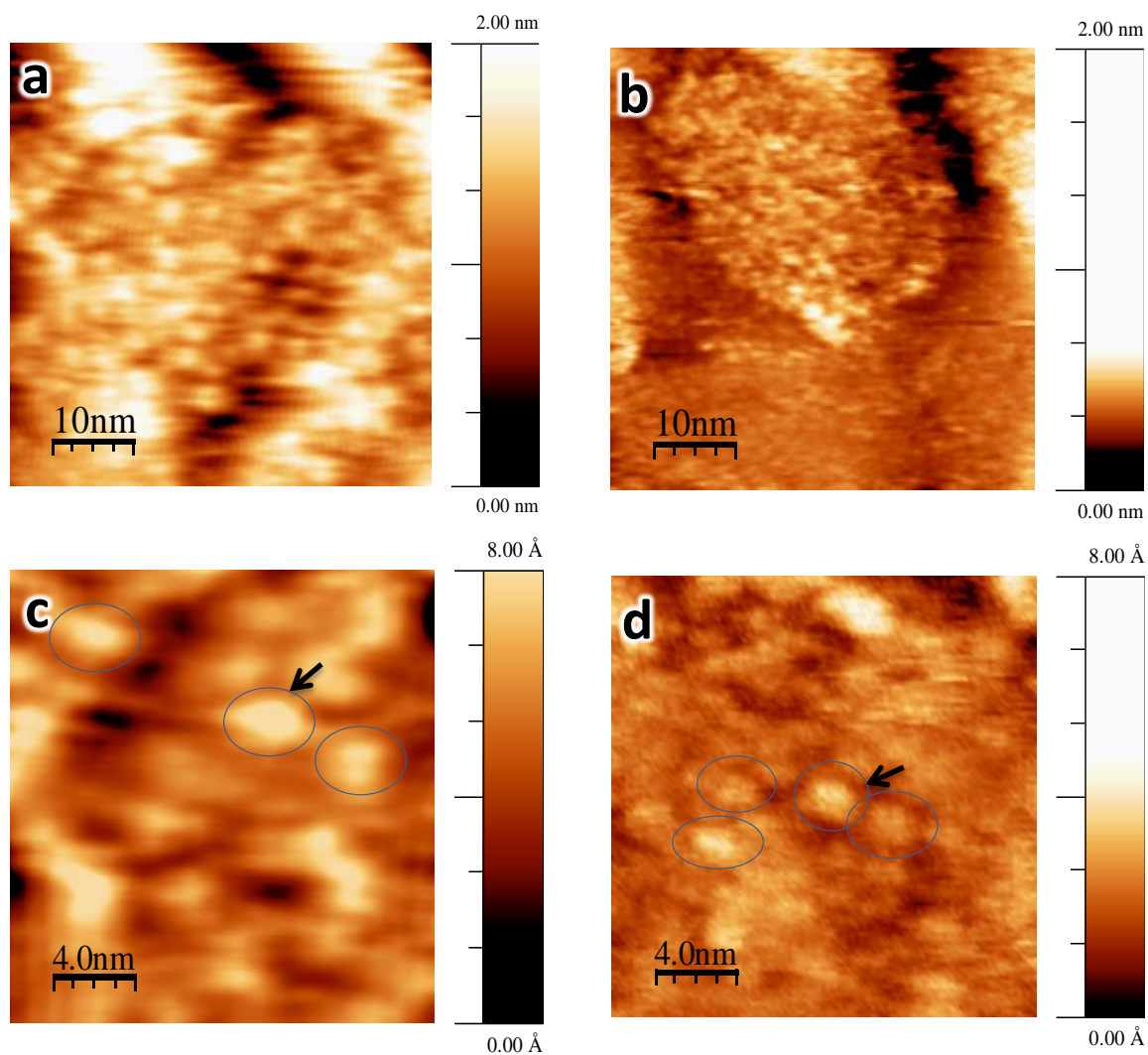


Figure 5.9: STM images of Au₉ clusters deposited on titania nanosheets: (a) as-deposited, (b) after annealing to 200 °C. Images (c) and (d) are magnifications of (a) and (b). Image size is 50 x 50 nm² for a and b and 20 x 20 nm² for c and d. STM operation conditions were (a) +1.5V, 20pA; (b) +2.0V, 18pA; (c) +1.5V, 20pA; (d) +2.5V, 25pA. Heights and widths of clusters surrounded by open blue circles were used for histogram analysis (Fig. 5.11).

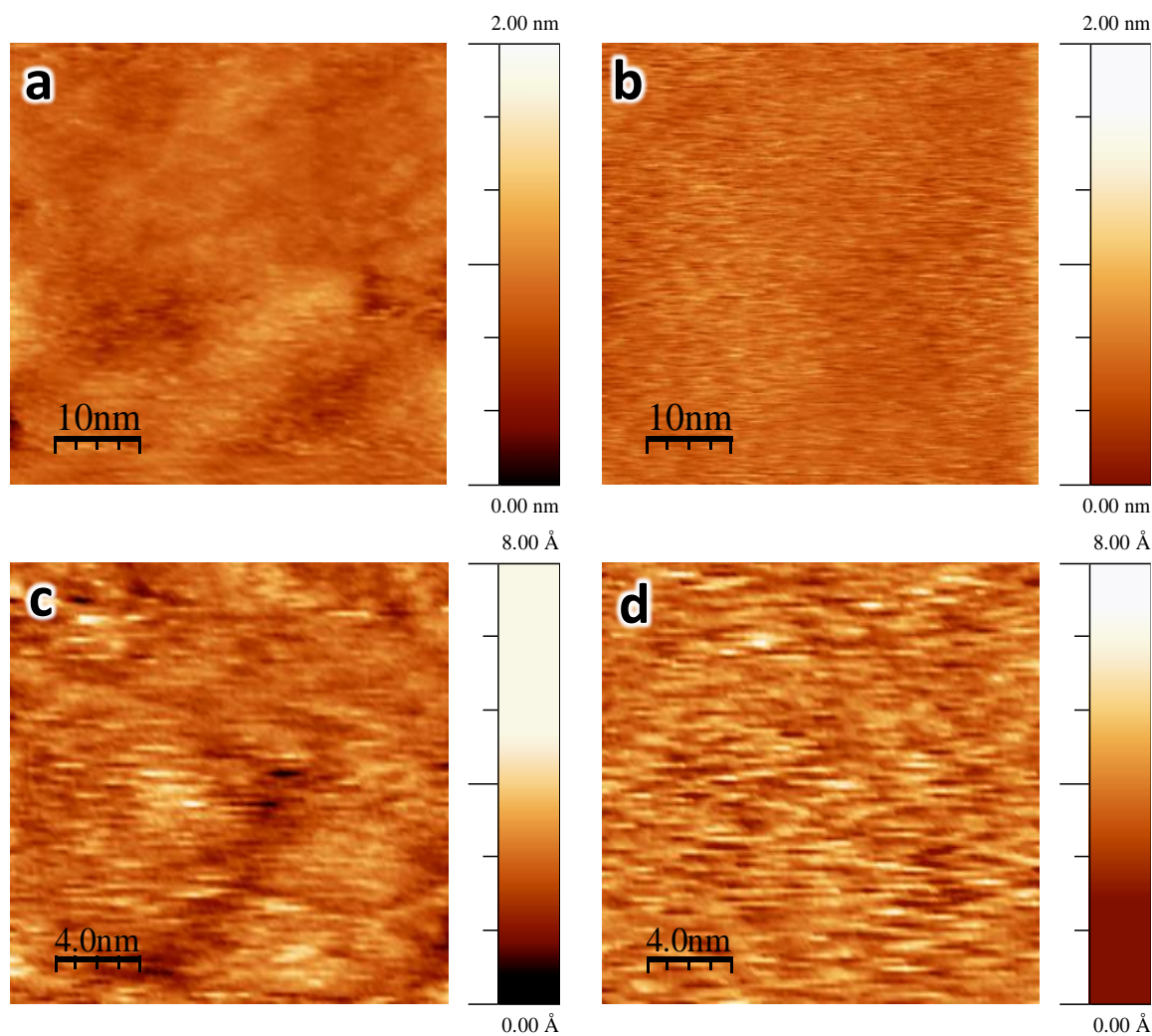


Figure 5.10: STM images of (a) MeOH titania nanosheet, (b) annealed MeOH titania nanosheet, (c) Zommed- MeOH titania nanosheet, and (d) Zommed-annealed MeOH blank sample. Image size is $50 \times 50 \text{ nm}^2$ for a and b, while $20 \times 20 \text{ nm}^2$ for c and d. a: +2.0V, 25pA; b: +2.5V, 20pA; c: +2.5V, 25pA; d: +2.5V, 20pA.

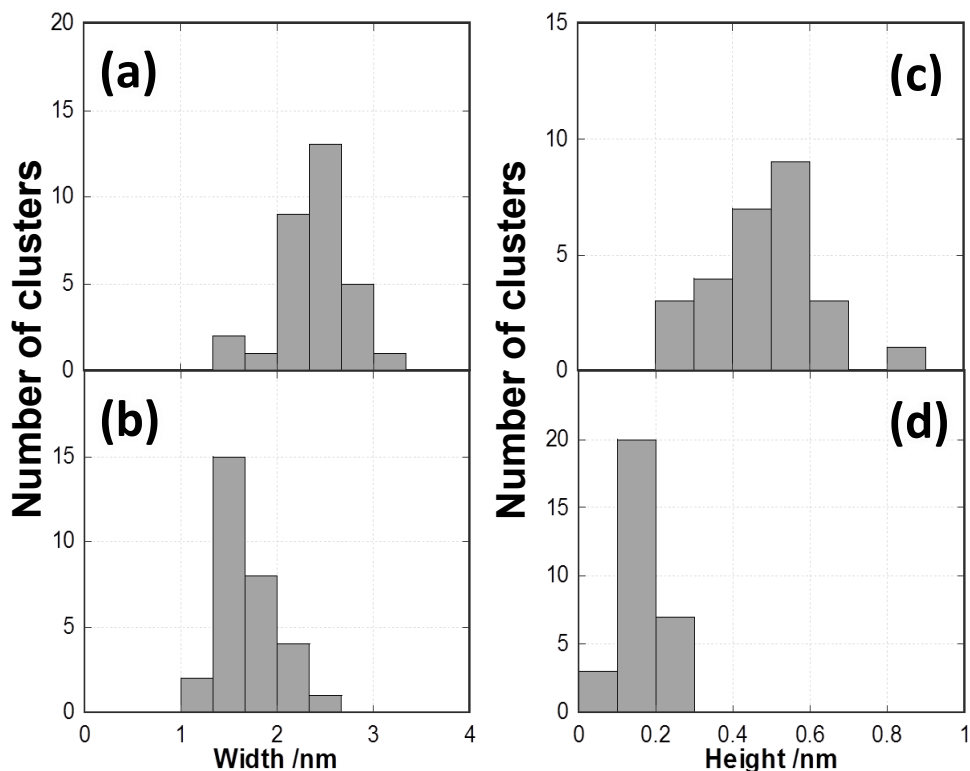


Figure 5.11: Histogram of features in STM images attributed to Au clusters. Width is shown in (a) for as-deposited samples and (b) after annealing. Height is shown in (c) for as-deposited samples and (d) after annealing.

After annealing at 200 °C for 20 minutes under UHV, STM measurements were repeated for the same sample. Figures 5.9b and 5.9d show STM images of annealed Au clusters. Brighter spots were identified in the same way as for non-annealed samples (Figure 5.9a and 5.9c). A black arrow in Figure 5.9d indicates an individual Au NC. Bright spots were not observed in the heated blank sample (Figure 5.10d). In Figures 5.11b and 5.11d the width and height distribution of features after annealing of samples are shown. In comparison with non-annealed samples, width distribution decreased to 1.3 - 2.3 nm with an average of 1.7 ± 0.3 nm, and height distribution decreased to 0.1 - 0.2 nm with an average 0.17 ± 0.05 nm. The significant decrease in cluster width is compatible with the assumption that ligands were removed through the annealing process, while height was less than what is expected from

the cluster core. However, it is important to note that the 2D cluster reported in our previous paper should have much smaller height of around 0.2 nm^{12} , in good agreement with the measured height in this work. The scanning process of the STM tip is illustrated in Figure 5.5b. As for non-heated samples, the STM tip did not reach to the layer underlying the top Au₉ layer, thus height variation is less than the height of an individual cluster core.

5.4.3 XPS RESULTS OF AU₉ CLUSTERS ON TITANIA NANOSHEET

High resolution XPS spectra of Au clusters deposited on titania nanosheet have been measured for the Au 4f, P 2p, Si 2p, Ti 2p, C 1s and O 1s regions. In the present work, we focused on Au 4f and P 2p peaks. The main C 1s peak was assigned to 285 eV and used to calibrate peak position for all other elements. Au showed the Au 4f doublet with Au 4f_{7/2} peak at 84.8 eV (Figure 5.12a) for the non-heated sample and was close to the binding energy found for as-deposited, non-agglomerated Au₉ clusters.^{9, 23-24} The binding energy of bulk Au was $84 \pm 0.2 \text{ eV}$. The difference in Au 4f_{7/2} peak position between bulk Au and isolated Au₉ clusters was attributed to the final state effect found for isolated Au₉ clusters, as described in detail in our previous work.²³⁻²⁴ The Au spectrum of the annealed titania nanosheet/Au₉ sample in Figure 5.12b shows two Au 4f doublets; a narrow peak at 83.8 eV consistent with the value for bulk Au. The decrease in binding energy from 84.8 to 83.8 eV was attributed to aggregated particles larger than Au₉ clusters due to the heating procedure. Binding energy of Au NCs with 101 atoms were found at $\sim 84 \text{ eV}$, similar to Au bulk.²⁴ The second, broader Au 4f_{7/2} peak was found at higher binding energy (85.3 eV). This peak was attributed to non-agglomerated Au₉ clusters that lost ligands and were in close contact with the titania substrate.^{24, 57} The P 2p_{3/2} peak was found at 131.6 eV and was attributed to ligands attached to Au NCs (Figure 5.12c). After annealing, no P signal was found which means that the ligands detached from the Au₉ cluster core through the heating procedure and left the sample.

CHAPTER 5

Titanium signal $2p_{3/2}$ was found at 459 eV for all samples (Figure 5.13). There was a small shoulder at 457.5 eV in the Ti spectra owing to the presence of reduced titania surfaces (Ti^{3+}) as an effect of UV irradiation inducing O vacancy in the titania nanosheet.^{8, 43, 58} After vacuum annealing the Ti^{3+} peak increased due to an increase in the number of defects.

Interpretation of XPS results for non-annealed samples is illustrated in Figure 5.5. It is important to note that the electron mean free path of samples investigated here was about 1.5 nm, thus information depth is around 4 to 5 nm. Irrespective of whether clusters form larger groups of Au_9 clusters or are isolated on the surface, each individual cluster has its own cluster core and the emission of electrons from a given cluster is influenced by the final state effect, as illustrated in Figure 5.5a. Thus, all Au_9 clusters appear as individual and isolated clusters irrespective whether another Au_9 cluster is located in close proximity or not. After removing the ligands through annealing, the clusters formed groups in which the cluster core either merged into a larger particle, like the larger block in the middle of Figure 5.5b, or formed groups with individual clusters in close proximity but cluster cores retained as individual clusters. The latter option is illustrated on the right and left in Figure 5.5b, and the top layer in the centre of the figure.

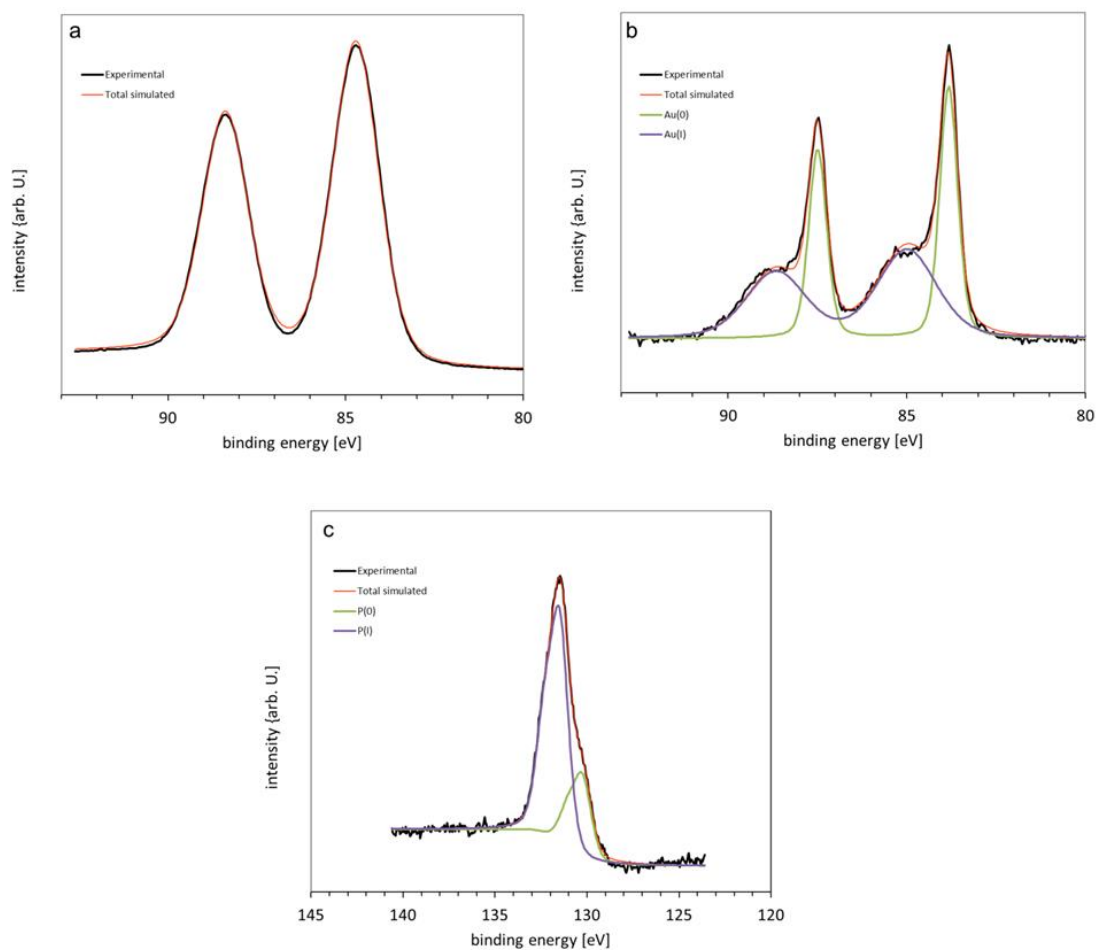


Figure 5.12: XPS of $[Au_9(PPh_3)_8](NO_3)_3$ clusters on titania nanosheet (a) 4f Au spectrum of as-deposited samples, (b) after annealing and (c) the 2p P peak of as-deposited samples.

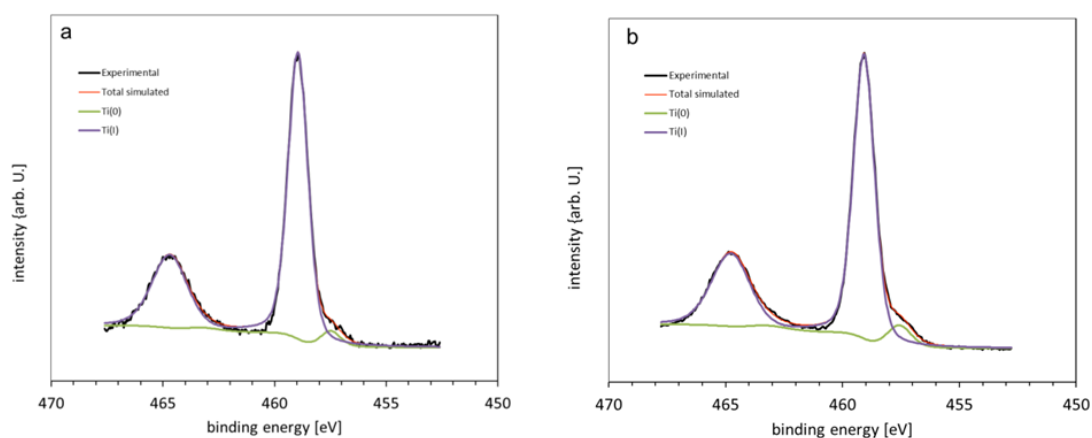


Figure 5.13: XPS peak position of $[Au_9(PPh_3)_8](NO_3)_3$ clusters on titania nanosheet (a) 2p Ti peak as-deposited and (b) 2p Ti peak as-annealed related to titania nanosheet.

5.4.4 INTEGRATING AFM, STM AND XPS RESULTS

AFM, STM and XPS measurements reveal complementary information about properties of Au₉ clusters deposited onto titania nanosheet which can be integrated into a single interpretation (schematically illustrated in Figure 5.5). AFM measurements allowed height analysis of features attributed to Au₉ clusters. Before heating the majority of features in AFM images showed a height corresponding to the smallest diameter of individual Au₉ clusters. Identifying individual Au NCs was not possible with AFM due to large tip curvature and large interaction range between the AFM tip and the sample. After annealing of samples, Au₉ clusters lost the PPh₃ ligands. Cluster cores either retained their identity as Au₉ clusters cores or merged into larger particles (schematically illustrated in Figure 5.5b). AFM measurements show that partial agglomeration occurred leading to an increase of feature heights. However, a significant number of features retained the height of single clusters.

The STM measurement is affected by the potential applied to the tip. Thus, STM is measuring the electronic state not a real height of gold clusters. STM was used to investigate small areas of a few nanometres in size with high lateral resolution sufficient to resolve individual Au NCs. Before annealing, STM images were used to identify individual Au₉ clusters, even when they form groups of clusters within close proximity to each other. In contrast to AFM, it is very difficult to determine the total height of a group of clusters using STM. Due to the complexity of the sample including the Si, SiO₂, TiO₂, ligands and gold core systems, it is hard to identify the specific electronic states that the electron tunneling from the tip to sample in STM measurements. In addition, we could not find a single gold cluster during our STM measurements. They may have been swept away in the scanning process. Therefore, there is a difficulty to find approximate height for the individual gold cluster separately and not in groups. After annealing of samples, STM results cannot be used

CHAPTER 5

to derive information about overall size of groups formed by clusters, but do provide information about the fine structure of the top layer of a group. Thus, STM results allowed identification of individual clusters. STM did not lead to a conclusion regarding whether individual clusters in the top layer merged electronically or retained their individual structure.

Based on the final state effect found in XPS results, it was concluded that the Au₉ clusters before annealing are individual and separate clusters. After annealing of samples, XPS showed that at least a fraction of Au₉ clusters retained their individual electronic structure and did not merge to form a bulk electronic structure. This conclusion is based on the XPS Au 4f_{7/2} eV peak found at 85.3 eV which can only be due to small clusters. STM also cannot be used to reveal information about the layer below the top Au cluster layer. The layer below could be substrate, or a layer of agglomerated Au clusters (as sketched in the centre section of Figure 5.5b), or could be individual Au clusters. The layer below the top layer could be formed by agglomerated clusters which may explain the XPS Au 4f_{7/2} eV peak found at 83.8 eV which is related to larger Au particles. In this context, it is important to note that the information depth of XPS is much larger than that of STM.

In our previous study, we investigated deposition of Au₉ clusters onto plasma treated ALD titania.¹⁰ The coverage of ALD titania with Au in¹⁰ was approximately 40 times lower than in the present case (Au/Ti ratio in¹⁰ below 0.1 and Au/Ti ratio 3.5 here). We assume that the higher coverage of the titania nanosheet surface with non-agglomerated Au₉ clusters is due to a larger number of defects induced compared to ALD titania.

5.5 CONCLUSION

Au₉ clusters deposited on titania nanosheets were investigated with AFM, STM and XPS techniques. Each method allowed determination of specific information about the structure of Au₉ clusters before and after annealing which was integrated into an overall interpretation of the Au₉/titania surface. After deposition, Au₉ clusters attached to the surface in a range of configurations from individual clusters to groups of clusters. All clusters retained their individual electronic structure. Heating of samples to 200 °C lead to partial agglomeration of Au NCs and the formation of larger Au particles. However, some clusters were not involved in agglomeration and were left as individual isolated clusters on the surface. The electronic structure of agglomerated Au particles was different to that of isolated individual clusters. Agglomeration did not necessarily include all clusters within a group. At least in the top layer of these groups, individual clusters that most likely retained the electronic structure of individual clusters were identified.

5.6 REFERENCES

1. Imaoka, T.; Kitazawa, H.; Chun, W.-J.; Omura, S.; Albrecht, K.; Yamamoto, K., Magic Number Pt₁₃ and Misshapen Pt₁₂ Clusters: Which One is the Better Catalyst? *Journal of the American Chemical Society* **2013**, *135* (35), 13089-13095.
2. Baletto, F.; Ferrando, R., Structural properties of nanoclusters: Energetic, thermodynamic, and kinetic effects. *Reviews of Modern Physics* **2005**, *77* (1), 371-423.
3. de Heer, W. A., The physics of simple metal clusters: experimental aspects and simple models. *Reviews of Modern Physics* **1993**, *65* (3), 611-676.
4. Schmid, G.; Baumle, M.; Geerkens, M.; Heim, I.; Osemann, C.; Sawitowski, T., Current and future applications of nanoclusters. *Chemical Society Reviews* **1999**, *28* (3), 179-185.
5. Lewis, L. N., Chemical catalysis by colloids and clusters. *Chem. Rev. (Washington, D. C.)* **1993**, *93* (8), 2693-730.
6. Daniel, M.-C.; Astruc, D., Gold Nanoparticles: Assembly, Supramolecular Chemistry, Quantum-Size-Related Properties, and Applications toward Biology, Catalysis, and Nanotechnology. *Chemical Reviews* **2004**, *104* (1), 293-346.
7. Ferrando, R.; Jellinek, J.; Johnston, R. L., Nanoalloys: From Theory to Applications of Alloy Clusters and Nanoparticles. *Chemical Reviews* **2008**, *108* (3), 845-910.
8. Bennett, T.; Adnan, R. H.; Alvino, J. F.; Kler, R.; Golovko, V. B.; Metha, G. F.; Andersson, G. G., Effect of Gold Nanoclusters on the Production of Ti³⁺ Defect Sites in Titanium Dioxide Nanoparticles under Ultraviolet and Soft X-ray Radiation. *The Journal of Physical Chemistry C* **2015**, *119* (20), 11171-11177.

CHAPTER 5

9. Ruzicka, J.-Y.; Abu Bakar, F.; Hoeck, C.; Adnan, R.; McNicoll, C.; Kemmitt, T.; Cowie, B. C.; Metha, G. F.; Andersson, G. G.; Golovko, V. B., Toward Control of Gold Cluster Aggregation on TiO₂ via Surface Treatments. *The Journal of Physical Chemistry C* **2015**, *119* (43), 24465-24474.
10. Andersson, G. G.; Golovko, V. B.; Alvino, J. F.; Bennett, T.; Wrede, O.; Mejia, S. M.; Al Qahtani, H. S.; Adnan, R.; Gunby, N.; Anderson, D. P.; Metha, G. F., Phosphine-stabilised Au₉ clusters interacting with titania and silica surfaces: The first evidence for the density of states signature of the support-immobilised cluster. *The Journal of Chemical Physics* **2014**, *141* (1), 014702.
11. Alvino, J. F.; Bennett, T.; Anderson, D.; Donoeva, B.; Ovoshchnikov, D.; Adnan, R. H.; Appadoo, D.; Golovko, V.; Andersson, G.; Metha, G. F., Far-infrared absorption spectra of synthetically-prepared, ligated metal clusters with Au₆, Au₈, Au₉ and Au₆Pd metal cores. *RSC Advances* **2013**, *3* (44), 22140-22149.
12. Al Qahtani, H. S.; Kimoto, K.; Bennett, T.; Alvino, J. F.; Andersson, G. G.; Metha, G. F.; Golovko, V. B.; Sasaki, T.; Nakayama, T., Atomically resolved structure of ligand-protected Au₉ clusters on TiO₂ nanosheets using aberration-corrected STEM. *The Journal of Chemical Physics* **2016**, *144* (11), 114703.
13. Wang, Z. W.; Toikkanen, O.; Quinn, B. M.; Palmer, R. E., Real-Space Observation of Prolate Monolayer-Protected Au₃₈ Clusters Using Aberration-Corrected Scanning Transmission Electron Microscopy. *Small* **2011**, *7* (11), 1542-1545.
14. Batenburg, K. J.; Erni, R.; Rossell, M. D.; Van Aert, S.; Van Tendeloo, G., Three-dimensional atomic imaging of crystalline nanoparticles. *Nature* **2011**, *470*, 374+.

CHAPTER 5

15. Yoon, B.; Häkkinen, H.; Landman, U.; Wörz, A. S.; Antonietti, J.-M.; Abbet, S.; Judai, K.; Heiz, U., Charging Effects on Bonding and Catalyzed Oxidation of CO on Au₈ Clusters on MgO. *Science* **2005**, *307* (5708), 403-407.
16. Lee, D.; Donkers, R. L.; Wang, G.; Harper, A. S.; Murray, R. W., Electrochemistry and Optical Absorbance and Luminescence of Molecule-like Au₃₈ Nanoparticles. *Journal of the American Chemical Society* **2004**, *126* (19), 6193-6199.
17. Jung, J.; Kim, H.; Han, Y.-K., Can an Electron-Shell Closing Model Explain the Structure and Stability of Ligand-Stabilized Metal Clusters? *Journal of the American Chemical Society* **2011**, *133* (15), 6090-6095.
18. Ramakrishna, G.; Varnavski, O.; Kim, J.; Lee, D.; Goodson, T., Quantum-Sized Gold Clusters as Efficient Two-Photon Absorbers. *Journal of the American Chemical Society* **2008**, *130* (15), 5032-5033.
19. Valden, M.; Lai, X.; Goodman, D. W., Onset of Catalytic Activity of Gold Clusters on Titania with the Appearance of Nonmetallic Properties. *Science* **1998**, *281* (5383), 1647-1650.
20. Haruta, M., Size- and support-dependency in the catalysis of gold. *Catalysis Today* **1997**, *36* (1), 153-166.
21. Judai, K.; Abbet, S.; Wörz, A. S.; Heiz, U.; Henry, C. R., Low-Temperature Cluster Catalysis. *Journal of the American Chemical Society* **2004**, *126* (9), 2732-2737.
22. Kunz, S.; Hartl, K.; Nesselberger, M.; Schweinberger, F. F.; Kwon, G.; Hanzlik, M.; Mayrhofer, K. J. J.; Heiz, U.; Arenz, M., Size-selected clusters as heterogeneous model catalysts under applied reaction conditions. *Physical Chemistry Chemical Physics* **2010**, *12* (35), 10288-10291.

CHAPTER 5

23. Anderson, D. P.; Adnan, R. H.; Alvino, J. F.; Shipper, O.; Donoeva, B.; Ruzicka, J.-Y.; Al Qahtani, H.; Harris, H. H.; Cowie, B.; Aitken, J. B.; Golovko, V. B.; Metha, G. F.; Andersson, G. G., Chemically synthesised atomically precise gold clusters deposited and activated on titania. Part II. *Physical Chemistry Chemical Physics* **2013**, *15* (35), 14806-14813.
24. Anderson, D. P.; Alvino, J. F.; Gentleman, A.; Qahtani, H. A.; Thomsen, L.; Polson, M. I. J.; Metha, G. F.; Golovko, V. B.; Andersson, G. G., Chemically-synthesised, atomically-precise gold clusters deposited and activated on titania. *Physical Chemistry Chemical Physics* **2013**, *15* (11), 3917-3929.
25. Chen, M. S.; Goodman, D. W., Structure–activity relationships in supported Au catalysts. *Catalysis Today* **2006**, *111* (1–2), 22-33.
26. Pyykkö, P., Theoretical Chemistry of Gold. *Angewandte Chemie International Edition* **2004**, *43* (34), 4412-4456.
27. Li, X.-G.; Zhang, X. G.; Cheng, H.-P., Conformational Electroresistance and Hysteresis in Nanoclusters. *Nano Letters* **2014**, *14* (8), 4476-4479.
28. Zhu, Y.; Qian, H.; Jin, R., Catalysis opportunities of atomically precise gold nanoclusters. *Journal of Materials Chemistry* **2011**, *21* (19), 6793-6799.
29. Zhu, Y.; Qian, H.; Drake, B. A.; Jin, R., Atomically Precise Au₂₅(SR)₁₈ Nanoparticles as Catalysts for the Selective Hydrogenation of α,β -Unsaturated Ketones and Aldehydes. *Angewandte Chemie* **2010**, *122* (7), 1317-1320.
30. Liu, Y.; Tsunoyama, H.; Akita, T.; Xie, S.; Tsukuda, T., Aerobic Oxidation of Cyclohexane Catalyzed by Size-Controlled Au Clusters on Hydroxyapatite: Size Effect in the Sub-2 nm Regime. *ACS Catalysis* **2011**, *1* (1), 2-6.

CHAPTER 5

31. Haruta, M.; Tsubota, S.; Kobayashi, T.; Kageyama, H.; Genet, M. J.; Delmon, B., Low-Temperature Oxidation of CO over Gold Supported on TiO₂, α -Fe₂O₃, and Co₃O₄. *Journal of Catalysis* **1993**, *144* (1), 175-192.
32. Meyer, R.; Lemire, C.; Shaikhutdinov, S. K.; Freund, H. J., Surface chemistry of catalysis by gold. *Gold Bull* **2004**, *37* (1-2), 72-124.
33. Adnan, R. H.; Andersson, G. G.; Polson, M. I. J.; Metha, G. F.; Golovko, V. B., Factors influencing the catalytic oxidation of benzyl alcohol using supported phosphine-capped gold nanoparticles. *Catalysis Science & Technology* **2015**, *5* (2), 1323-1333.
34. Rodríguez-Zamora, P.; Yin, F.; Palmer, R. E., Enhanced Immobilization of Gold Nanoclusters on Graphite. *The Journal of Physical Chemistry A* **2014**, *118* (37), 8182-8187.
35. Chusuei, C. C.; Lai, X.; Davis, K. A.; Bowers, E. K.; Fackler, J. P.; Goodman, D. W., A Nanoscale Model Catalyst Preparation: Solution Deposition of Phosphine-Stabilized Gold Clusters onto a Planar TiO₂(110) Support. *Langmuir* **2001**, *17* (13), 4113-4117.
36. Kolmakov, A.; Goodman, D. W., Scanning tunneling microscopy of gold clusters on TiO₂(110): CO oxidation at elevated pressures. *Surface Science* **2001**, *490* (1-2), L597-L601.
37. Spiridis, N.; Haber, J.; Korecki, J., STM studies of Au nano-clusters on TiO₂(1 1 0). *Vacuum* **2001**, *63* (1-2), 99-105.
38. Tong, X.; Benz, L.; Kemper, P.; Metiu, H.; Bowers, M. T.; Buratto, S. K., Intact Size-Selected Au Clusters on a TiO₂(110)-(1 × 1) Surface at Room Temperature. *Journal of the American Chemical Society* **2005**, *127* (39), 13516-13518.

CHAPTER 5

39. Wahlström, E.; Lopez, N.; Schaub, R.; Thostrup, P.; Rønnau, A.; Africh, C.; Lægsgaard, E.; Nørskov, J. K.; Besenbacher, F., Bonding of Gold Nanoclusters to Oxygen Vacancies on Rutile *Physical Review Letters* **2003**, *90* (2), 026101.
40. Batson, P. E., Motion of Gold Atoms on Carbon in the Aberration-Corrected STEM. *Microscopy and Microanalysis* **2008**, *14* (01), 89-97.
41. Li, Z. Y.; Young, N. P.; Di Vece, M.; Palomba, S.; Palmer, R. E.; Bleloch, A. L.; Curley, B. C.; Johnston, R. L.; Jiang, J.; Yuan, J., Three-dimensional atomic-scale structure of size-selected gold nanoclusters. *Nature* **2008**, *451* (7174), 46-48.
42. Porsgaard, S.; Jiang, P.; Borondics, F.; Wendt, S.; Liu, Z.; Bluhm, H.; Besenbacher, F.; Salmeron, M., Charge State of Gold Nanoparticles Supported on Titania under Oxygen Pressure. *Angewandte Chemie International Edition* **2011**, *50* (10), 2266-2269.
43. Chen, M.; Goodman, D. W., Catalytically active gold on ordered titania supports. *Chemical Society Reviews* **2008**, *37* (9), 1860-1870.
44. Wörz, A. S.; Heiz, U.; Cinquini, F.; Pacchioni, G., Charging of Au Atoms on TiO₂ Thin Films from CO Vibrational Spectroscopy and DFT Calculations. *The Journal of Physical Chemistry B* **2005**, *109* (39), 18418-18426.
45. Diebold, U., The surface science of titanium dioxide. *Surface Science Reports* **2003**, *48* (5–8), 53-229.
46. Fujishima, A.; Zhang, X.; Tryk, D. A., TiO₂ photocatalysis and related surface phenomena. *Surface Science Reports* **2008**, *63* (12), 515-582.
47. Osada, M.; Sasaki, T., Two-Dimensional Dielectric Nanosheets: Novel Nanoelectronics From Nanocrystal Building Blocks. *Advanced Materials* **2012**, *24* (2), 210-228.

CHAPTER 5

48. Freund, H.-J.; Pacchioni, G., Oxide ultra-thin films on metals: new materials for the design of supported metal catalysts. *Chemical Society Reviews* **2008**, 37 (10), 2224-2242.
49. Rudneva, M.; Kozlova, T.; Zandbergen, H. W., The use of STEM imaging to analyze thickness variations due to electromigration-induced mass transport in thin polycrystalline nanobridges. *Ultramicroscopy* **2013**, 134, 155-159.
50. Wen, F.; Englert, U.; Gutrath, B.; Simon, U., Crystal Structure, Electrochemical and Optical Properties of [Au₉(PPh₃)₈](NO₃)₃. *European Journal of Inorganic Chemistry* **2008**, 2008 (1), 106-111.
51. Söderlund, J.; Kiss, L. B.; Niklasson, G. A.; Granqvist, C. G., Lognormal Size Distributions in Particle Growth Processes without Coagulation. *Physical Review Letters* **1998**, 80 (11), 2386-2388.
52. Granqvist, C. G.; Buhrman, R. A., Ultrafine metal particles. *Journal of Applied Physics* **1976**, 47 (5), 2200-2219.
53. Susan-Resiga, D.; Socoliuc, V.; Boros, T.; Borbáth, T.; Marinica, O.; Han, A.; Vékás, L., The influence of particle clustering on the rheological properties of highly concentrated magnetic nanofluids. *Journal of Colloid and Interface Science* **2012**, 373 (1), 110-115.
54. Bosch-Navarro, C.; Laker, Z. P. L.; Thomas, H. R.; Marsden, A. J.; Sloan, J.; Wilson, N. R.; Rourke, J. P., Covalently Binding Atomically Designed Au₉ Clusters to Chemically Modified Graphene. *Angewandte Chemie International Edition* **2015**.
55. Fukamori, Y.; König, M.; Yoon, B.; Wang, B.; Esch, F.; Heiz, U.; Landman, U., Fundamental Insight into the Substrate-Dependent Ripening of Monodisperse Clusters. *ChemCatChem* **2013**, 5 (11), 3330-3341.

CHAPTER 5

56. Kolmakov, A.; Goodman, D. W., Imaging gold clusters on TiO₂(110) at elevated pressures and temperatures. *Catalysis Letters* **2000**, *70* (3-4), 93-97.
57. Stakheev, A. Y.; Kustov, L. M., Effects of the support on the morphology and electronic properties of supported metal clusters: modern concepts and progress in 1990s. *Applied Catalysis A: General* **1999**, *188* (1-2), 3-35.
58. Ohwada, M.; Kimoto, K.; Mizoguchi, T.; Ebina, Y.; Sasaki, T., Atomic structure of titania nanosheet with vacancies. *Scientific Reports* **2013**, *3*, 2801.

CHAPTER 6

Aggregation behaviour of ligands protected Au₉ clusters on sputtered ALD TiO₂

This chapter is a reformatted version of the manuscript planned to submit to *ACS Applied
Materials & Interfaces*

6.1 ABSTRACT

[Au₉ (PPh₃)₈] (NO₃) (Au₉) clusters were deposited onto sputtered atomic layer deposition (ALD) titania surfaces. Atomic force microscopy (AFM) was used to determine height and distributions of Au₉ clusters over the ALD titania surface. Synchrotron x-ray photoelectron spectroscopy (XPS) was used to derive information about the degree of agglomeration of Au₉ clusters due to the annealing process. Both AFM and XPS showed that Au₉ clusters deposited on titania were partially agglomerated after annealing. The sputtering pre-deposition method makes the ALD titania a rich surface for attaching Au clusters.

6.2 INTRODUCTION

Gold nanoparticles (Au NPs) are of interest for modifying surfaces to tailor surface properties to specific functionalities by adsorbing nanoparticles.¹⁻⁹ Nanoparticles modify surfaces due to their specific chemical composition and crystal structure. Gold nanoclusters (Au NCs) are smaller in size than Au NPs and are also used to modify surface properties. In contrast to NPs, for NCs it is not the crystal structure but geometric fluxionality and size dependence of the electronic structure which is important for surface modification.¹⁰⁻²⁷ Au NCs form specific atomic structures depending on the number of atoms, while Au NPs typically adopt a face-centered cubic (fcc) structure.^{18, 28} NCs have discrete electron energy levels like molecules, while NPs have a continuous electronic energy band structure similar to bulk Au.²⁹⁻³⁰ For this reason, the number of atoms forming an Au NC strongly influences the properties of NC modified surfaces.³¹⁻³⁵ One example is the catalytic properties of surfaces modified with Au NCs which are directly dependent on the size, morphology and electronic structure of Au NCs.³⁶⁻⁴⁹ The catalytic properties of cluster modified surfaces change with the size of Au NCs and the size of NCs needs to be preserved for retaining specific surface properties. Agglomeration of NCs leads to an increase in NC size or formation of NPs and should be avoided. Thus, it is important to understand the conditions which lead to agglomeration of NCs deposited on surfaces.

Au NCs can be prepared and deposited onto surfaces from the gas phase under UHV conditions^{37, 50-52} or from the liquid phase when using chemical synthesis processes.^{29, 35, 53-58} Compared with the gas phase method, chemical methods have the benefit of easy scale-up. The series of chemically synthesised precise Au NCs, formulated as $\text{Au}_n(\text{PPh}_3)_m$ where n and m represent the respective number of Au atoms and triphenylphosphine ligands, deposited on titania surfaces were discussed in our previous publications.⁵⁴⁻⁵⁵ The cluster

core size of this phosphine-coordinated Au NCs family is well defined⁵⁹⁻⁶² and has been shown to exhibit clearly distinguishable properties depending on cluster size.^{54-57, 60, 63} The binding peak position of Au is influenced by the size of clusters through the final state effect and has been used to identify the size of metal clusters.^{29, 50, 54-55, 64-65} When depositing NCs onto surfaces it is important to understand whether or not clusters agglomerate during the deposition process, the conditions that lead to agglomeration and how electronic and geometric properties of clusters change during deposition.

The characterisation of electronic and geometrical properties of Au NCs deposited on surfaces requires a combination of different surface science techniques, each providing specific information and complementing information obtained through other techniques. In this work, a combination of microscopic and spectroscopic techniques were applied to investigate $[\text{Au}_9(\text{PPh}_3)_8](\text{NO}_3)_3$ clusters (abbreviated as Au_9) deposited on ALD titania to determine agglomeration of Au_9 clusters after deposition. AFM allowed imaging to determine cluster size distribution of Au NCs and dispersion over titania surfaces. XPS was used to analyse the chemical state and electronic structure of Au NCs deposited onto titania. Samples were investigated before and after heat treatment to 200 °C. The focus of the present work is on change in size of clusters after heat treatment for removing protective phosphine ligands.

6.3 EXPERIMENTAL

ALD titania were immersed for 30 minutes in Au_9 methanol solution with concentrations between 0.02 and 0.0002 mM, then rinsed briefly in ultrapure methanol (Methanol Infinity Pure, Wako company-Japan) and subsequently dried under N_2 . This deposition method lead to homogenous distribution of ligand protected Au NCs on silica surfaces.⁶⁶

CHAPTER 6

ALD titania were treated prior to Au₉ deposition by magnetron sputtering for 0.5 min with Ar-ions to create defect sites for adsorbing of Au₉. Magnetron sputtering was operated at 3V and 1.3×10^{-4} mbar argon partial pressure with sputtering current at 45 mA. 1 monolayer is $\sim 5 - 10 \times 10^{14}$ atoms/cm². Thus a current of 10^{14} Ar⁺ ions/cm² will sputter about 1 monolayer (preferential sputtering⁶⁷). We had a current of 10^{-4} A which will sputter less than monolayer. A monolayer is approximately 0.2 nm in thickness. In the next step, protecting ligands were removed by heating ALD titania substrates covered with Au₉. Heat treatment was applied at 200 °C for 20 minutes under high vacuum (10^{-4} mbar).

Treatment of the ALD surface with sulphuric acid was also attempted because it had been previously identified that acidic treatment of titania results in a lower degree of agglomeration of Au NCs on titania surfaces during the annealing process,⁵⁵ compared to samples where the titania substrate was not pre-treated prior to Au cluster deposition.⁵⁴ However, the resulting surface roughness of ALD titania after acidic treatment was in the order of the size of Au₉ clusters (Figure 6.1). Thus, identifying Au₉ clusters on acidic treated ALD surfaces is not possible and acidic treatment was not further pursued.

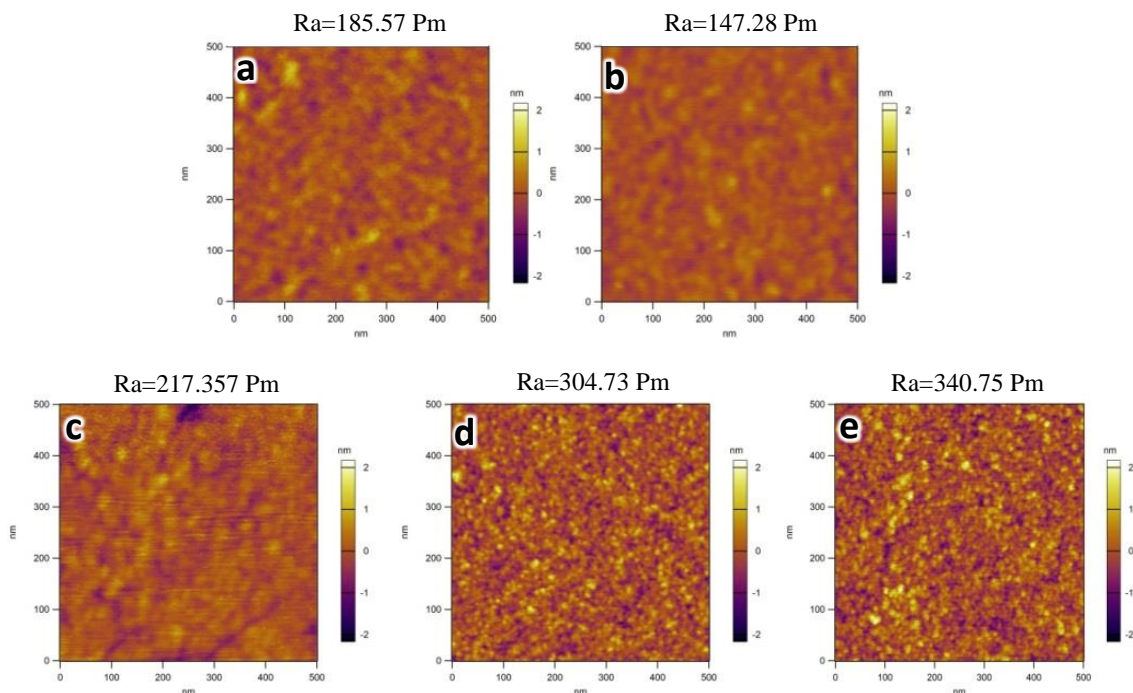


Figure 6.1: AFM topographies of ALD titania (a) exposed to MeOH, (b) sputtered for 30 seconds and exposed to MeOH, (c) exposed to MeOH and subsequently acid treated for 30 seconds, (d) exposed to MeOH and subsequently acid treated for 5 minutes, and (e) exposed to MeOH and subsequently acid treated for 10 minutes. Surface roughness is shown as route mean square (R_a) for each image. Image size is $500 \times 500 \text{ nm}^2$.

6.4 Results and Discussion

6.4.1 AFM-OBSERVATION AND HEIGHT DISTRIBUTION OF Au₉ CLUSTERS ON ALD TITANIA

In Figure 6.2, AFM 3D images are shown. These 3D images are zoomed in areas from the topographical images shown in Figure 6.3. Figure 6.2a shows ALD titania after exposure to methanol which is the solvent used in the adsorption process of Au₉ onto ALD titania. Figures 6.2b, 6.2c and 6.2d are typical examples of ALD titania exposed to Au₉/methanol solutions with a range of different concentrations (0.0002mM – 0.02mM). The figures show random distribution of spikes with a height not found in the image of the sample exposed

CHAPTER 6

only to solvent (Figure 6.2a). The spike densities are not proportional to the concentration of Au clusters solutions due the following reasons. There is an adsorption isotherm which not necessarily will increase linear. However, we have only three different concentrations and that is not enough for determining the adsorption isotherm. Secondly, if clusters go into groups, then we would not count clusters but features related to clusters. In the end, we do not know how many clusters are represented by one single feature in AFM. Samples with deposited Au NCs show larger variation in height compared to samples exposed to solvent. Based on this observation it can be assumed that the spikes in Figures 6.2 b, 6.2c and 6.2d mostly show Au₉ clusters. The height variation in Figure 6.2a is due to roughness of the ALD titania substrates. Figures 6.2f, 6.2g and 6.2h show AFM images of ALD titania samples with Au₉ clusters deposited from solutions with the same concentration range as those shown in Figures 6.2b, 6.2c and 6.2d and which were annealed at 200°C subsequent to the deposition process. Figure 6.2e shows an AFM image of an ALD titania sample exposed only to solvent and subsequently annealed at 200°C. Again, the images in Figures 6.2f, 6.2g and 6.2h show spikes with a height not found in Figure 6.2e which are also attributed to Au NCs.

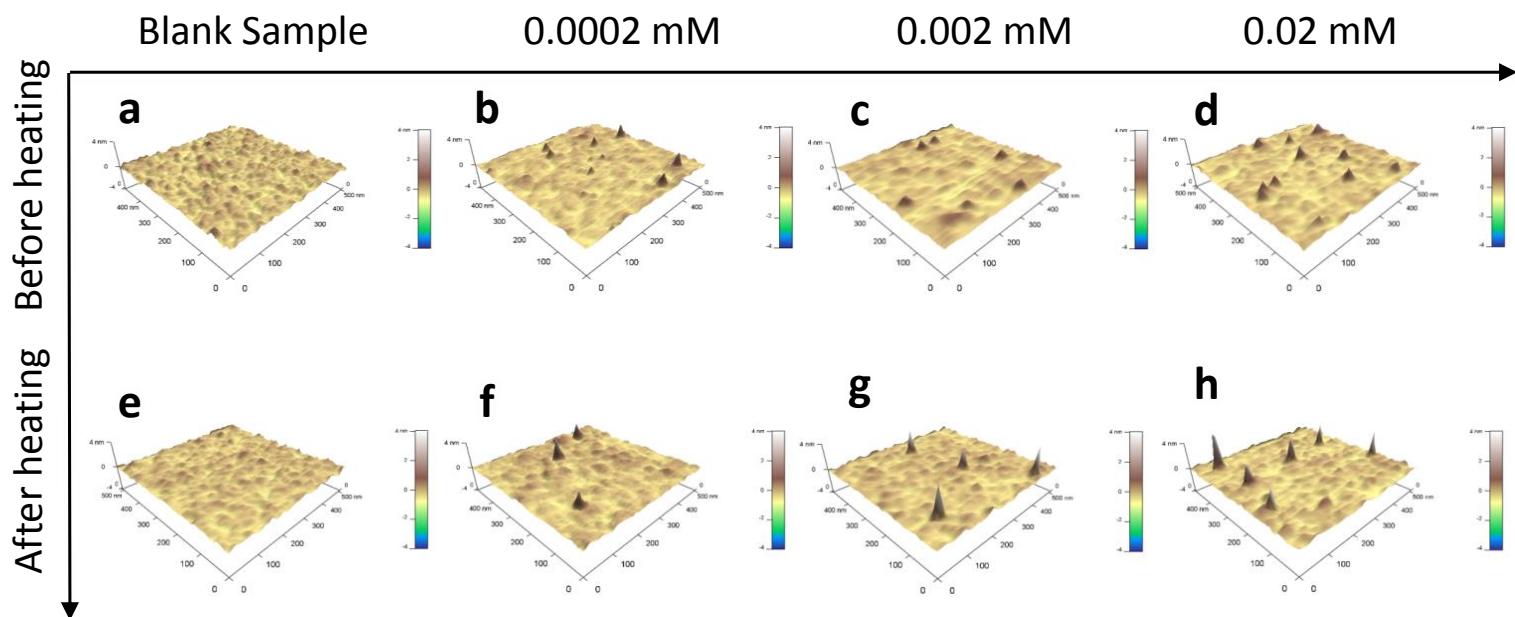


Figure 6.2: AFM 3D images of sputtered ALD titania (a) exposed only to MeOH, (b-d) after deposition of Au₉ clusters with a range of different concentration from MeOH solutions (0.0002mM – 0.02mM), (e) annealed blank sample without deposited Au NCs, and (f-h) annealed after Au NC deposition with the same concentrations as b-d. The size of images are 500 x 500nm².

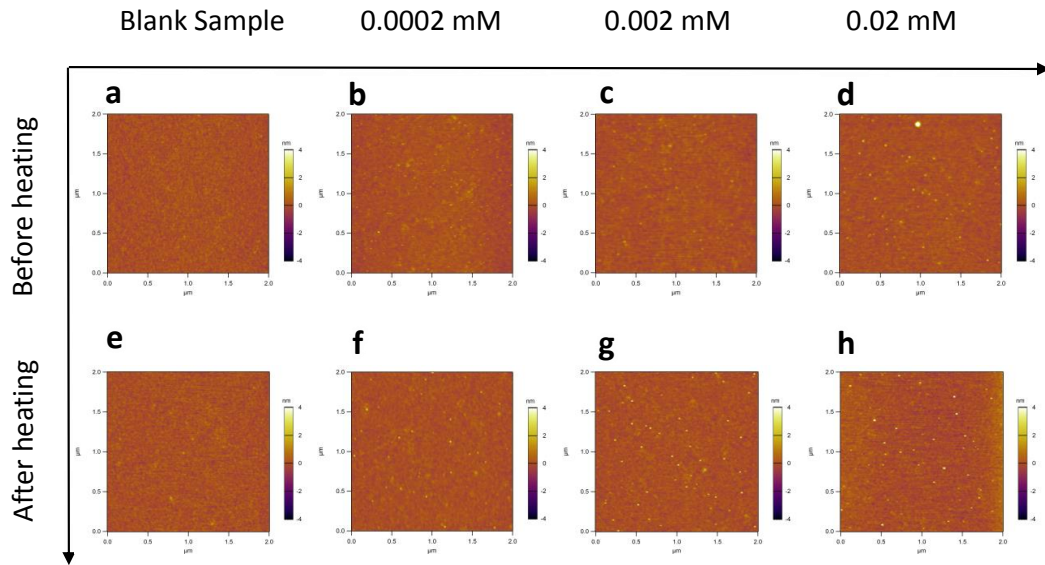


Figure 6.3: AFM topographies of sputtered ALD titania (a) exposed only to MeOH, (b-d) after deposition of Au₉ clusters with a range of different concentrations from MeOH solutions (0.0002mM – 0.02mM), (e) annealed blank sample without deposited Au NCs, and (f-h) annealed after Au NC deposition with the same concentrations as b-d. The size of images are 2.0 x 2.0 μm².

From AFM images the height distribution of Au NCs can be determined, but not lateral width. The reason is that curvature of the AFM tip and also the range of interaction forces between the AFM tip and the sample are much larger than the size of Au₉ clusters. Consequently, the lateral width of Au NCs could appear to be larger than the actual size of individual Au NCs. A large number of features in the AFM images were analysed and identified as Au NCs. All features in the AFM images of surfaces with adsorbed Au₉ clusters less than 1 nm were excluded from statistical analysis due to the R_{rms} of 1 nm. In Figures 6.4a and 6.4b, height distributions of the cluster on ALD titania before and after the heating process are shown. The fraction of Au NC features found for a given height interval were calculated by:

$$fraction_i = \frac{N_i}{\sum_i N_i}$$

CHAPTER 6

where $fraction_i$ is the percentage of features found in a given height interval and N_i is the number of features found in a given height interval.

Before discussing experimental AFM height distribution, the theoretical size of Au₉ clusters and Au₉ cluster cores (de-ligated clusters) must be considered. Based on the theoretical calculation of isolated Au₉ clusters, the distance across the cluster, including PPh₃ ligands, is around 1.75 nm. The overall shape of Au₉ clusters is best described as oblate spheroid. The mean axes of clusters have a length of 1.75 nm, 1.66 nm and 1.47 nm. Because of the interaction between clusters and substrate, it can be assumed that clusters prefer to orient on the surface such that the shortest mean axis (1.47 nm) orients parallel to the normal surface. Experimentally, height distributions show a mean value of 1.7 ± 0.6 nm for non-annealed samples (Figure 6.4a). The average height of Au₉ clusters of non-annealed samples was in agreement with the calculated height of ligated clusters within the uncertainty range. This suggests that the ligands were still attached to Au₉ clusters after adsorption onto the titania surface from the methanol solution, in line with earlier findings.⁵⁴⁻⁵⁵ Theoretically, Au₉ clusters after ligand removal should show a size of about 0.5 nm which is twice the average distance between two Au atoms forming the cluster.⁵⁷ Height distributions after annealing show a mean value of 2.9 ± 1.6 nm (Figure 6.4b). AFM measurements show that the annealing process affects height distribution of features in AFM images and leads to an increase in height of identified features. A fraction of the small features are found at a height around 1 nm. The fraction dropped from around 10% for non-annealed samples (Figure 6.4a) to around 4% for annealed samples (Figure 6.4b). The average height of features after removal of ligands was larger than average size of the Au₉ cluster core. The reason for this finding is most likely that a number of Au₉ cluster cores agglomerated or Ostwald ripening occurred.⁶⁸ Thus, features found in AFM images are described as agglomerated Au NCs or

Au NPs. In our statistical analysis some de-ligated clusters were not considered because cluster heights below 1 nm were excluded.

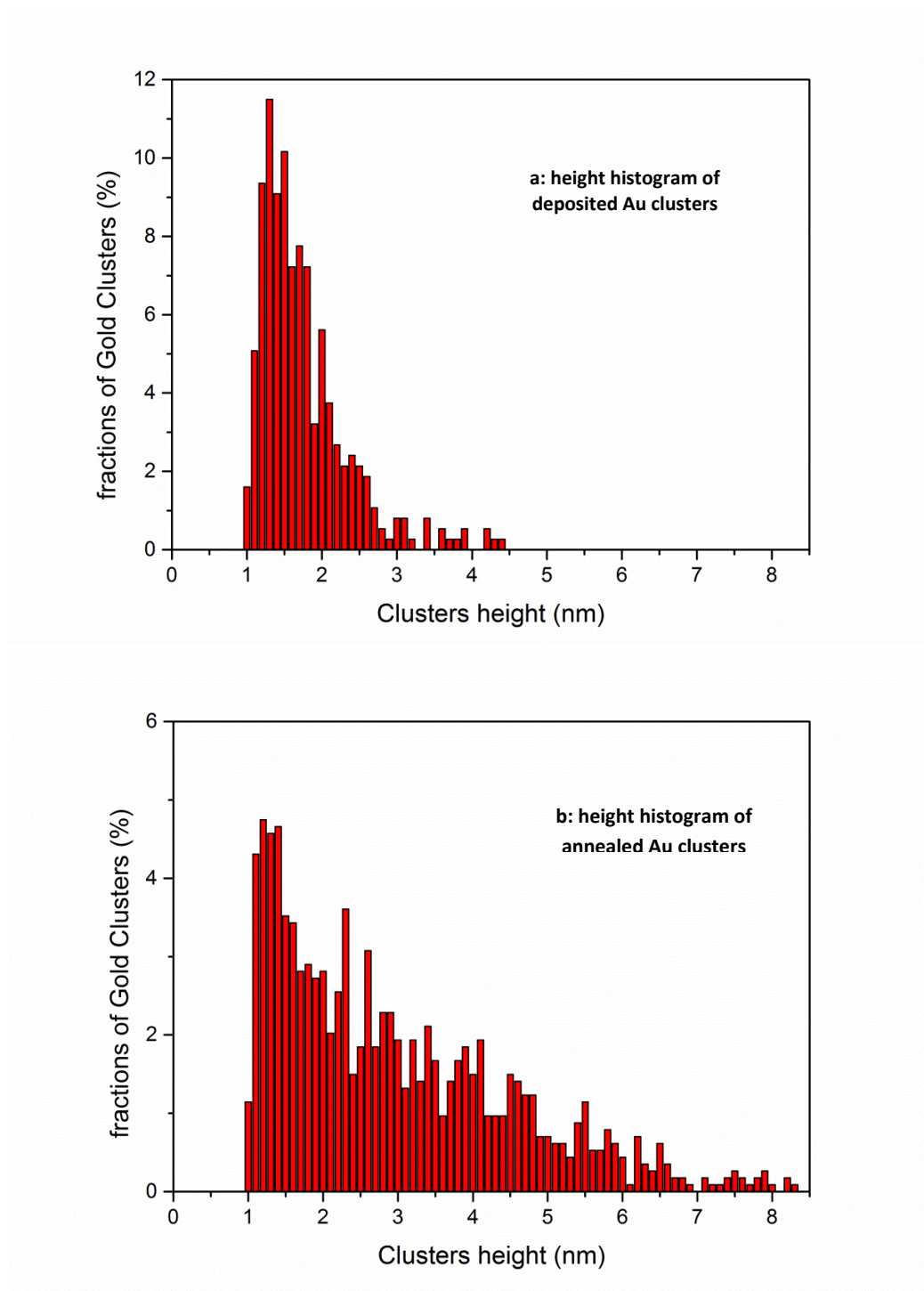


Figure 6.4: Height distribution of features in AFM images: (a) as deposited Au NCs, and (b) after annealing to 200 °C. The cluster mean height before annealing is 1.7 ± 0.6 nm, while after annealing it is 2.9 ± 1.6 nm.

CHAPTER 6

We investigated whether other AFM modes could be used to assess ALD titania surfaces after deposition of Au₉ clusters. It was found earlier that AFM tips can exert forces on clusters in contact mode condition which can lead to movement of clusters over the surface.⁶⁹ Figure 6.5a shows a tapping mode image after taking a contact mode image over the central image area. Figure 6.5b shows the zoomed-in edge of the scanned contact mode image. AFM contact mode scanning of Au₉ clusters deposited on the ALD titania surface showed in every case that even one scan can remove all clusters from the scanned region as indicated in Figure 6.5a and sweep clusters to the side of the scanned region. Performing imaging in tapping mode after applying contact mode imaging on the same samples implied that clusters remain in the positions as left after applying tapping mode when the region is scanned in tapping mode. The white arrows in Figure 6.5 highlight individual Au NCs which seem to be swept to the side of the region scanned in contact mode, but seem to stay at these positions after applying tapping mode. This indicates that the contact mode AFM scan does not change the position and size of Au NCs deposited onto ALD titania. We calculated the number of Au clusters in 1 micro m² and it was about 45 gold clusters. The swept clusters after the contact mode AFM was roughly 80 gold clusters which is close to number that would have been expected. This is another indication that these gold clusters still preserved their own identity after being accumulated. The black arrow in Figure 6.5 shows instability of the feedback scan. This can be explained by the weaker bond between Au NCs and substrate which easily affect tip cluster behaviour. Another example for this phenomenon can also be seen in Figure 6.6.

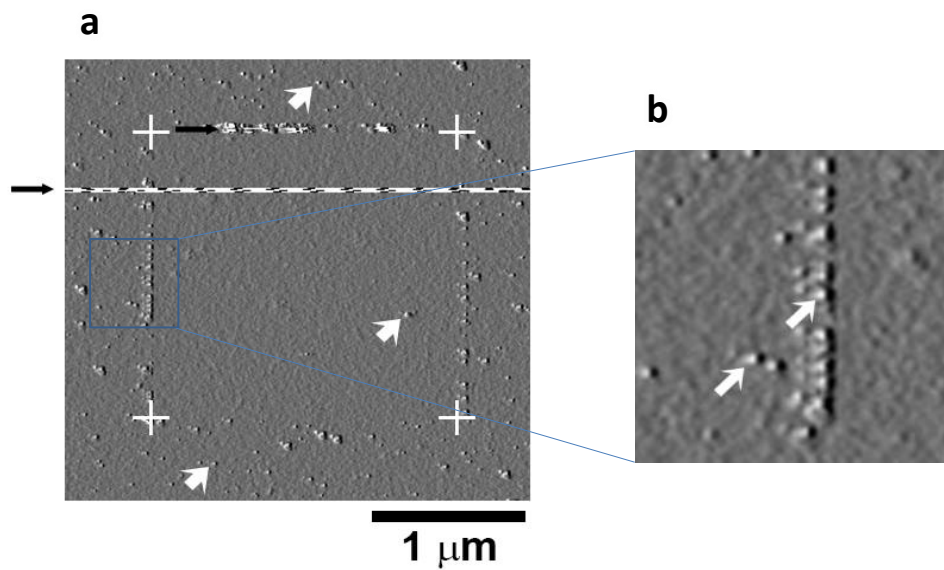


Figure 6.5: NC-AFM Amplitude images of Au_9 nanoclusters deposited on ALD titania pretreated by Ar^+ sputtering. (a) amplitude image after a C-AFM scan shown in the white marked subregion. Clusters inside the C-AFM area are swept to the edge of the scanned region. (b) is a magnification image after C-AFM scan. The white arrow points at individual Au NCs. Au NCs have the same features after removal by the contact scan. The black arrow indicates an area with instability in the feedback loop.

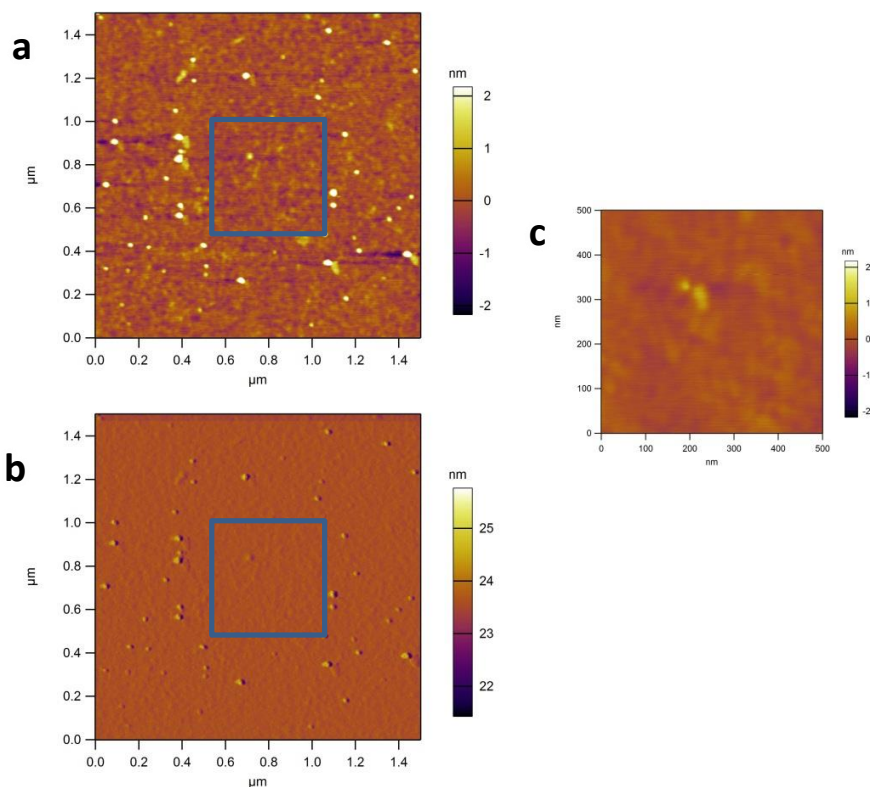


Figure 6.6: NC-AFM topography and amplitude images of Au₉ nanoclusters deposited on ALD titania pre-treated by Ar⁺ sputtering. The same sample (a) topography and (b) amplitude image after a C-AFM scan (c) in the marked subregion. Clusters inside the C-AFM area are swept to the edge of the scanned zone.

6.4.2 XPS RESULTS OF AU₉ CLUSTERS ON ALD TITANIA

High resolution XP spectra for Au 4f, P 2p, Si 2p, Ti 2p, C 1s and O 1s regions of Au NCs deposited on ALD titania were measured and evaluated. In this present work, we focused on Au 4f and P 2p peaks as they are the main components of Au NCs. The main C 1s peak was assigned to 285 eV and used to calibrate the energy scale for all spectra. The Au peak of non-annealed samples show the Au 4f doublet with the Au 4f_{7/2} peak at 84.8 ± 0.2 eV (Figure 6.7a) which is close to the binding energy found for deposited, non-agglomerated Au₉ clusters.⁵⁴⁻⁵⁵ The binding energy of bulk Au can be found at a binding energy of 84 ± 0.2 eV. The difference in Au 4f_{7/2} peak position between bulk Au and Au₉ clusters is attributed to the final state effect found for isolated Au₉ clusters.^{54-55, 64} The Au spectrum of the heated

CHAPTER 6

ALD titania/Au₉ sample is shown in Figure 6.7b. Two Au 4f doublets were required for fitting the Au spectrum. A narrow Au peak was found at 83.6 ± 0.2 eV close to the value for bulk Au. The decrease in binding energy from 84.8 ± 0.2 eV to 83.6 ± 0.2 eV was attributed to the agglomeration of Au₉ cluster cores due to annealing of samples. The second Au 4f_{7/2} peak was found at 85.1 ± 0.2 eV and attributed to non-agglomerated Au₉ clusters which lost ligands and might have been in close contact with the titania substrate.⁵⁵ Before heating Au NCs, the P 2p_{3/2} peak was found at 131.7 ± 0.2 eV and attributed to triphenylphosphine ligands attached to Au NCs (Figure 6.7c). The P contribution shifted to 133.2 ± 0.4 eV after heating (Figure 6.7d) and was attributed to oxidised P. Oxidised P was mostly likely due to ligands detached from the Au NC core which interacted with the titania substrate.⁵⁴⁻⁵⁵ In all samples, the titanium signal displayed from 2p region with two distinct peaks at 458.9 ± 0.2 and 457.5 ± 0.2 eV corresponded to Ti⁴⁺ and Ti³⁺, respectively (Figure 6.8).⁷⁰ Ti³⁺ ions in TiO₂ are known to extend adsorption of materials into the visible light region of the spectrum.⁷¹ Also, thermal treatment is known to increase Ti³⁺ percentage in titania materials.⁷² Titanium reduction (Ti³⁺) in this study was found to depend on pre- and post-deposition treatment. Sputtering pre-deposition induced oxygen vacancy in the ALD titania surface as potential sites for adsorbing Au NCs.⁷³ In the previous study, the percentage of the Ti³⁺ population in untreated titania NPs (P-25) was approximately 7% .³⁵ In this study, Ti³⁺ percentage dropped dramatically with different pre-deposition treatments.³⁵ The Ti³⁺ population on pure ALD titania was $1.2 \pm 1\%$ (Table 6.1). These percentages have been calculated from the ratio of fitted Ti XPS peak intensity. It was assumed that the composition is homogeneous over the thickness of ALD film. The defect density affected by sputtering and annealing process. On the same substrate Ti³⁺ percentage increased to $8 \pm 1\%$ after sputtering. The Ti³⁺ fraction increased even further to $11.5 \pm 1\%$ after subsequent annealing.

It is likely that sputtering pre-deposition shows a considerably higher Ti^{3+} population compared with other pre-deposition treatment methods used in the previous study.³⁵

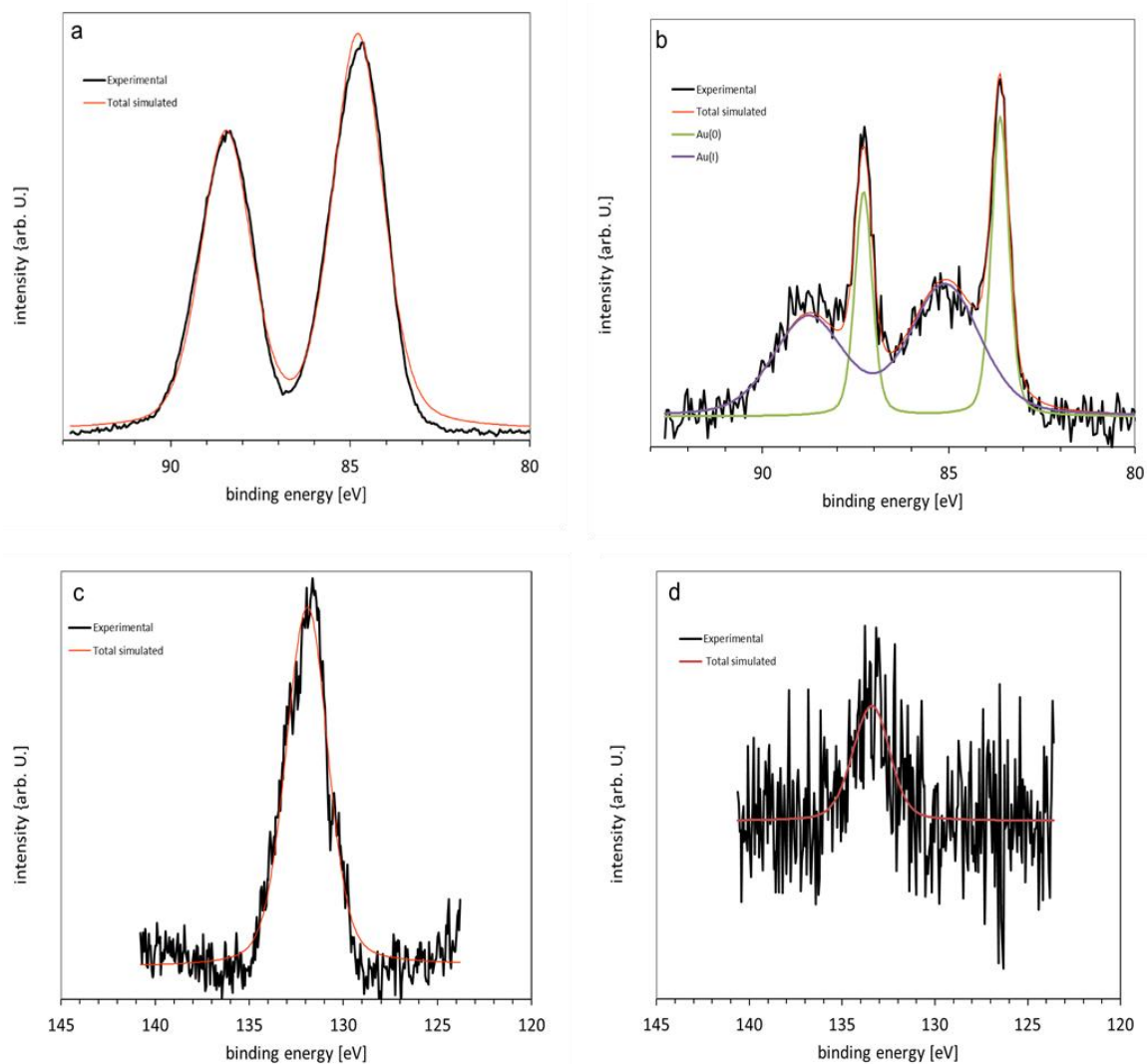


Figure 6.7: XPS spectra of $[\text{Au}_9(\text{PPh}_3)_8](\text{NO}_3)_3$ clusters on ALD titania (a) Au 4f region of as-deposited samples, (b) after annealing, (c) P 2p spectrum of as-deposited samples and (d) after annealing. Au(0) is the LBP-Au, while Au(I) is the HBP-Au.

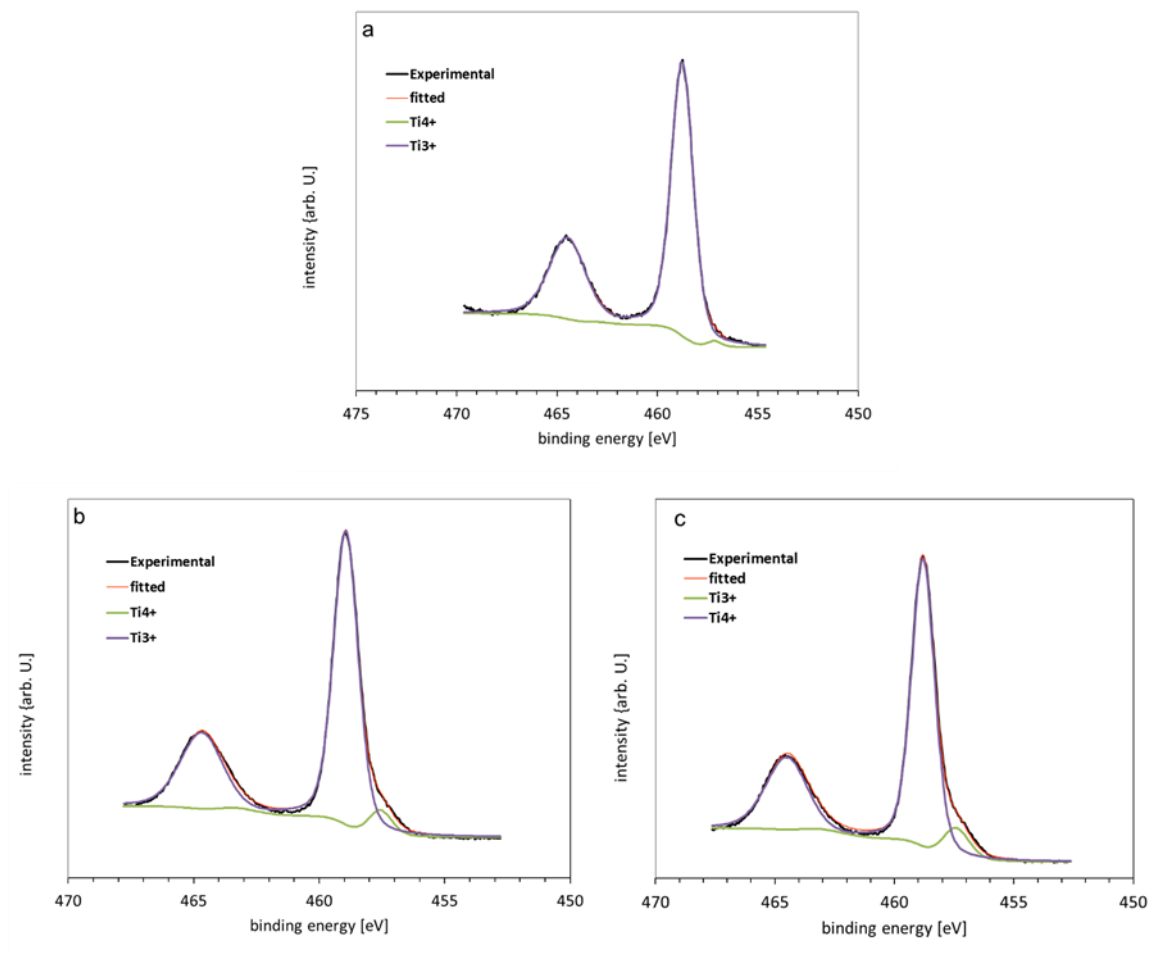


Figure 6.8: XPS spectra of Ti 2p (a) of pure ALD titania, (b) of Au₉ clusters deposited on sputtered ALD titania and (c) Au₉ clusters on sputtered ALD titania after annealing.

Table 6.1: Fraction of Ti³⁺ and Ti⁴⁺ in the Ti 2p XPS spectrum for various ALD titania samples. Error in the intensities was estimated to be ±1%. Au NCs were deposited on sputtered ALD titania.

Surface	Ti ³⁺ [%]	Ti ⁴⁺ [%]
Pure ALD titania	1.2	98.8
Sputtered ALD titania	8	92.2
Annealed ALD titania after sputtered	11.5	88.5

6.4.3 DISCUSSION AFM AND XPS RESULTS

AFM and XPS measurements in this work investigated the properties of Au₉ clusters deposited onto ALD titania and outcomes were integrated into a single interpretation. On the other hand, this interpretation was integrated with our previous studies.⁶³ AFM measurements allowed for imaging and height analysis of features attributed to Au₉ clusters. Before heating, the majority of Au NCs were attributed to single Au₉ clusters according to height analysis. The height of these clusters was in agreement with calculations of individual Au NCs including stabilised ligands. It needs to be emphasised that, due to lateral resolution of AFM, the features in an AFM image cannot be used to distinguish between individual clusters and groups of clusters when clusters form 2-D groups or islands.⁶³ XPS results show that after deposition clusters are adsorbed onto the surface as individual clusters cluster cores had not agglomerated. However, from XPS results it is not possible to derive a conclusion about the distance between individual clusters, i.e. whether clusters form groups of individual and separated clusters in close proximity or whether clusters are randomly distributed over the surface. After annealing, XPS shows that ligands were removed from the cluster core and both AFM and XPS show that Au NCs partially agglomerated.

In a previous study we used titania nanosheets instead of ALD titania as substrate for deposition of Au₉ clusters.⁶³ Titania nanosheets are single crystallites with a thickness of one monolayer of titanium oxide. In contrast, ALD titania used here forms an amorphous surface and has a thickness of about 5 nm. In our previous study we found a similar height distribution of Au₉ clusters before and after annealing, as in the present work, and Au 4f XP spectra were similar to those shown here. The difference in height distribution of AFM features is that in the present case a larger range is covered in height distribution compared to our previous study.⁶³ Based on XPS and AFM results it cannot be excluded that Au₉

clusters in the present study also form 2-D groups after deposition, despite the fact that Au₉ surface interaction is different for titania nanosheets and ALD titania. One example for the difference between titania nanosheets and ALD titania is that the number of Ti³⁺ sites is higher for titania nanosheets than for ALD titania. Ti³⁺ sites are attractive for adsorbing Au NCs.⁷⁴ Thus, as individual and randomly distributed clusters adsorption is more likely to occur on sputtered ALD titania than on titania nanosheets. As 2-D distribution of Au₉ clusters have to move a shorter distance for merging with another Au₉ cluster, these groups have a higher likelihood of agglomeration as compared to randomly distributed clusters.

In comparison to titania nanosheet measurements, we attempted to measure STM for ALD titania decorated by Au NCs. It was a difficult to apply STM in this case due to surface roughness of ALD titania being 1 R_{rms}. Due to roughness, STM tip position could not be stabilised and therefore it was hard to maintain the tunnelling current. For this reason, we unsure if individual Au NCs adsorb as groups on ALD titania or as individual clusters.

In another former study we investigated deposition of Au₉ clusters onto plasma treated ALD titania.⁵⁶ It was found that after annealing non-agglomerated Au₉ clusters were retained up to a Au₉ concentration of 0.75 mM in methanol solution. Coverage of ALD titania with Au in⁵⁶ was approximately eight times lower than in the present case (Au/Ti ratio in⁵⁶ below 0.1 and Au/Ti ratio 0.87 here). We assume that the higher coverage of sputtered ALD titania surface with non-agglomerated Au₉ clusters is due to a larger number of Ti³⁺ defects induced by sputtering compared to plasma cleaning.

6.5 CONCLUSION

Sputtering of ALD titania substrates induced a number of Ti³⁺ defects for attracting Au NCs. Sputter pre-treatment increased coverage of non-agglomerated Au₉ clusters compared with

CHAPTER 6

other pre-treatment conditions. It is difficult to conclude that Au NCs are adsorbed onto sputtered ALD titania randomly and as separate clusters rather than forming 2-D groups. However, due to the larger number of Ti^{3+} defects on sputtered ALD titania compared to nanosheets it is likely that the fraction of clusters adsorbed onto the surface as individual clusters in sputtered ALD titania is higher than in nanosheets. Knowing whether Au_9 adsorb as separate and individual clusters rather than in 2-D groups is important because in the first case agglomeration is more likely than in the second case.

6.6 REFERENCES

1. Homberger, M.; Simon, U., On the application potential of gold nanoparticles in nanoelectronics and biomedicine. *Philosophical Transactions of the Royal Society of London A: Mathematical, Physical and Engineering Sciences* **2010**, *368* (1915), 1405-1453.
2. Murray, R. W., Nanoelectrochemistry: Metal Nanoparticles, Nanoelectrodes, and Nanopores. *Chemical Reviews* **2008**, *108* (7), 2688-2720.
3. Franke, M. E.; Koplín, T. J.; Simon, U., Metal and Metal Oxide Nanoparticles in Chemiresistors: Does the Nanoscale Matter? *Small* **2006**, *2* (1), 36-50.
4. Zhang, X.; Guo, Q.; Cui, D., Recent Advances in Nanotechnology Applied to Biosensors. *Sensors* **2009**, *9* (2), 1033.
5. Wilson, R., The use of gold nanoparticles in diagnostics and detection. *Chemical Society Reviews* **2008**, *37* (9), 2028-2045.
6. Schmid, G.; Reuter, T.; Simon, U.; Noyong, M.; Blech, K.; Santhanam, V.; Jäger, D.; Slomka, H.; Lüth, H.; Lepsa, M. I., Generation and electrical contacting of gold quantum dots. *Colloid Polym Sci* **2008**, *286* (8-9), 1029-1037.
7. Jin, R., The impacts of nanotechnology on catalysis by precious metal nanoparticles. In *Nanotechnology Reviews*, **2012**; Vol. 1, p 31.
8. Zhang, Y.; Cui, X.; Shi, F.; Deng, Y., Nano-Gold Catalysis in Fine Chemical Synthesis. *Chemical Reviews* **2012**, *112* (4), 2467-2505.
9. Tan, X.; Jin, R., Ultrasmall metal nanoclusters for bio-related applications. *Wiley Interdisciplinary Reviews: Nanomedicine and Nanobiotechnology* **2013**, *5* (6), 569-581.

CHAPTER 6

10. White, R.; Bennett, T.; Golovko, V.; Andersson, G. G.; Metha, G. F., A Systematic Density Functional Theory Study of the Complete De-ligation of Ru₃(CO)₁₂. *accepted for publication in ChemistrySelect* **2016**.
11. Alvino, J. F.; Bennett, T.; Anderson, D.; Donoeva, B.; Ovoshchnikov, D.; Adnan, R. H.; Appadoo, D.; Golovko, V.; Andersson, G.; Metha, G. F., Far-infrared absorption spectra of synthetically-prepared, ligated metal clusters with Au₆, Au₈, Au₉ and Au₆Pd metal cores. *RSC Advances* **2013**, 3 (44), 22140-22149.
12. Schmid, G.; Simon, U., Gold nanoparticles: assembly and electrical properties in 1-3 dimensions. *Chemical Communications* **2005**, (6), 697-710.
13. Schmid, G., Large clusters and colloids. Metals in the embryonic state. *Chemical Reviews* **1992**, 92 (8), 1709-1727.
14. Della Pina, C.; Falletta, E.; Prati, L.; Rossi, M., Selective oxidation using gold. *Chemical Society Reviews* **2008**, 37 (9), 2077-2095.
15. Corma, A.; Garcia, H., Supported gold nanoparticles as catalysts for organic reactions. *Chemical Society Reviews* **2008**, 37 (9), 2096-2126.
16. Eustis, S.; El-Sayed, M. A., Why gold nanoparticles are more precious than pretty gold: Noble metal surface plasmon resonance and its enhancement of the radiative and nonradiative properties of nanocrystals of different shapes. *Chemical Society Reviews* **2006**, 35 (3), 209-217.
17. Chen, W.; Chen, S., Oxygen Electroreduction Catalyzed by Gold Nanoclusters: Strong Core Size Effects. *Angewandte Chemie International Edition* **2009**, 48 (24), 4386-4389.
18. Qian, H.; Zhu, M.; Wu, Z.; Jin, R., Quantum Sized Gold Nanoclusters with Atomic Precision. *Accounts of Chemical Research* **2012**, 45 (9), 1470-1479.

CHAPTER 6

19. Chen, M. S.; Goodman, D. W., Structure–activity relationships in supported Au catalysts. *Catalysis Today* **2006**, *111* (1–2), 22-33.
20. Boronat, M.; Corma, A., Molecular approaches to catalysis: Naked gold nanoparticles as quasi-molecular catalysts for green processes. *Journal of Catalysis* **2011**, *284* (2), 138-147.
21. Wilcoxon, J. P.; Abrams, B. L., Synthesis, structure and properties of metal nanoclusters. *Chemical Society Reviews* **2006**, *35* (11), 1162-1194.
22. Yamazoe, S.; Koyasu, K.; Tsukuda, T., Nonscalable Oxidation Catalysis of Gold Clusters. *Accounts of Chemical Research* **2014**, *47* (3), 816-824.
23. Schmid, G., The relevance of shape and size of Au₅₅ clusters. *Chemical Society Reviews* **2008**, *37* (9), 1909-1930.
24. Zeng, C.; Qian, H.; Li, T.; Li, G.; Rosi, N. L.; Yoon, B.; Barnett, R. N.; Whetten, R. L.; Landman, U.; Jin, R., Total Structure and Electronic Properties of the Gold Nanocrystal Au₃₆(SR)₂₄. *Angewandte Chemie* **2012**, *124* (52), 13291-13295.
25. Qin, W.; Lohrman, J.; Ren, S., Magnetic and Optoelectronic Properties of Gold Nanocluster–Thiophene Assembly. *Angewandte Chemie International Edition* **2014**, *53* (28), 7316-7319.
26. Bennett, T.; Falcinella, A. J.; White, R. J.; Adnan, R. H.; Golovko, V.; Andersson, G. G.; Metha, G. F., The effect of counter ions on the far-infrared spectra of tris(triphenylphosphinegold)oxonium dimer salts. *RSC Advances* **2015**, *5* (91), 74499-74505.
27. Bennett, T.; Adnan, R. H.; Alvino, J. F.; Golovko, V.; Andersson, G. G.; Metha, G. F., Identification of the Vibrational Modes in the Far-Infrared Spectra of Ruthenium Carbonyl Clusters and the Effect of Gold Substitution. *Inorganic Chemistry* **2014**, *53* (9), 4340-4349.

CHAPTER 6

28. Wu, Z.; Chen, J.; Jin, R., One-Pot Synthesis of Au₂₅(SG)₁₈ 2- and 4-nm Gold Nanoparticles and Comparison of Their Size-Dependent Properties. *Advanced Functional Materials* **2011**, *21* (1), 177-183.
29. Chusuei, C. C.; Lai, X.; Davis, K. A.; Bowers, E. K.; Fackler, J. P.; Goodman, D. W., A Nanoscale Model Catalyst Preparation: Solution Deposition of Phosphine-Stabilized Gold Clusters onto a Planar TiO₂(110) Support. *Langmuir* **2001**, *17* (13), 4113-4117.
30. Wan, X.-K.; Lin, Z.-W.; Wang, Q.-M., Au₂₀ Nanocluster Protected by Hemilabile Phosphines. *Journal of the American Chemical Society* **2012**, *134* (36), 14750-14752.
31. Tsukuda, T., Toward an atomic-level understanding of size-specific properties of protected and stabilized gold clusters. *Bulletin of the Chemical Society of Japan* **2012**, *85* (2), 151-168.
32. Zhu, Y.; Qian, H.; Jin, R., An Atomic-Level Strategy for Unraveling Gold Nanocatalysis from the Perspective of Au_n(SR)_m Nanoclusters. *Chemistry – A European Journal* **2010**, *16* (37), 11455-11462.
33. Parker, J. F.; Fields-Zinna, C. A.; Murray, R. W., The Story of a Monodisperse Gold Nanoparticle: Au₂₅L₁₈. *Accounts of Chemical Research* **2010**, *43* (9), 1289-1296.
34. Adnan, R. H.; Andersson, G. G.; Polson, M. I. J.; Metha, G. F.; Golovko, V. B., Factors influencing the catalytic oxidation of benzyl alcohol using supported phosphine-capped gold nanoparticles. *Catalysis Science & Technology* **2015**, *5* (2), 1323-1333.
35. Ruzicka, J.-Y.; Abu Bakar, F.; Hoeck, C.; Adnan, R.; McNicoll, C.; Kemmitt, T.; Cowie, B. C.; Metha, G. F.; Andersson, G. G.; Golovko, V. B., Toward Control of

- Gold Cluster Aggregation on TiO₂ via Surface Treatments. *The Journal of Physical Chemistry C* **2015**, *119* (43), 24465-24474.
36. Casaletto, M. P.; Longo, A.; Martorana, A.; Prestianni, A.; Venezia, A. M., XPS study of supported gold catalysts: the role of Au⁰ and Au^{+δ} species as active sites. *Surface and Interface Analysis* **2006**, *38* (4), 215-218.
37. Valden, M.; Lai, X.; Goodman, D. W., Onset of Catalytic Activity of Gold Clusters on Titania with the Appearance of Nonmetallic Properties. *Science* **1998**, *281* (5383), 1647-1650.
38. Zhu, M.; Aikens, C. M.; Hollander, F. J.; Schatz, G. C.; Jin, R., Correlating the Crystal Structure of A Thiol-Protected Au₂₅ Cluster and Optical Properties. *Journal of the American Chemical Society* **2008**, *130* (18), 5883-5885.
39. Sanchez, A.; Abbet, S.; Heiz, U.; Schneider, W. D.; Häkkinen, H.; Barnett, R. N.; Landman, U., When Gold Is Not Noble: Nanoscale Gold Catalysts. *The Journal of Physical Chemistry A* **1999**, *103* (48), 9573-9578.
40. Janssens, T. V. W.; Carlsson, A.; Puig-Molina, A.; Clausen, B. S., Relation between nanoscale Au particle structure and activity for CO oxidation on supported gold catalysts. *Journal of Catalysis* **2006**, *240* (2), 108-113.
41. Miller, J. T.; Kropf, A. J.; Zha, Y.; Regalbuto, J. R.; Delannoy, L.; Louis, C.; Bus, E.; van Bokhoven, J. A., The effect of gold particle size on AuAu bond length and reactivity toward oxygen in supported catalysts. *Journal of Catalysis* **2006**, *240* (2), 222-234.
42. Gao, W.; Chen, X. F.; Li, J. C.; Jiang, Q., Is Au₅₅ or Au₃₈ Cluster a Threshold Catalyst for Styrene Epoxidation? *The Journal of Physical Chemistry C* **2010**, *114* (2), 1148-1153.

CHAPTER 6

43. Liu, J.; Krishna, K. S.; Losovyj, Y. B.; Chattopadhyay, S.; Lozova, N.; Miller, J. T.; Spivey, J. J.; Kumar, C. S. S. R., Ligand-Stabilized and Atomically Precise Gold Nanocluster Catalysis: A Case Study for Correlating Fundamental Electronic Properties with Catalysis. *Chemistry – A European Journal* **2013**, *19* (31), 10201-10208.
44. Li, G.; Jin, R., Atomically Precise Gold Nanoclusters as New Model Catalysts. *Accounts of Chemical Research* **2013**, *46* (8), 1749-1758.
45. Jin, R., Quantum sized, thiolate-protected gold nanoclusters. *Nanoscale* **2010**, *2* (3), 343-362.
46. Gaur, S.; Miller, J. T.; Stellwagen, D.; Sanampudi, A.; Kumar, C. S. S. R.; Spivey, J. J., Synthesis, characterization, and testing of supported Au catalysts prepared from atomically-tailored Au₃₈(SC₁₂H₂₅)₂₄ clusters. *Physical Chemistry Chemical Physics* **2012**, *14* (5), 1627-1634.
47. Zhu, Y.; Qian, H.; Jin, R., Catalysis opportunities of atomically precise gold nanoclusters. *Journal of Materials Chemistry* **2011**, *21* (19), 6793-6799.
48. Gao, Y.; Shao, N.; Pei, Y.; Chen, Z.; Zeng, X. C., Catalytic Activities of Subnanometer Gold Clusters (Au₁₆–Au₁₈, Au₂₀, and Au₂₇–Au₃₅) for CO Oxidation. *ACS Nano* **2011**, *5* (10), 7818-7829.
49. Liu, Y.; Tsunoyama, H.; Akita, T.; Tsukuda, T., Efficient and selective epoxidation of styrene with TBHP catalyzed by Au₂₅ clusters on hydroxyapatite. *Chemical Communications* **2010**, *46* (4), 550-552.
50. Lim, D.-C.; Hwang, C.-C.; Gantefor, G.; Kim, Y. D., Model catalysts of supported Au nanoparticles and mass-selected clusters. *Physical Chemistry Chemical Physics* **2010**, *12* (46), 15172-15180.

CHAPTER 6

51. Benz, L.; Tong, X.; Kemper, P.; Metiu, H.; Bowers, M. T.; Buratto, S. K., Pinning Mononuclear Au on the Surface of Titania. *The Journal of Physical Chemistry B* **2006**, *110* (2), 663-666.
52. Yoon, B.; Häkkinen, H.; Landman, U.; Wörz, A. S.; Antonietti, J.-M.; Abbet, S.; Judai, K.; Heiz, U., Charging Effects on Bonding and Catalyzed Oxidation of CO on Au₈ Clusters on MgO. *Science* **2005**, *307* (5708), 403-407.
53. Turner, M.; Golovko, V. B.; Vaughan, O. P. H.; Abdulkin, P.; Berenguer-Murcia, A.; Tikhov, M. S.; Johnson, B. F. G.; Lambert, R. M., Selective oxidation with dioxygen by gold nanoparticle catalysts derived from 55-atom clusters. *Nature* **2008**, *454* (7207), 981-983.
54. Anderson, D. P.; Adnan, R. H.; Alvino, J. F.; Shipper, O.; Donoeva, B.; Ruzicka, J.-Y.; Al Qahtani, H.; Harris, H. H.; Cowie, B.; Aitken, J. B.; Golovko, V. B.; Metha, G. F.; Andersson, G. G., Chemically synthesised atomically precise gold clusters deposited and activated on titania. Part II. *Physical Chemistry Chemical Physics* **2013**, *15* (35), 14806-14813.
55. Anderson, D. P.; Alvino, J. F.; Gentleman, A.; Qahtani, H. A.; Thomsen, L.; Polson, M. I. J.; Metha, G. F.; Golovko, V. B.; Andersson, G. G., Chemically-synthesised, atomically-precise gold clusters deposited and activated on titania. *Physical Chemistry Chemical Physics* **2013**, *15* (11), 3917-3929.
56. Andersson, G. G.; Golovko, V. B.; Alvino, J. F.; Bennett, T.; Wrede, O.; Mejia, S. M.; Al Qahtani, H. S.; Adnan, R.; Gunby, N.; Anderson, D. P.; Metha, G. F., Phosphine-stabilised Au₉ clusters interacting with titania and silica surfaces: The first evidence for the density of states signature of the support-immobilised cluster. *The Journal of Chemical Physics* **2014**, *141* (1), 014702.

CHAPTER 6

57. Bosch-Navarro, C.; Laker, Z. P. L.; Thomas, H. R.; Marsden, A. J.; Sloan, J.; Wilson, N. R.; Rourke, J. P., Covalently Binding Atomically Designed Au₉ Clusters to Chemically Modified Graphene. *Angewandte Chemie International Edition* **2015**, *54* (33), 9560-9563.
58. Bennett, T.; Adnan, R. H.; Alvino, J. F.; Kler, R.; Golovko, V. B.; Metha, G. F.; Andersson, G. G., Effect of Gold Nanoclusters on the Production of Ti³⁺ Defect Sites in Titanium Dioxide Nanoparticles under Ultraviolet and Soft X-ray Radiation. *The Journal of Physical Chemistry C* **2015**, *119* (20), 11171-11177.
59. Shichibu, Y.; Zhang, M.; Kamei, Y.; Konishi, K., [Au₇]³⁺: A Missing Link in the Four-Electron Gold Cluster Family. *Journal of the American Chemical Society* **2014**, *136* (37), 12892-12895.
60. Wen, F.; Englert, U.; Gutrath, B.; Simon, U., Crystal Structure, Electrochemical and Optical Properties of [Au₉(PPh₃)₈](NO₃)₃. *European Journal of Inorganic Chemistry* **2008**, *2008* (1), 106-111.
61. Gutrath, B. S.; Opperl, I. M.; Presly, O.; Beljakov, I.; Meded, V.; Wenzel, W.; Simon, U., [Au₁₄(PPh₃)₈(NO₃)₄]: An Example of a New Class of Au(NO₃)-Ligated Superatom Complexes. *Angewandte Chemie International Edition* **2013**, *52* (12), 3529-3532.
62. Al Qahtani, H. S.; Kimoto, K.; Bennett, T.; Alvino, J. F.; Andersson, G. G.; Metha, G. F.; Golovko, V. B.; Sasaki, T.; Nakayama, T., Atomically resolved structure of ligand-protected Au₉ clusters on TiO₂ nanosheets using aberration-corrected STEM. *The Journal of Chemical Physics* **2016**, *144* (11), 114703.
63. Al Qahtani, H. S.; Higuchi, R.; Sasaki, T.; Metha, G. F.; Golovko, V. B.; Andersson, G. G.; Nakayama, T., grouping and aggregation of ligand Protected Au₉ Clusters on TiO₂ nanosheet. *Planned to submitted to Physical Review B* **2016**.

CHAPTER 6

64. Borman, V. D.; Pushkin, M. A.; Tronin, V. N.; Troyan, V. I., Evolution of the electronic properties of transition metal nanoclusters on graphite surface. *J. Exp. Theor. Phys.* **2010**, *110* (6), 1005-1025.
65. Kitsudo, Y.; Iwamoto, A.; Matsumoto, H.; Mitsuhashi, K.; Nishimura, T.; Takizawa, M.; Akita, T.; Maeda, Y.; Kido, Y., Final state effect for Au 4f line from gold-nanoparticles grown on oxides and HOPG supports. *Surface Science* **2009**, *603* (13), 2108-2114.
66. Liu, Y.; Tsunoyama, H.; Akita, T.; Tsukuda, T., Preparation of ~1 nm Gold Clusters Confined within Mesoporous Silica and Microwave-Assisted Catalytic Application for Alcohol Oxidation. *The Journal of Physical Chemistry C* **2009**, *113* (31), 13457-13461.
67. Hofmann, S.; Wang, J. Y., Determination of the Depth Scale in Sputter Depth Profiling.(The Sputtered Depth in Depth Profiling). *Journal of Surface Analysis* **2002**, *9* (3), 306-309.
68. Fukamori, Y.; König, M.; Yoon, B.; Wang, B.; Esch, F.; Heiz, U.; Landman, U., Fundamental Insight into the Substrate-Dependent Ripening of Monodisperse Clusters. *ChemCatChem* **2013**, *5* (11), 3330-3341.
69. Dietzel, D.; Mönninghoff, T.; Herding, C.; Feldmann, M.; Fuchs, H.; Stegemann, B.; Ritter, C.; Schwarz, U. D.; Schirmeisen, A., Frictional duality of metallic nanoparticles: Influence of particle morphology, orientation, and air exposure. *Physical Review B* **2010**, *82* (3), 035401.
70. Jagadale, T. C.; Takale, S. P.; Sonawane, R. S.; Joshi, H. M.; Patil, S. I.; Kale, B. B.; Ogale, S. B., N-Doped TiO₂ Nanoparticle Based Visible Light Photocatalyst by Modified Peroxide Sol–Gel Method. *The Journal of Physical Chemistry C* **2008**, *112* (37), 14595-14602.

CHAPTER 6

71. Zuo, F.; Wang, L.; Wu, T.; Zhang, Z.; Borchardt, D.; Feng, P., Self-Doped Ti³⁺ Enhanced Photocatalyst for Hydrogen Production under Visible Light. *Journal of the American Chemical Society* **2010**, *132* (34), 11856-11857.
72. Amano, F.; Nakata, M.; Asami, K.; Yamakata, A., Photocatalytic activity of titania particles calcined at high temperature: Investigating deactivation. *Chemical Physics Letters* **2013**, *579*, 111-113.
73. Wahlström, E.; Lopez, N.; Schaub, R.; Thostrup, P.; Rønnau, A.; Africh, C.; Lægsgaard, E.; Nørskov, J. K.; Besenbacher, F., Bonding of Gold Nanoclusters to Oxygen Vacancies on Rutile. *Physical Review Letters* **2003**, *90* (2), 026101.
74. Li, M.; Hebenstreit, W.; Diebold, U.; Tyryshkin, A. M.; Bowman, M. K.; Dunham, G. G.; Henderson, M. A., The Influence of the Bulk Reduction State on the Surface Structure and Morphology of Rutile TiO₂(110) Single Crystals. *The Journal of Physical Chemistry B* **2000**, *104* (20), 4944-4950.

CHAPTER 7

Investigation of phosphine-stabilised Au₉ Clusters on Acidic pre-treated ALD TiO₂

7.1 ABSTRACT

Chemically synthesised, atomically precise phosphine-stabilised clusters ($\text{Au}_9(\text{PPh}_3)_8(\text{NO}_3)_3$) were deposited onto acid pre-treated titania at various concentrations and samples were heated under vacuum to remove ligands. Metastable Induced Electron Spectroscopy (MIES) was used to determine density of state at the surface. X-ray Photoelectron Spectroscopy (XPS) was used to determine chemical composition of the surface. It was found that Au clusters partially agglomerated after heat treatment. The experimental MIE spectra was fitted with three base spectra assigned to the spectra of Au clusters anchored to titania after removal of ligands, the hydrocarbon including phosphine ligands, and sulphur on the substrate.

7.2 INTRODUCTION

Over the last centuries, gold was thought to be chemically inert and catalytically inactive.¹ During the past two decades this view has changed with various studies showing that Au nanoparticles are highly active catalysts for a number of reactions including CO oxidation²⁻⁵ and hydrogenation.⁶⁻⁷ Au nanoparticles are important for catalysis due to their size specific properties.⁸⁻⁹ Au reactivity properties become more dramatic when particle size is less than 1 nm, where each particle can be considered a nanocluster (or cluster) formed by a few atoms. For example, gas phase Au₈ clusters deposited onto MgO surfaces have experimentally shown CO oxidation at 150 K, whereas smaller clusters are inert.¹⁰⁻¹¹ Heiz and co-workers studied the photocatalytic water reduction reaction on CdS nanorods as a function of Pt cluster size.¹² They found that the maximum H₂ production for Pt₄₆ was attributed to size dependent electronic properties of clusters. Similarly, Hutchings and co-workers reported the relationship between Au clusters of ~10 atoms and enhancement of catalytic activity of CO oxidation for large immobilised Au particles on iron-oxide.¹³ Another study by Flytzani-Stephanopoulos and co-workers showed a huge difference in catalytic performance between sub-1nm and >3nm gold particles for reactions such as producing methanol-steam and water gas shift.¹⁴ The electronic structure of Au clusters supported on oxide surfaces has a strong influence on catalytic performance. Specifically, charge transfer between clusters and oxide surfaces is often considered crucial.^{1, 15-20} The electronic structure of ultra-small clusters strongly depends on the number of atoms forming the cluster and has been measured in both gas phase²¹⁻²² and on metal oxide surfaces.²³ Scanning Tunneling Microscopy (STM) is used for such studies with ideally flat surfaces.²³⁻²⁴ Another method used for determining surface structure is Metastable Induced Electron Spectroscopy (MIES) which is a technique exclusively sensitive to the outermost layer.²⁵⁻²⁶

CHAPTER 7

Size selected Au atomic clusters can be formed from the gas phase²⁷⁻²⁹ or liquid phase using solutions of chemically synthesised, atomically precise nanoclusters to deposit clusters on a surface with a narrow cluster size distribution.³⁰⁻³¹ The latter type of cluster has a cluster core protected by ligands. Removal of ligands from the cluster core is assumed to be an important step for making surface sites onto which the cluster adsorbs catalytically active. Chemical oxidation using KMnO_4 ³², oxygen plasma³³, and electron bombardment³⁰ can be used to remove ligands. The heat treatment under vacuum is effective to remove ligands for chemically synthesised and colloid Au clusters to enhance catalytic activity of Au clusters.³⁴⁻

36

Metal oxide surfaces are used as the support for clusters.³⁷ Titanium oxide is used widely as a support for metal based catalysts. For example, Haruta and co-workers discovered that Au nanoclusters react actively for low-temperature CO oxidation when supported with TiO_2 .³⁸ Titania is used as a support material due to chemical stability, low toxicity, high surface area and strong metal support interaction.³⁹ Surface pre-treatments have been explored to prevent Au cluster aggregation. In previous studies, oxide surfaces, such as P-25 and atomic layer deposited (ALD) titania, have been pre-treated in several ways including heat treatments, oxygen plasma treatment, calcination etc.^{26, 31, 40-41} Chemically synthesised atomically precise Au clusters deposited onto P-25 aerioxide pre-treated with eight different procedures and followed by post-treatments have been investigated using x-ray photoelectron spectroscopy (XPS).⁴¹ The study clearly illustrated the importance of support pre-treatment for control of Au nanocluster agglomeration and provides evidence that pre-treatment with H_2SO_4 is the most promising means for maintaining un-aggregated clusters under calcination and ozonolysis. Another study involves chemically synthesised atomically precise Au clusters deposited onto the surface of oxygen plasma pre-treated ALD titania and shows that heat treatment leads to agglomeration of Au clusters at higher loadings.²⁶ Therefore, acidic

pre-treatment ALD titania was used in this study to increase the strength of Au cluster bonds to the titania surface compared to plasma treated ALD titania, thus reducing agglomeration of clusters.

The aim of this work was to deposit chemically synthesised atomically precise Au clusters stabilised by triphenylphosphine ligands ($\text{Au}_9(\text{PPh}_3)_8(\text{NO}_3)_3$) (from now on abbreviated as Au_9) on an acidic pre-treatment ALD titania surface and determine electronic structure and chemical composition of samples before and after heat treatments under vacuum. MIES is a useful surface sensitive analytical technique to study the electronic structure of the sample surface specifically after removal of ligands. The substrate used in this research was acidic pre-treated ALD titania. XPS was used to study chemical composition of the sample surface and the size of Au clusters. We also aimed to investigate samples using the atomic force microscopy (AFM) technique, but the roughness after acidic treatment was too large to identify clusters on the ALD titania surface.

7.3 EXPERIMENTAL

1 molal sulphuric acid solution was prepared by mixing 50 ml of milliQ water (18 m Ω) and 4.9 g of concentrated sulphuric acid (sulphuric acid 98% (sun metals)). The samples were immersed into the sulphuric acid solution for 20 minutes, then rinsed with methanol (supragradient HPLC grade 99.9%, Scharlau) and dried in a stream of dry nitrogen. The sulphuric acid pre-treatment process increases the surface roughness of ALD titania to the dimension of single clusters. Thus, it is difficult to determine Au cluster distributions on titania surfaces via AFM.

The Au cluster methanol solution was prepared by varying concentration of Au clusters between 0.001 mM and 0.1 mM. For adsorbing Au clusters onto ALD titania, acidic pre-

treated substrates were immersed into Au cluster solutions for 30 minutes, rinsed with methanol and dried in a stream of dry nitrogen. This method has been used previously for depositing chemically made Au clusters with a highly homogeneous distribution over the surface.^{26, 42} The heat treatment was applied in UHV by ramping the temperature by 10 degree per minute to 200°C. The samples were kept at 200°C for 20 minutes.

Metastable Induced Electron Spectroscopy (MIES) was used to study valence electronic structure (i.e. density of states) of the outermost layer of deposited Au cluster samples. The organic polymer (P3HT and PCBM in the ratio 1:1) spin coated on silica wafer were used and taken in intervals of several hours to calibrate the intensity of the MIES source.

7.4 RESULTS AND DISCUSSION

7.4.1 XPS RESULTS OF Au₉ CLUSTERS ON ALD TITANIA

Peaks due to the elements gold, phosphorous, sulfur, titanium, carbon, silicon and oxygen were found in the survey spectra of the Au₉/ALD titania samples. High resolution spectra were taken for carbon (C 1s), titania (Ti 2p), gold (Au 4f), phosphorus (P 2p), sulfur (S 2p), silicon (Si 2p) and oxygen (O 1s). Intensity of the peak area is a measure for the amount of the respective element present on the surface. The majority of carbon on samples is either carbon of Au cluster triphenylphosphine ligands or adventitious hydrocarbons. Thus, the carbon peak can be used for calibration of the binding energy scale. The main C peak (C (1)) was set to 285eV corresponding to the C-C bond. The C 1s spectra were fitted with three peaks including the main carbon peak. Additional to the C-C peak, further C (2) species were found at 286.0 eV corresponding to a C-O or C-N bond (e.g. C-O-C⁴³) and at 289.4 ± 0.3 eV corresponding to C (3) in the O-C=O bond.⁴⁴ It should be noted that the nature of C (2) and C (3) is not exactly known. Figure 7.1 shows the experimentally measured carbon peak

with fitted peaks including Shirley background. The peak of silicon was found at 99.1 ± 0.2 eV due to using silica wafer as a substrate. The peak of oxygen was found at 530.4 ± 0.2 eV mostly due to titanium dioxide and also at 532.4 ± 0.2 eV due to silicon dioxide.

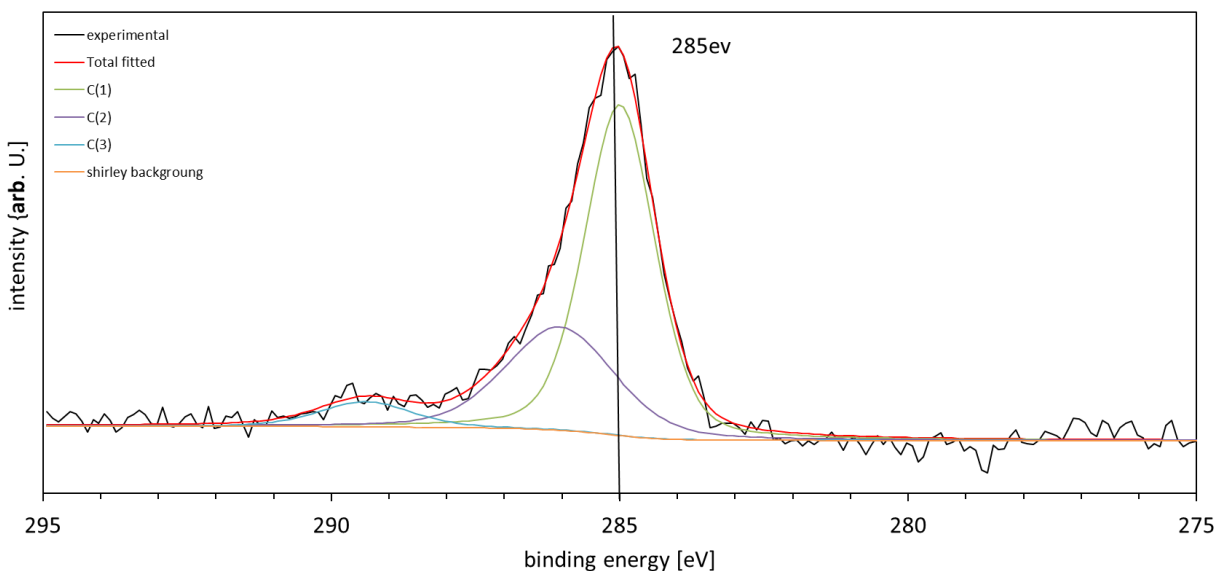


Figure 7.1: XPS spectra of carbon (calibration) with fitted peaks including Shirley background.

GOLD PEAKS BEFORE AND AFTER HEAT TREATMENT

Figure 7.2 shows the XPS Au-spectra of Au₉ clusters as deposited on acid pre-treated ALD TiO₂ for higher (0.1 mM Au₉) and lower (0.001 mM Au₉) loading. The Au peaks were fitted with the single higher binding peak (HBP). The HBP is at binding energy > 84.5 eV and LBP is at < 84.5 eV. This if there is only one single peak > 84.5 eV there is only one single HBP. The Au spectrum was fitted with two sets of $4f_{7/2}$ and $4f_{5/2}$ doublets and splitting was fixed at 3.67 eV.⁴⁵ For all Au spectra the background was slightly non-linear. This non-linearity has to be considered because Au are small compared to the background. Therefore, the regions right and left of the Au peaks were fitted with a third order polynomial. Figure 7.3 shows the Au peak position and FWHM of Au higher binding peak (Au-HBP) before heating for both concentrations. The Au peak positions were in the range of 85.3 ± 0.3 eV

and close to the binding energy found for deposited, non-agglomerated Au₉ clusters.^{31, 40, 46} The Au 4f_{7/2} peak of bulk Au was found at a binding energy of 84 within a range of ± 0.2 eV.⁴⁷⁻⁵⁰ This value was used to determine the shift between Au 4f_{7/2} of Au clusters and binding energy of the bulk Au. This shift was attributed to the final state effect found for isolated Au₉ clusters. The HBP FWHM of different concentrations of Au clusters is almost constant but larger than the FWHM of the LBP and in the range of 1.8 ± 0.2 eV. The broader FWHM was attributed to the final state effect.³¹ The atoms in the cluster react differently in the final state effect causing the broadening. This is a second indication that Au clusters did not agglomerate. Furthermore, 0.001 and 0.006 mM concentrations had low Au peak intensity.

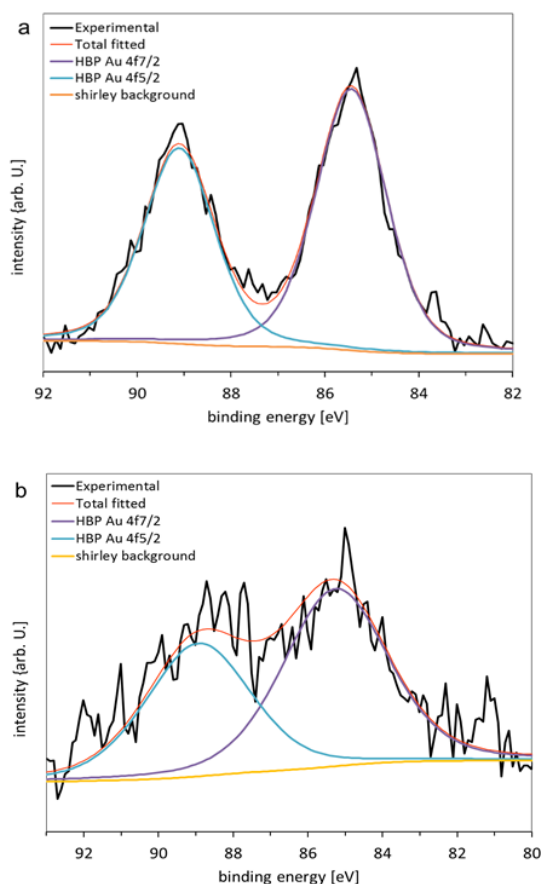


Figure 7.2: Au XP spectra of deposited Au cluster before heating for (a) 0.1 mM and (b) 0.001 mM.

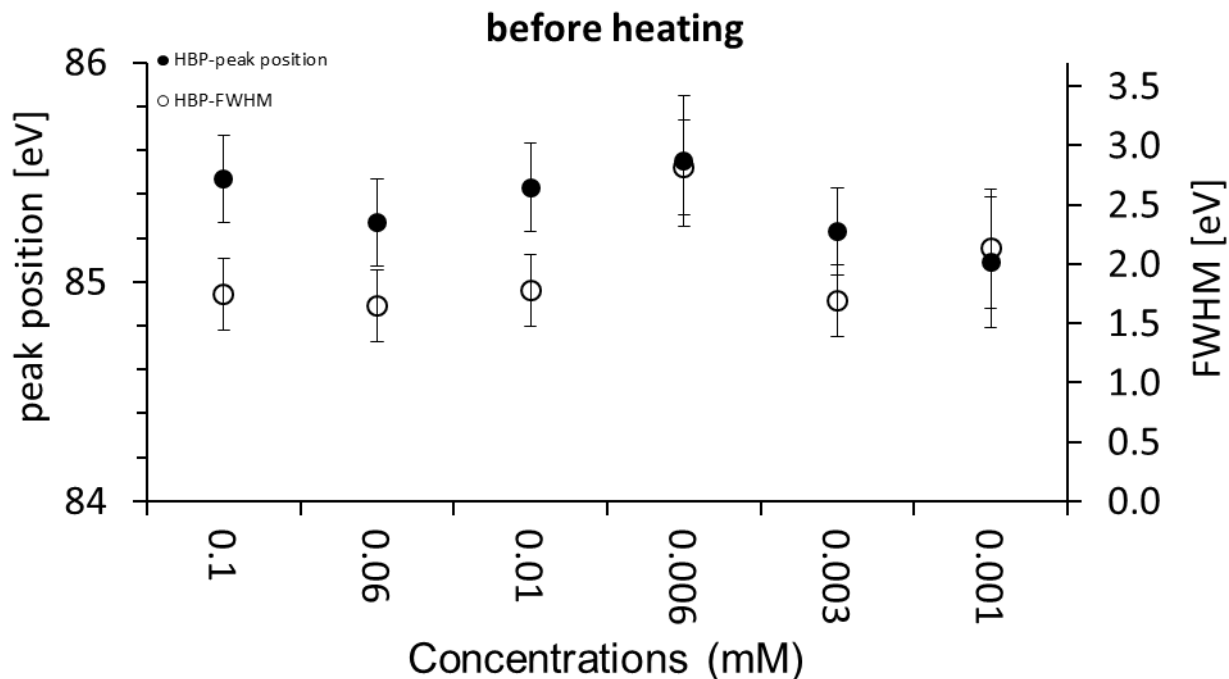


Figure 7.3: Au-HBP position and FWHM for all Au₉ concentrations before heating.

Figure 7.4 shows the Au 4f spectra of heated samples for high (0.1 mM Au₉) and low loading (0.001 mM Au₉). At high loading, it is clear that two doublets are required to fit the experimental spectra (Figure 7.4a), while only one doublet is needed for fitting the low loading spectrum (Figure 7.4b). The Au peak positions and FWHM of deposited Au clusters after heat treatment are shown in Figure 7.5. The peak positions of Au lower binding peak (Au-LBP) were found in the range of 84.3 ± 0.2 eV. The FWHM of these peaks is 1.2 ± 0.2 eV, which is smaller than that of Au clusters before heat treatment. We attribute the decrease in binding energy (Au-LBP) after heating to agglomeration of Au clusters. The HBP-Au peaks were found in the range of 85.4 ± 0.4 eV across all concentrations. The FWHM of these peaks is similar to that of deposited Au clusters. The binding energy of HBP-Au peaks was attributed to the final state effect found for isolated Au₉ clusters. Au-HBP increases slightly after heat treatment due to the cluster core interacting with substrate formation of Au-O bonds, but not fully oxidised Au clusters³¹ as the shift in peak position was

significantly less than the +2 eV shifts reported by others.⁵¹⁻⁵² The spectra of 0.001 and 0.006 mM concentrations could not be fitted with two separate peaks because the intensity peaks were small. Thus, there was only one fitted peak of lower energy than HBP-Au for other concentrations. The values of peak positions, FWHM and intensity of different concentrations of Au clusters before and after heating are shown in Table 7.1.

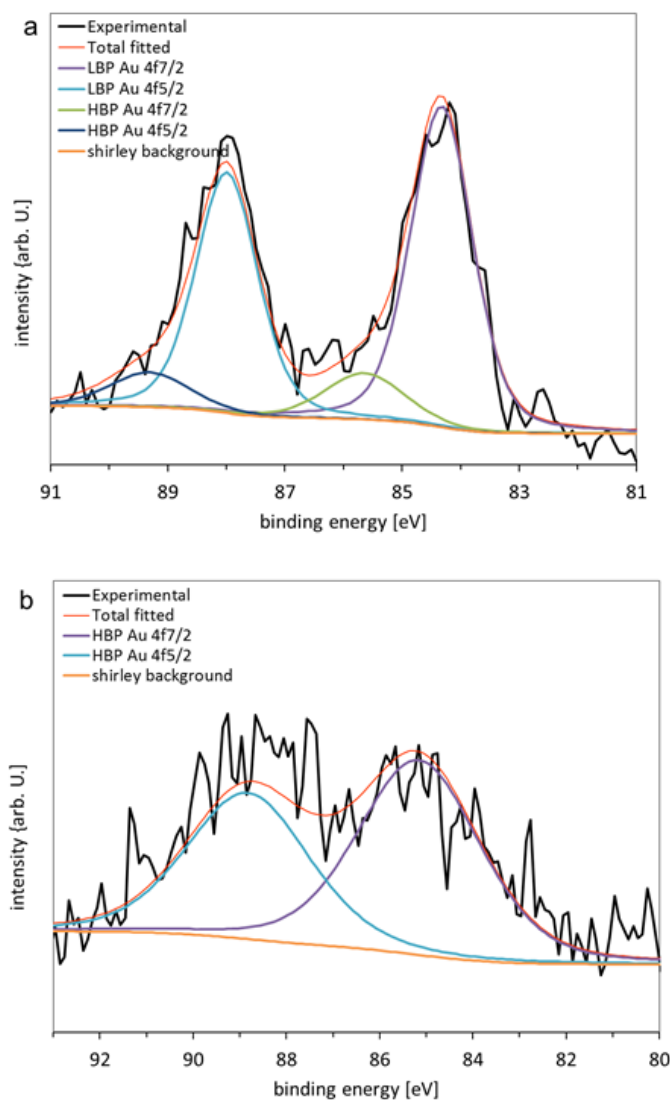


Figure 7.4: Au XP spectra of deposited Au cluster after heating for (a) 0.01 mM and (b) 0.001 mM loading.

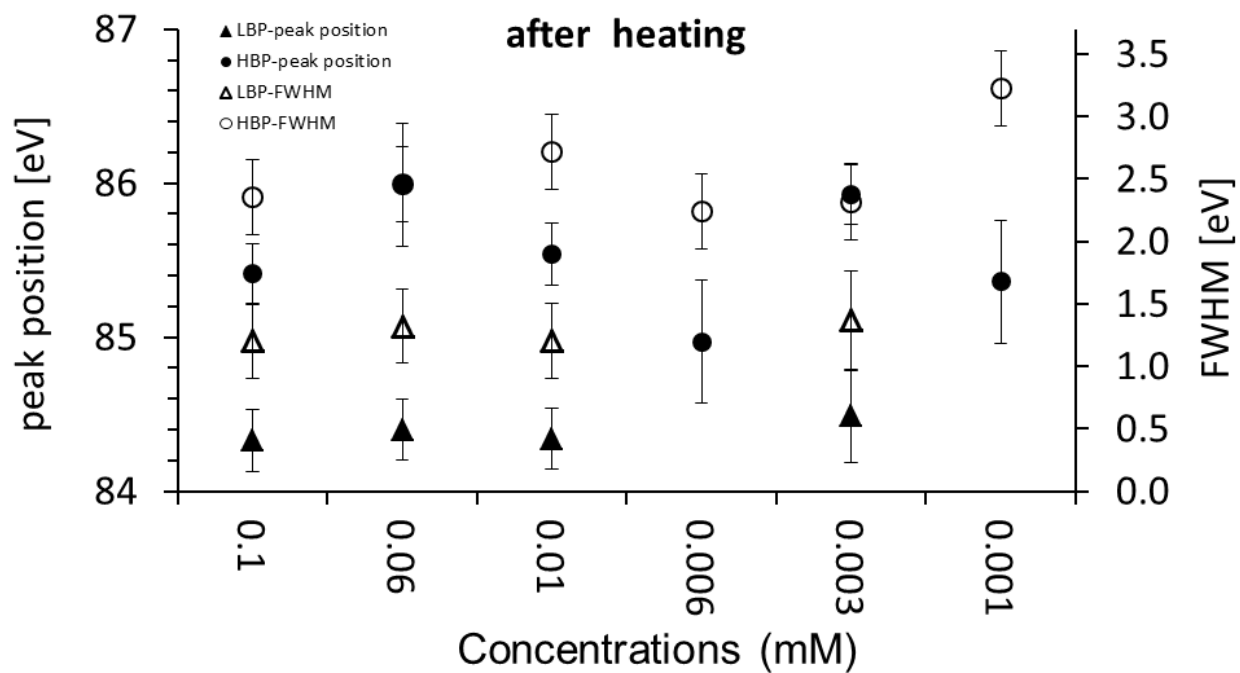


Figure 7.5: Au-LBP and Au-HBP position and FWHM for all Au₉ concentrations after heating.

Table 7.1: The values of Au-LBP and Au-HBP position and FWHM for all Au₉ concentrations.

Au	Before heating		After heating			
Concentration (mM)	Peak position Au-HBP (eV)	FWHM Au-HBP (eV)	Peak position (eV)		FWHM (eV)	
			Au-LBP	Au-HBP	Au-LBP	Au-HBP
0.1	85.4 ± 0.2	1.7 ± 0.3	84.3 ± 0.2	85.4 ± 0.2	1.2 ± 0.3	2.3 ± 0.3
0.06	85.2 ± 0.2	1.7 ± 0.3	84.4 ± 0.2	85.9 ± 0.4	1.3 ± 0.3	2.4 ± 0.3
0.01	85.4 ± 0.2	1.5 ± 0.3	84.3 ± 0.2	85.5 ± 0.2	1.2 ± 0.3	2.7 ± 0.3
0.006	85.5 ± 0.3	2.8 ± 0.4	-	85.0 ± 0.4	-	2.2 ± 0.3
0.003	85.2 ± 0.2	1.7 ± 0.3	84.4 ± 0.2	85.9 ± 0.2	1.4 ± 0.4	2.3 ± 0.3
0.001	85.1 ± 0.3	2.1 ± 0.5	-	85.3 ± 0.4	-	3.2 ± 0.3

PHOSPHORUS PEAK BEFORE AND AFTER HEAT TREATMENT

In Figure 7.6, the P spectrum of deposited Au clusters after heat treatment is shown. The experimental peak of P is fitted with the phosphorus lower binding peak (P-LBP) single peak at 132.3 ± 0.2 eV. The P spectrum fitted with one set of $2p_{3/2}$ and $2p_{1/2}$ doublet and the

splitting was fixed at 0.84 eV.⁴⁵ The P peak positions and FWHM of deposited Au clusters after heat treatment are shown in Figure 7.7. The P peak positions here is the same as reported in our previous studies.^{31,40} Hence, P-LBP is attributed to the phosphorus attached to the Au clusters. For some concentrations, the peak in the P spectra were rather small and fitting of the peaks resulted in a large uncertainty.

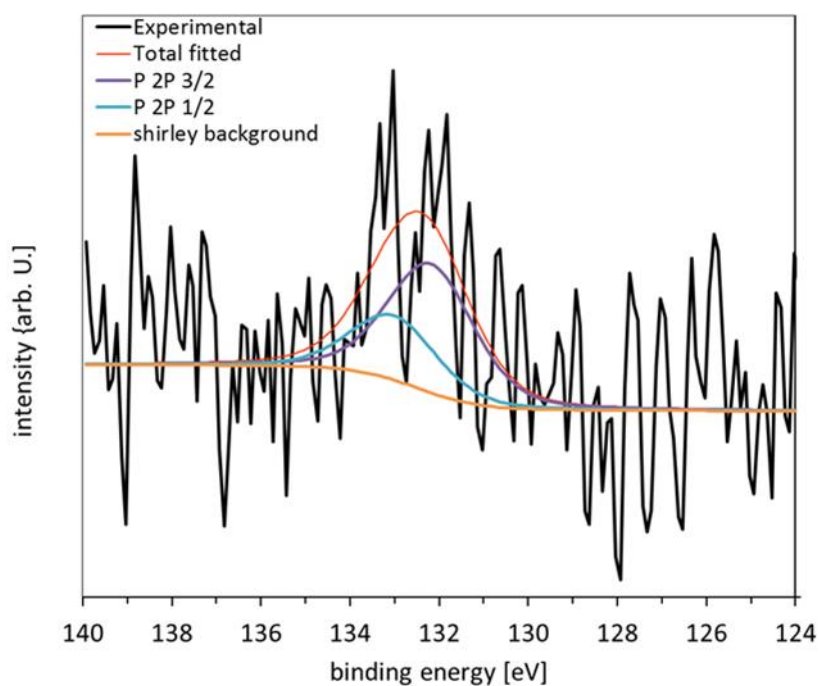


Figure 7.6: P XPS spectrum of deposited Au cluster before heating.

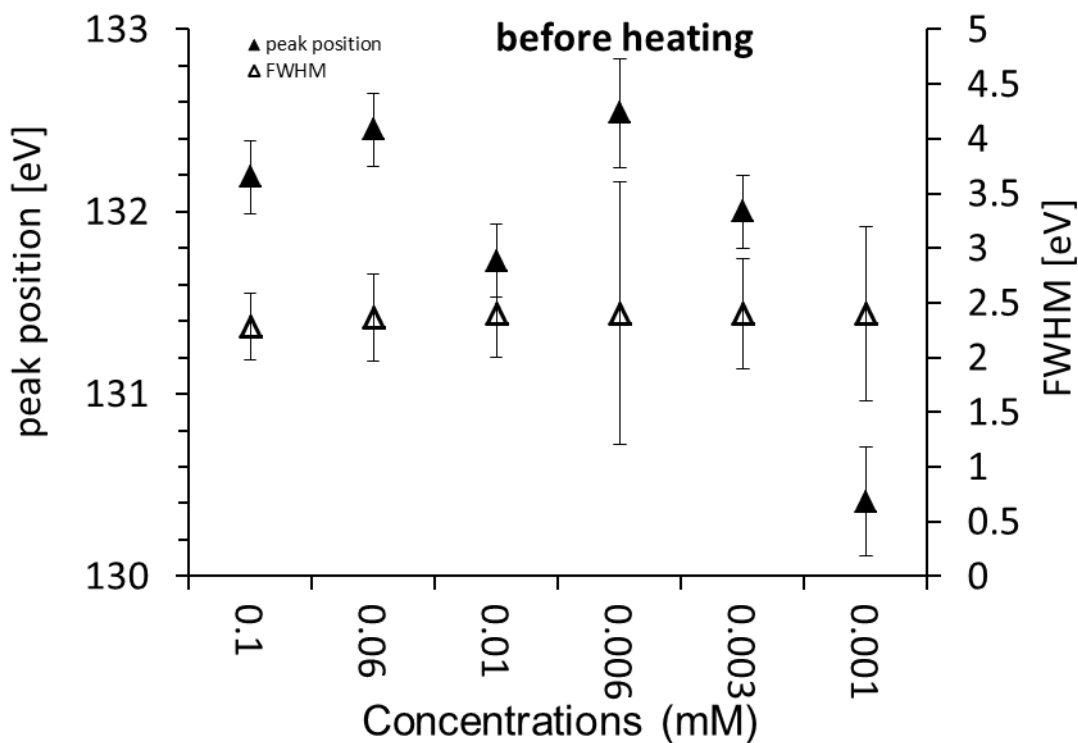


Figure 7.7: P-LBP position and FWHM for all Au₉ concentrations before heating.

Figure 7.8 shows the peak positions and FWHM of phosphorus after heat treatment. For all concentrations, ligands were removed from the Au cluster core and left the sample after heating except for 0.06 and 0.003 mM concentration samples. The spectra of these two samples showed traces of ligands remaining after heating. In these spectra, P-LBP is the dominant form and for a contribution of the phosphorus higher binding peak (P-HBP) at 133.1 ± 0.2 eV describing oxidised phosphorous cannot be identified. The peak positions, FWHM and intensity of phosphorus of various concentrations before and after heating are given in Table 7.2.

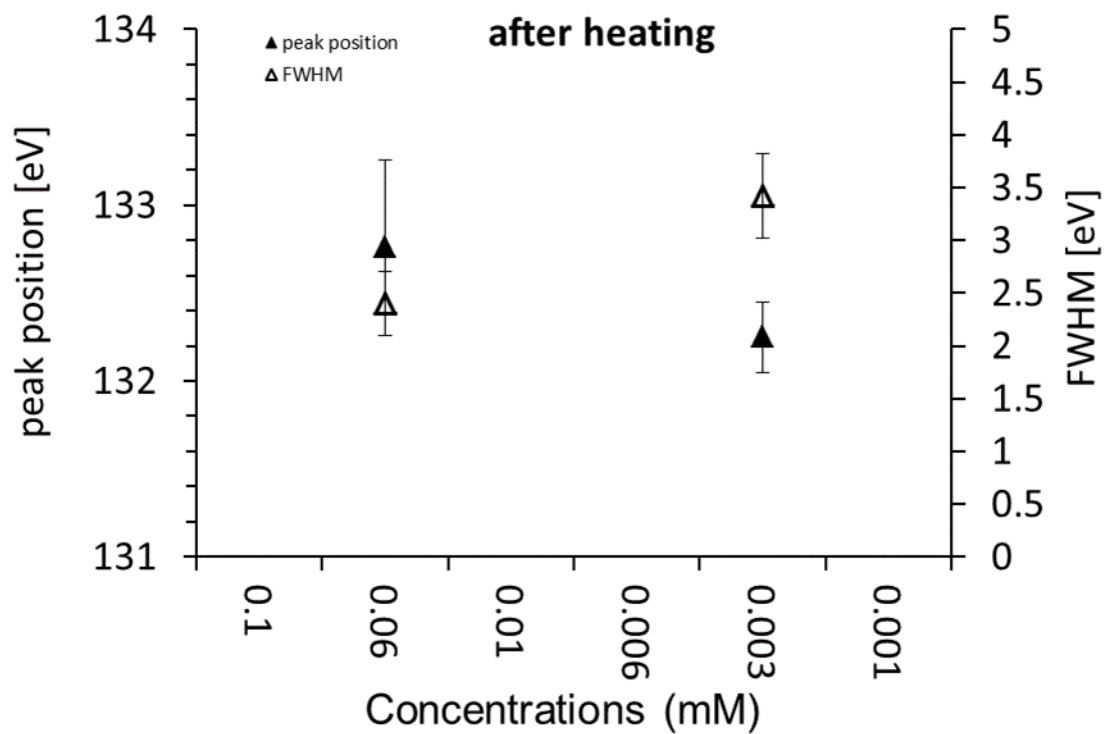


Figure 7.8: *P-LBP position and FWHM for all Au₉ concentrations after heating. The ligands were removed completely after heating treatment except for these two concentrations.*

Table 7.2: The values of P-LBP position and FWHM for all Au₉ concentrations.

Phosphorus	Before heating		After heating	
Concentration (mM)	Peak position (eV)	FWHM (eV)	Peak position (eV)	FWHM (eV)
0.1	132.2 ± 0.2	2.3 ± 0.3	-	-
0.06	132.4 ± 0.2	2.3 ± 0.4	132.7 ± 0.5	2.4 ± 0.3
0.01	131.7 ± 0.2	2.4 ± 0.4	-	-
0.006	132.5 ± 0.3	2.4 ± 1.2	-	-
0.003	132.0 ± 0.2	2.4 ± 0.5	132.2 ± 0.2	3.4 ± 0.4
0.001	130.3 ± 0.3	2.4 ± 0.8	-	-

The ratio intensity of phosphorus to Au should be less than unity since the number of triphenylphosphine ligands attached to the Au cluster surface is less than the number of Au atoms in (Au₉ (PPh₃)₈(NO₃)₃) clusters. Figure 7.9 shows the ratio of P-LBP to the sum of the Au 4f signal and that it is larger than unity. Peak intensities for both Au and P were quite small and uncertainty in the ratios very large. The phosphorus was completely removed from the majority of samples after heat treatment. Therefore, the ratio intensity of phosphorus to Au after heat treatment dropped below the ratios of untreated samples.

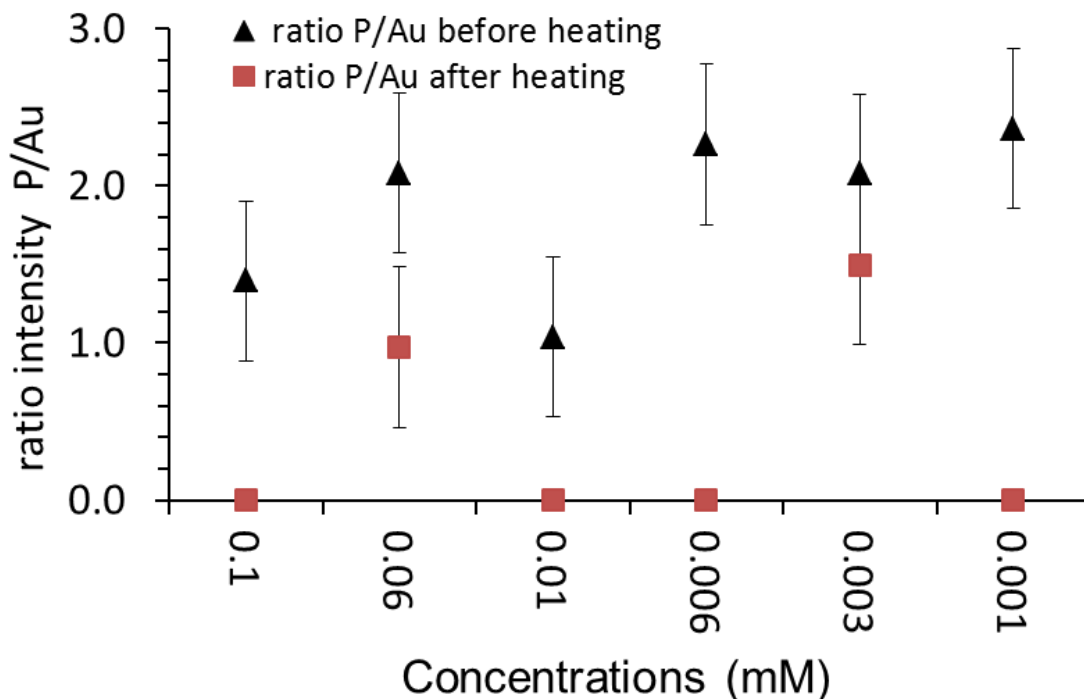


Figure 7.9: Ratio of the intensities of P-LBP to the sum of respective Au peak intensities (i.e. the sum of Au-LBP and Au-HBP).

TITANIA PEAKS BEFORE AND AFTER HEAT TREATMENT

Figure 7.10 shows experimental Ti-spectra for deposited Au clusters before and after heat treatments. The Ti spectrum was fitted with one set of $2\text{Ti}_{3/2}$ and $2\text{Ti}_{1/2}$ doublet. The peak positions of titania are usually found around 459.0 ± 0.2 eV before and after heat treatment. Figure 7.11 shows the intensity ratio of Au with respect to titania with the larger concentration of Au corresponding to larger coverage of Au on the titania surface. Coverage of Au on the titania surface was the same before and after heat treatment which confirms that coverage of Au on the titania surface depends on Au concentration. The amount of Au decreased after heat treatment for both 0.1 and 0.01 mM concentrations due to significant aggregation of Au clusters.

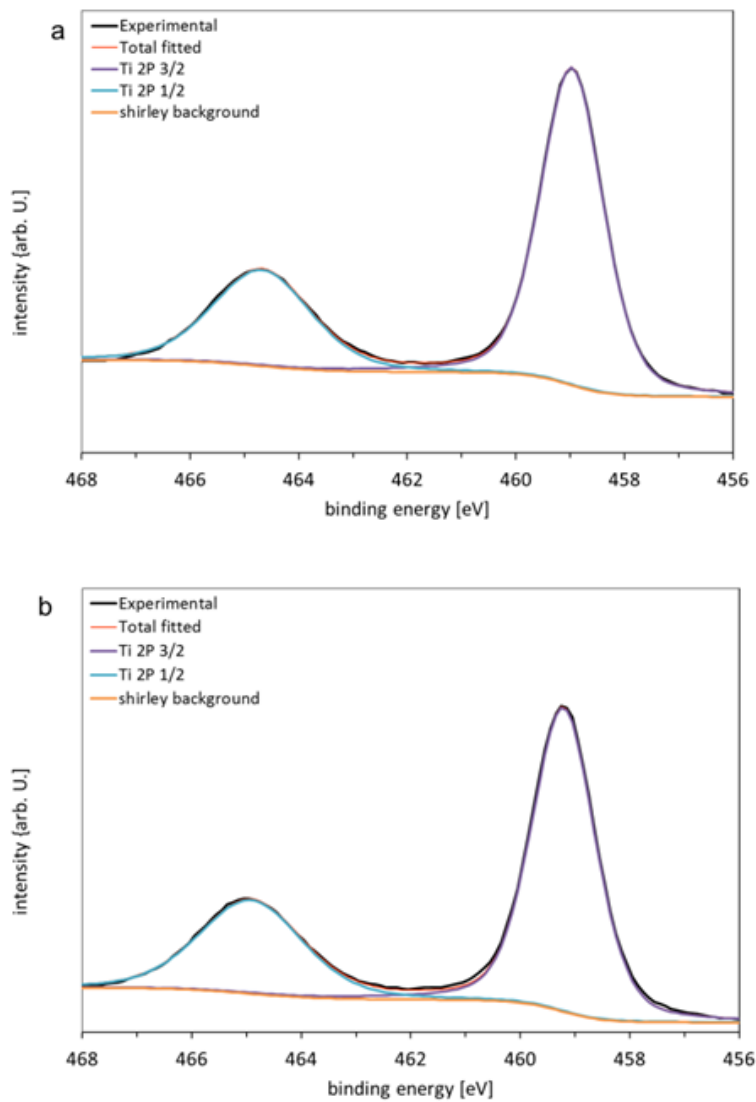


Figure 7.10: Ti XP spectra of deposited Au cluster sample (a) before and (b) after heating.

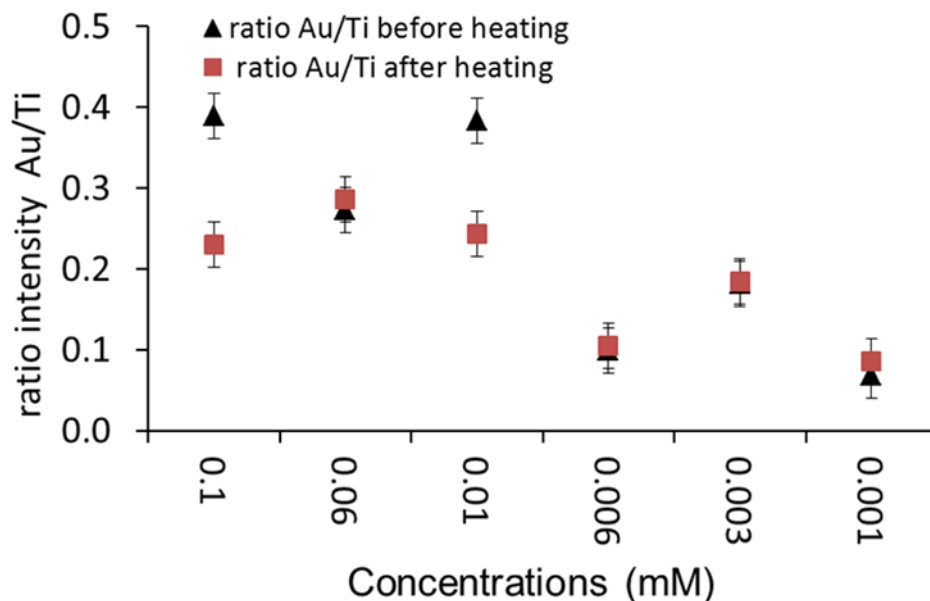


Figure 7.11: Ratio of the intensities of the sum of Au peak intensities to Ti intensity.

SULFUR PEAKS BEFORE AND AFTER HEAT TREATMENT

The peak of sulphur was found at 169.0 ± 0.2 eV before heating (Figure 7.12a) and at 169.3 ± 0.2 eV (Figure 7.12b) after heat treatment due to treatment of the titania support with H_2SO_4 prior to deposition of clusters. The S spectrum was fitted with one set of $2S_{3/2}$ and $2S_{1/2}$ doublet. Figure 7.13 shows the intensity ratio of sulphur with respect to titania before and after heat treatment. The amount of sulphur on the titania surface decreased after heat treatment. Sulphur on the titania surface partially evaporated during heat treatment. In Figure 7.14, coverage of Au clusters increases proportionally to coverage with sulphur. Therefore, it can be assumed that the acid pre-treatment binds Au clusters on the titania surface

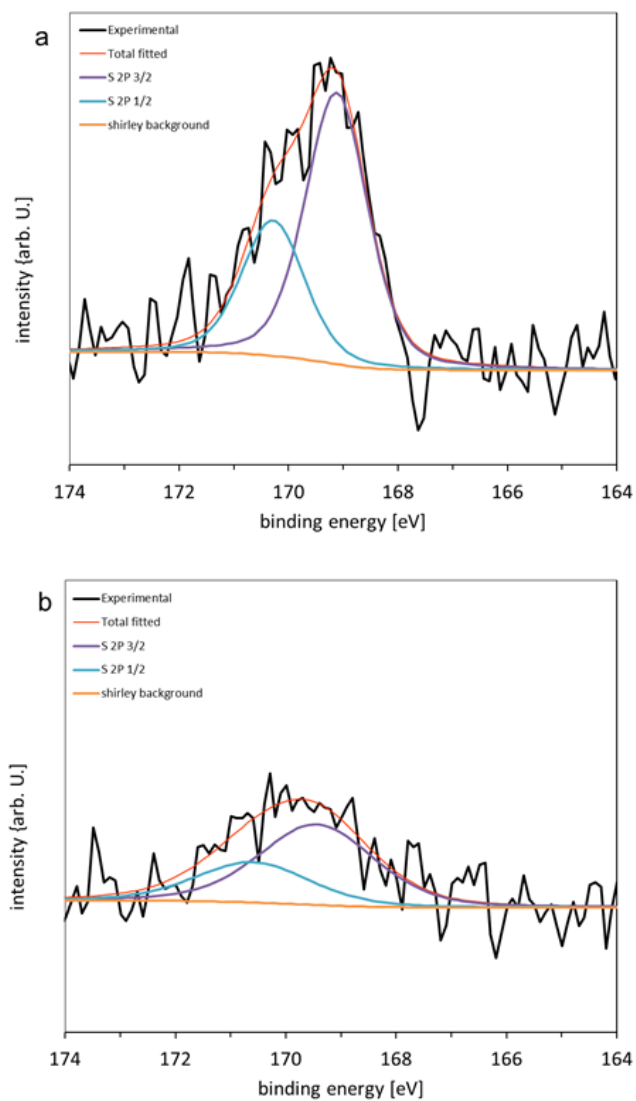


Figure 7.12: S XPS spectra of deposited Au cluster sample (a) before and (b) after heating.

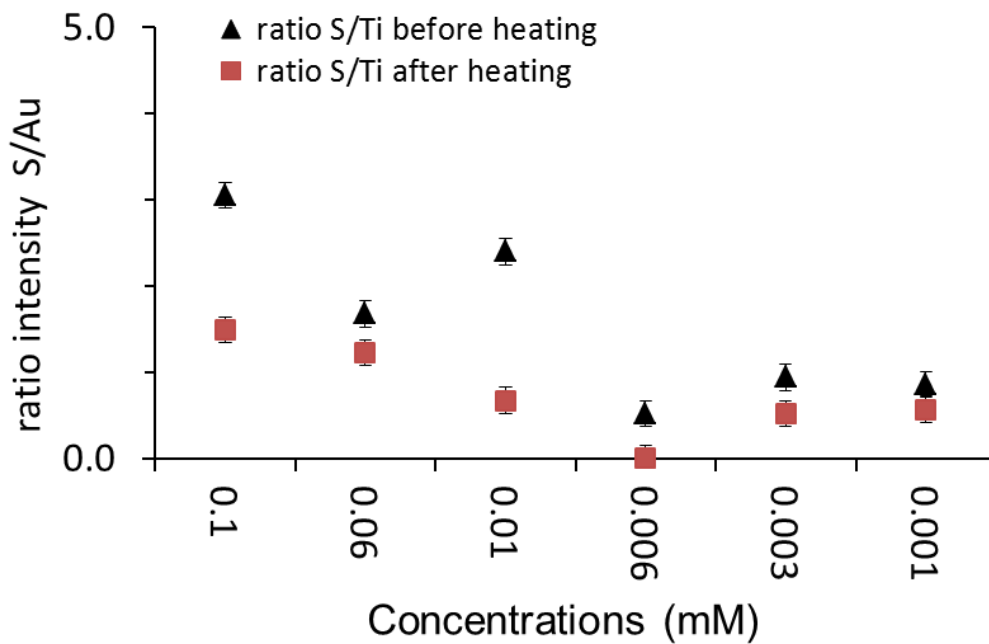


Figure 7.13: Ratio of intensities of the S peak to intensities of Ti peak.

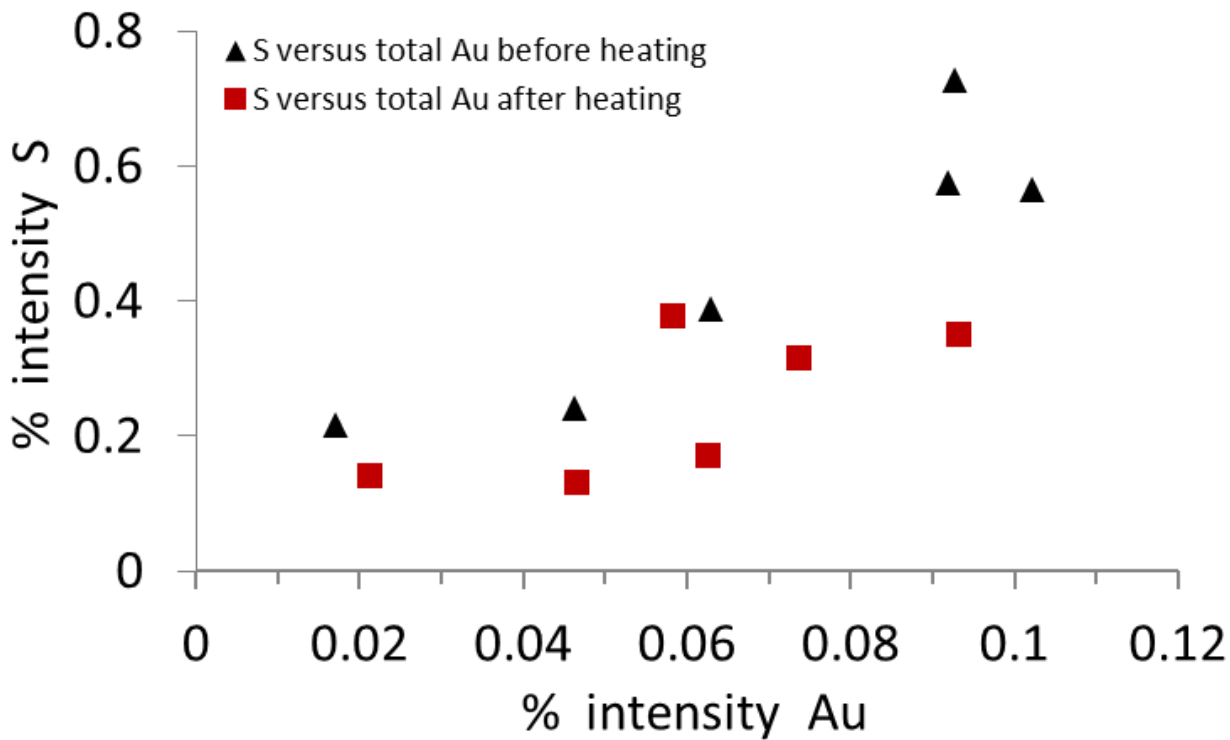


Figure 7.14: Relative intensities of the S peak to the sum of intensities of respective Au peaks.

In summary, based on the final state effect found in Au XPS results, it can be concluded that Au₉ clusters deposited on acid pre-treated ALD titania are individual clusters. Before heating, ligands are attached to Au cluster cores. After heating, the 4f_{7/2} Au binding energies were found at ~ 84 eV (due to agglomerated clusters) and ~ 85.5 eV. The slight increase of Au-HBP after applying heat treatment could be attributed to cluster cores interacting with the substrate. The stabilised ligands de-attach from Au cluster cores and at least partially leave the samples. The acid pre-treated TiO₂ with H₂SO₄ solution increased the concentration of the hydroxyl group on TiO₂ surfaces compared with bare TiO₂ which generated a Brønsted acid on the surface.⁵³⁻⁵⁴ These sulphate ions on TiO₂ surfaces create unbalanced charges on Ti and vacancies and defects in the TiO₂ network.⁵⁵ It was found that Au particles strongly bind to TiO₂ defect rich surfaces after acidic pre-treatments.⁵⁶ In our experiments, we found that the amount of Au increases with the amount of sulphur on samples leading to the conclusion that sulphuric acid supports attachment of Au clusters to titania.

7.4.2 MIES RESULTS OF AU₉ CLUSTERS ON ALD TITANIA

The MIE spectra were analysed by the singular value decomposition (SVD) algorithm. The details of the procedure were described previously in Chapter 3.2 and here a brief summary of the method is provided. The procedure for the evaluation of the MIES spectra was as follows:

1. Determination of the number of base spectra required to fit the experimentally measured spectra using SVD algorithm.
2. Determination of meaningful reference spectra.
3. Interpretation of the nature of reference spectra.

1. Determining the number of required base spectra using singular value decomposition algorithm:

This step determined the number of base spectra required to fit the entire measured MIES spectra. The singular value decomposition (SVD) analysis of the MIES spectra of the sample heated to 200°C for 20 minutes revealed that the number of base spectra required for fitting the entire measured spectra was three.

2. Determining the meaningful reference spectra:

The second step determined the reference spectra that define physically meaningful surfaces. We found that three reference spectra were needed to describe the entire set of measured spectra in the first step. The reference spectrum was inferred by comparing the shape of MIE reference spectra with existing reference spectra and by comparing the course of relative XPS intensities with MIES weighting factors.

3. Interpretation of the nature of the reference spectra:

Figure 7.15 shows the three reference spectra reconstructed from the series of seven MIES spectra (Figure 7.16) as a result of applying the SVD algorithm. All MIES spectra have been fitted with these 3 reference spectra and this is a quite strong constraint. Samples prepared by immersing substrates in Au₉ solution with a concentration between 0.1 and 0.001 mM were fitted with three reference spectra to adequately fit SVD analysis. The fit of the 0.06 mM spectrum with the three reference spectra is shown as an example in Figure 7.17. The 0.06 mM sample fitted well with the three reference spectra within experimental uncertainty. It should be noted that the secondary electron background was not considered in the SVD procedure and spectra are fitted at energies < 12 eV only. The reason is that the secondary

electron background in shape and intensity does not necessarily change linearly with the composition of the outermost layer.

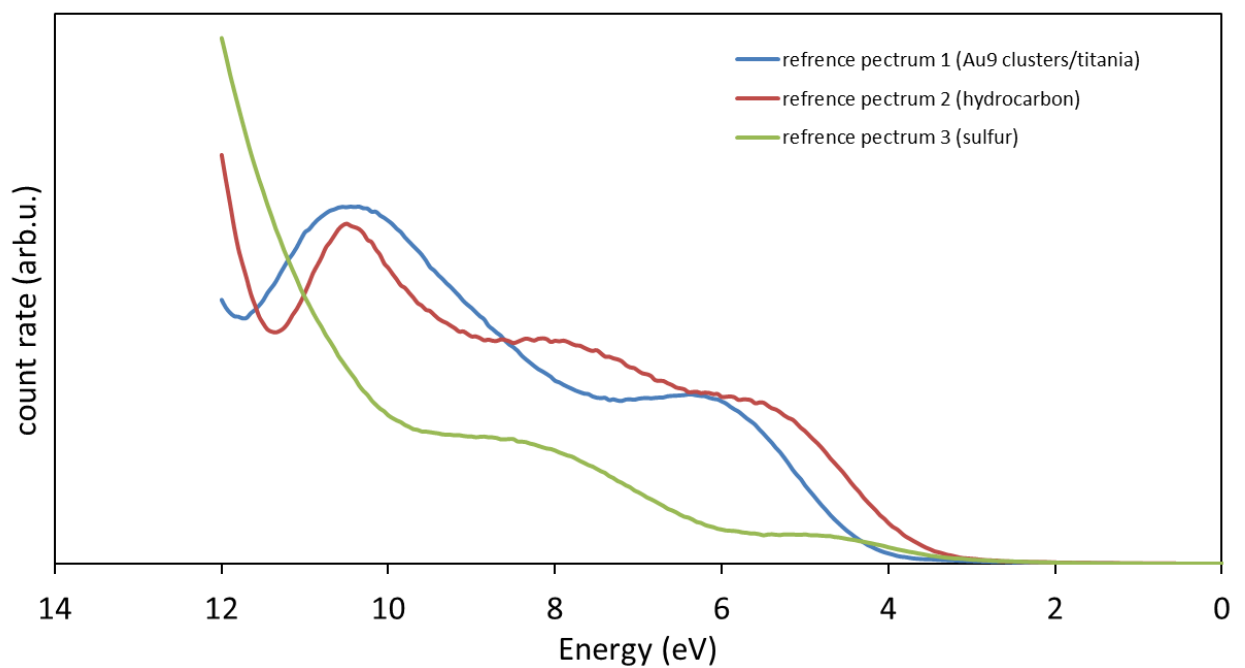


Figure 7.15: Reference spectra for fitting the series of Au₉/titania MIE spectra including the bare titania resulting from the singular value decomposition (SVD) algorithm.

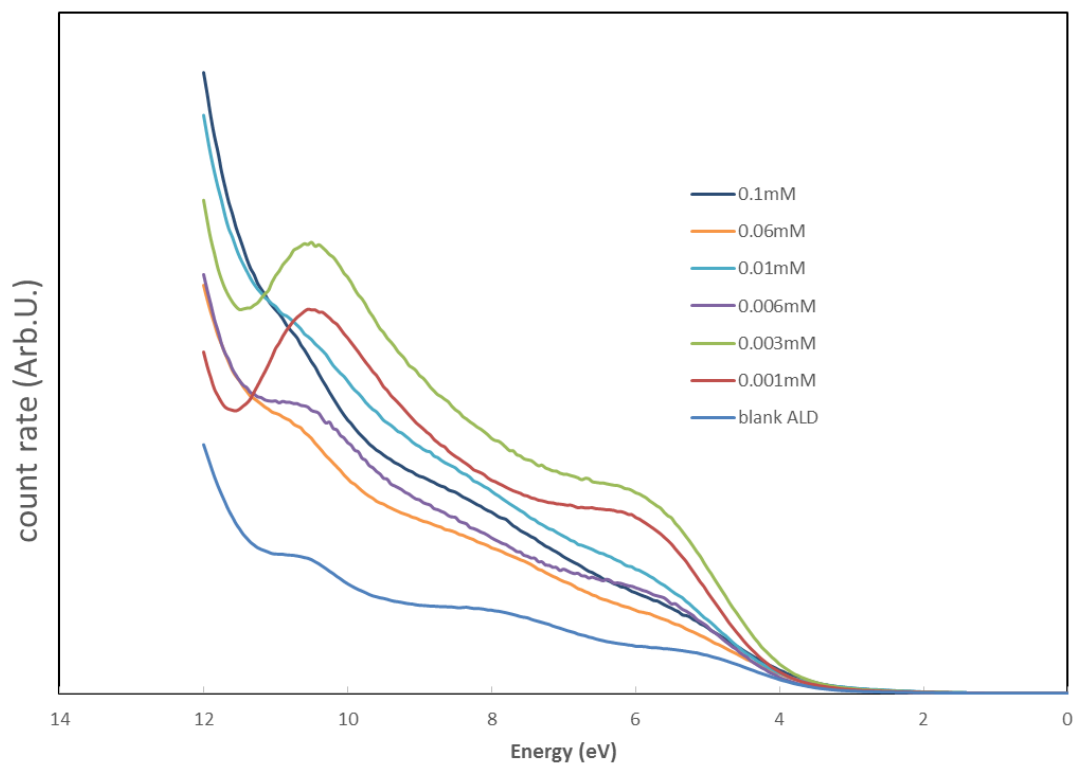


Figure 7.16: MIE experimental spectra of Au_9 clusters deposited on ALD titania heated to $200^\circ C$.

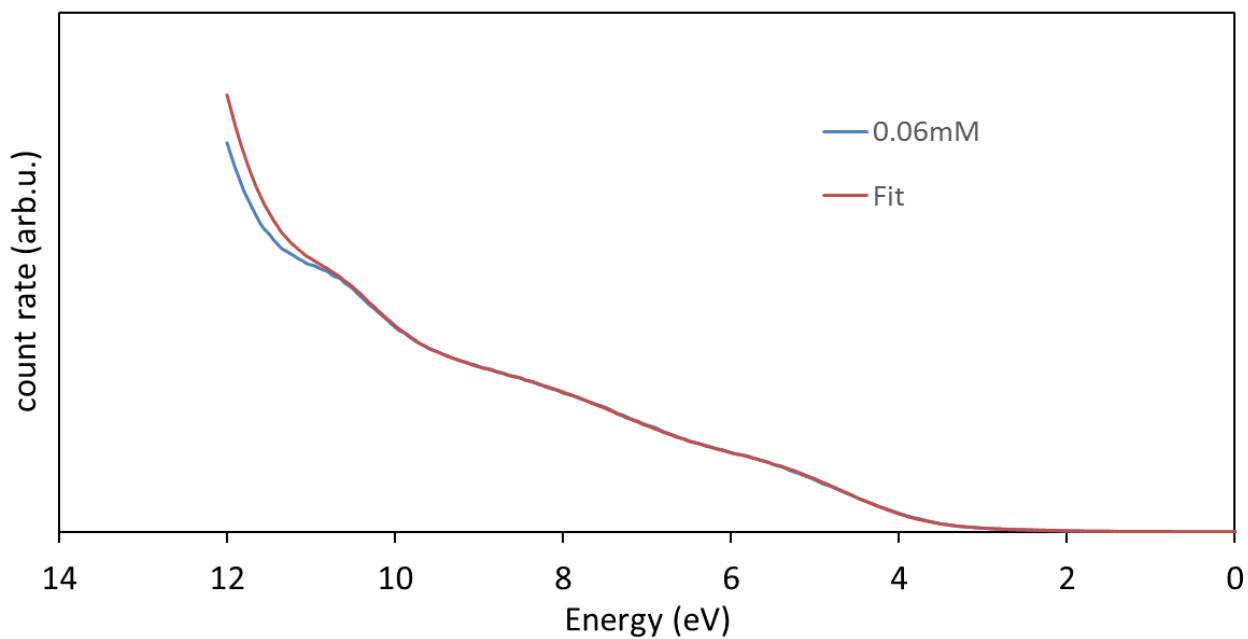


Figure 7.17: Fits of the ALD titania sample immersed into the 0.06 mM Au_9 solution and subsequently heated to $200^\circ C$ using all three reference spectra.

a. First reference spectrum

Figure 7.18 shows that a significant contribution of the weighting factor for reference spectrum 1 appears only in samples deposited from solutions within the concentration range of 0.001 to 0.1 mM and not in the blank sample. Figure 7.18 also shows that the intensity of XPS of HBP-Au clusters with experimental uncertainty as a function of Au₉ solution concentration coincides approximately with the shape of the weighting factor for reference spectrum 1. Agglomerated Au cluster XPS intensity (LBP-Au) does not follow the MIES weighting factors, while the individual Au₉ clusters (HBP-Au) does. The reason is that the ratio of the surface area affected by the presence of small Au clusters to the amount of Au in these small Au clusters is much larger for small clusters than for large clusters.

Figure 7.19 shows a comparison between Au reference spectrums measured in our previous study²⁶ with the current reference spectrum attributed to the presence of Au clusters on ALD titania. The general shape of these spectra shows similarities and differences. There are peaks at positions with similar binding energies at ~ 4.5, 5 and 8 eV in both Au reference spectra. The peak at 6 eV in the reference spectrum from²⁶ does not appear in the current Au spectrum. Despite the difference between the two spectra, we propose that the current first spectrum is close to our published Au spectrum.

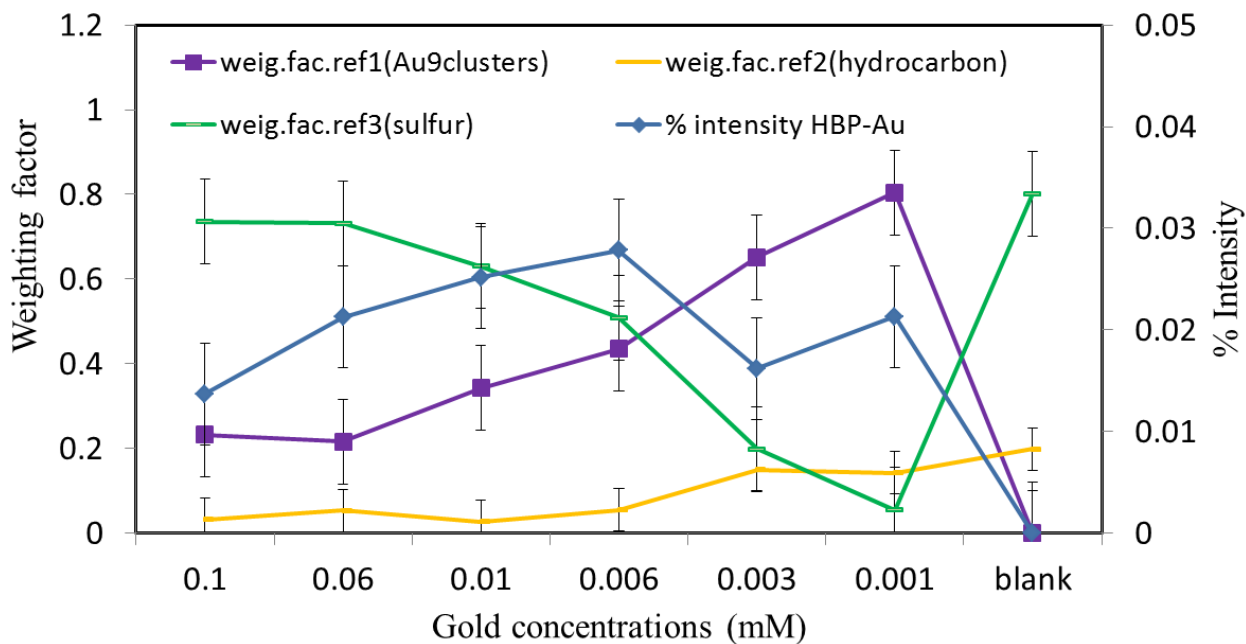


Figure 7.18. Weighting factors of the reference spectra for fitting the MIE spectra of the Au/ALD titania heated to 200°C together with Au-HBP intensity measured by XPS.

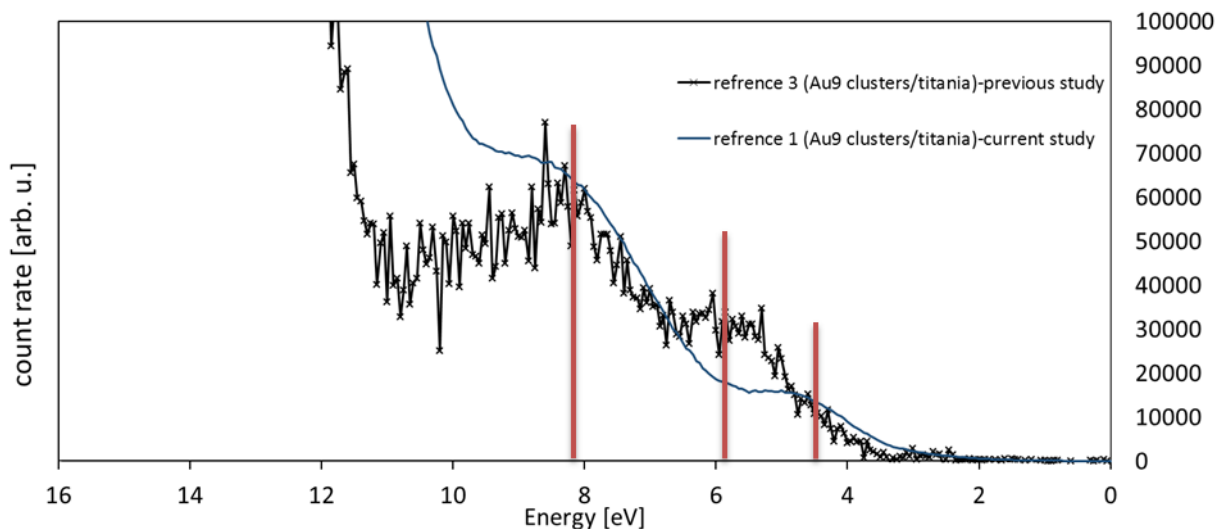


Figure 7.19: Comparison of the reference spectra of Au in our previous study²⁶ with the current reference spectrum.

b. Second reference spectrum

Figure 7.20 shows the second reference spectrum corresponding to hydrocarbons. This conclusion was drawn because the intensity of carbon in XPS is approximately proportional to the weighing factor for reference spectrum 2. The only exemption is the blank sample. In

this current study, we used carbon (C) for MIES-XPS correlation. In an earlier publication the correlation between P XPS and the reference spectra were considered. In this current study, we used C for MIES-XPS correlation and not phosphorous (P) as P XPS intensity is too low. Also, the reference spectrum PPh₃ ligands is not very different to the adventitious carbon.

Figure 7.21 shows a comparison between ligand reference spectrums measured in our previous study²⁶ with a current hydrocarbon reference spectrum. The features of both spectra are in reasonable agreement. There are three pronounced peaks at ~ 5, 8 and 11 eV. The hydrocarbon spectrum has higher intensity at 11eV compared with the ligand spectrum. The peak around 6 eV is missing in the hydrocarbon spectrum. It must be emphasised that the relative contributions of peaks to both spectra are different.

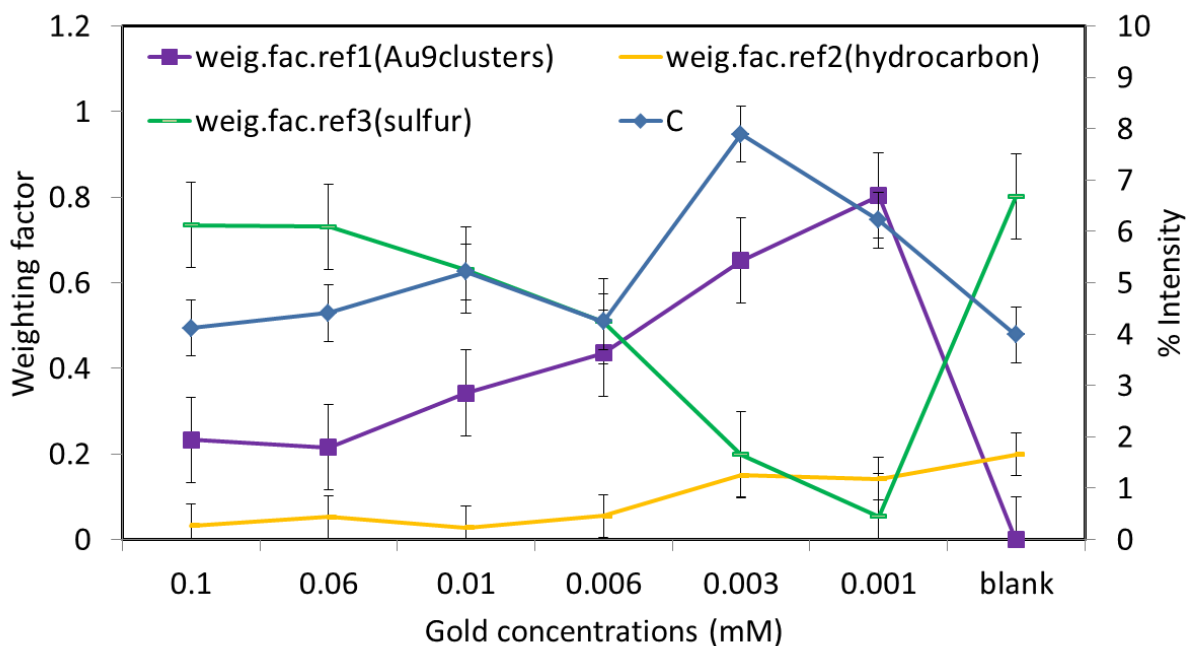


Figure 7.20: Weighting factors of reference spectra for fitting the MIE spectra of Au₉/ALD titania heated to 200°C together with C intensity measured by XPS.

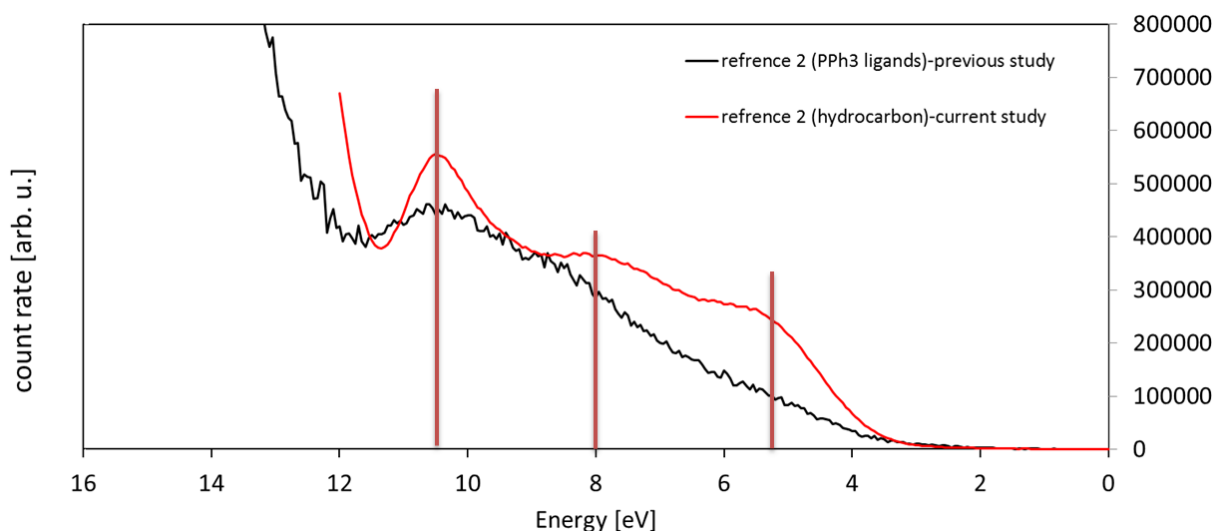


Figure 7.21: Comparison of the reference spectra of PPh_3 in our previous study²⁶ with the current spectrum.

c. Third reference spectrum

Figure 7.22 shows that the XPS intensity of sulphur generally follows the course of the weighting factors of reference spectrum 3. Therefore, the third reference spectrum is attributed to sulphuric acid attached to titania resulting from the acidic pre-treatment. In the previous study, the remaining reference spectra was a spectrum of bare titania²⁶ where the titania surface was not pre-treated with acid, but was treated with oxygen plasma. Thus, it is assumed that a spectrum of bare titania was found in the previous study, but not in the present study. The procedure used to determine the reference spectra in²⁶ was different to the approach taken here. In²⁶ the third reference spectrum in the first step of the fitting procedure was neglected and considered in the second step of data fitting and was thus treated as a small perturbation for the two main reference spectra. However, in this work all three reference spectra were taken into account in the same way.

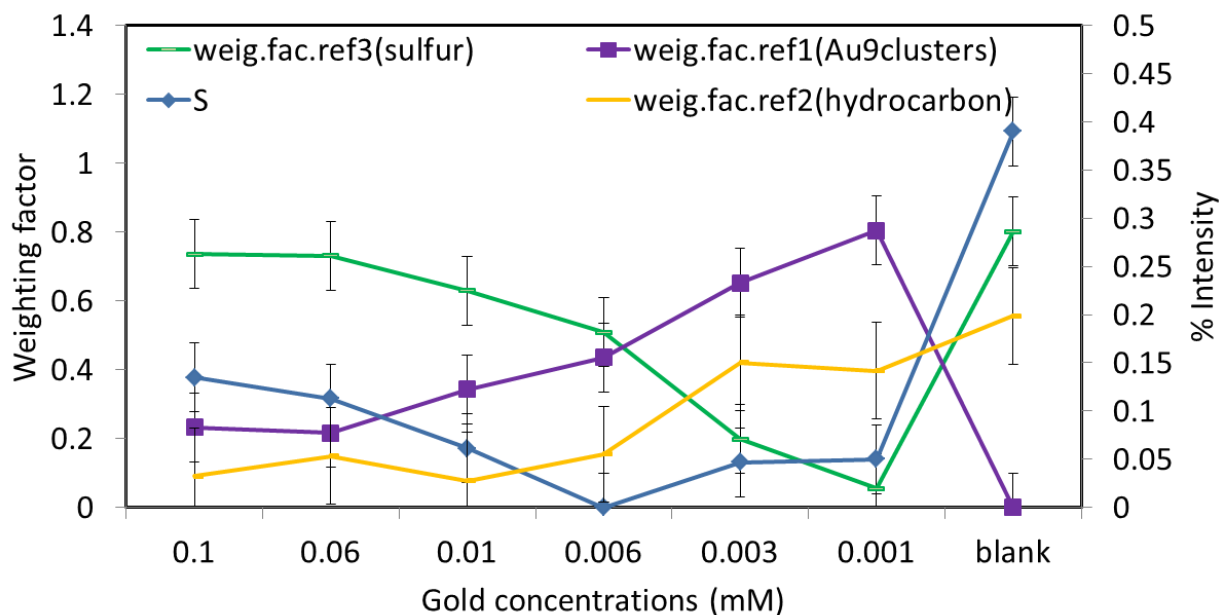


Figure 7.22: Weighting factors of the reference spectra for fitting the MIE spectra of the Au₉/ALD titania heated to 200°C together with S intensity measured by XPS.

It was discussed early in the XPS summary that sulphuric acid helps binding of clusters to the titania surface. The first reference spectrum required to fit the series of spectra with titania between 0.001mM to 0.1 mM is non-agglomerated clusters found after heating. Reference spectrum 1 is an important finding since the interface between Au clusters and titania is vital in understanding the electronic properties of the titania surface with adsorbed Au clusters which potentially plays an important role in catalytic activity.⁵⁷ For catalytic performance, it has been shown that sulphuric acid de-activated the catalytic reaction, such as CO oxidation.⁵⁸ It indicated that the SO₂ can block the active sites for CO oxidation on an Au based catalyst. It was shown in our previous study²⁶ that heating of Au₉ clusters deposited on titania leads to a reaction of ligands with the titania surface.

Coverage of plasma treated ALD titania with Au was approximately three times lower than in the present case (Au/Ti ratio in²⁶ below 0.1 and Au/Ti ration 0.3 here). In the study applying sputtering as pre-treatment of ALD titania substrates⁵⁹, the Au/Ti ratio was ~0.87

which is higher than the ratio in the current study. We show that Au coverage of acid treated titania is central between plasma treated ALD titania and sputter treated.

7.5 CONCLUSION

Chemically synthesised atomically precise phosphine protected Au clusters were deposited on acid pre-treated ALD titania surface by varying the concentration of Au cluster solutions from which Au clusters were deposited. The samples were investigated using XPS and MIES. XPS revealed that Au clusters were partially agglomerated after heat treatment. Heating Au₉/titania samples leads to removal of triphenylphosphine ligands from the surface of Au clusters. Therefore, acidic treatment of titania surfaces supports binding of Au₉ clusters on the titania surface and reduces agglomeration of Au into larger particles compared with plasma treated ALD titania. MIES revealed that three reference spectra were required to fit the entire series of measured MIES spectra. Weighting factors for fitting MIE spectra correlated with XPS intensity of existing elements. The first reference spectrum was attributed to non-agglomerated Au₉ clusters. The second reference spectrum was attributed to hydrocarbon, including phosphorous ligands. The third reference spectrum was attributed to sulphuric acid due to acidic pre-treatment. Au reference spectrum is an important finding for understanding electronic properties which play a major role in understanding catalytic properties of Au.

7.6 REFERENCES

1. Baker, T. A.; Liu, X.; Friend, C. M., The mystery of gold's chemical activity: local bonding, morphology and reactivity of atomic oxygen. *Physical Chemistry Chemical Physics* **2011**, *13* (1), 34-46.
2. Bollinger, M. A.; Vannice, M. A., A kinetic and DRIFTS study of low-temperature carbon monoxide oxidation over Au—TiO₂ catalysts. *Applied Catalysis B: Environmental* **1996**, *8* (4), 417-443.
3. Valden, M.; Pak, S.; Lai, X.; Goodman, D. W., Structure sensitivity of CO oxidation over model Au/TiO₂ catalysts. *Catalysis Letters* *56* (1), 7-10.
4. Grunwaldt, J.-D.; Kiener, C.; Wögerbauer, C.; Baiker, A., Preparation of Supported Gold Catalysts for Low-Temperature CO Oxidation via “Size-Controlled” Gold Colloids. *Journal of Catalysis* **1999**, *181* (2), 223-232.
5. Grunwaldt, J.-D.; Baiker, A., Gold/Titania Interfaces and Their Role in Carbon Monoxide Oxidation. *The Journal of Physical Chemistry B* **1999**, *103* (6), 1002-1012.
6. Zhu, Y.; Qian, H.; Zhu, M.; Jin, R., Thiolate-Protected Au_n Nanoclusters as Catalysts for Selective Oxidation and Hydrogenation Processes. *Advanced Materials* **2010**, *22* (17), 1915-1920.
7. Zhu, Y.; Qian, H.; Drake, B. A.; Jin, R., Atomically Precise Au₂₅(SR)₁₈ Nanoparticles as Catalysts for the Selective Hydrogenation of α,β -Unsaturated Ketones and Aldehydes. *Angewandte Chemie* **2010**, *122* (7), 1317-1320.
8. Li, G.; Jin, R., Atomically Precise Gold Nanoclusters as New Model Catalysts. *Accounts of Chemical Research* **2013**, *46* (8), 1749-1758.
9. Bond, G. C.; Louis, C.; Thompson, D. T., *Catalysis by gold*. World Scientific: **2006**; Vol. 6.

CHAPTER 7

10. Yoon, B.; Häkkinen, H.; Landman, U.; Würz, A. S.; Antonietti, J.-M.; Abbet, S.; Judai, K.; Heiz, U., Charging Effects on Bonding and Catalyzed Oxidation of CO on Au₈ Clusters on MgO. *Science* **2005**, *307* (5708), 403-407.
11. Heiz, U.; Sanchez, A.; Abbet, S.; Schneider, W.-D., The reactivity of gold and platinum metals in their cluster phase. *The European Physical Journal D - Atomic, Molecular, Optical and Plasma Physics* **1999**, *9* (1), 35-39.
12. Schweinberger, F. F.; Berr, M. J.; Döblinger, M.; Wolff, C.; Sanwald, K. E.; Crampton, A. S.; Ridge, C. J.; Jäckel, F.; Feldmann, J.; Tschurl, M.; Heiz, U., Cluster Size Effects in the Photocatalytic Hydrogen Evolution Reaction. *Journal of the American Chemical Society* **2013**, *135* (36), 13262-13265.
13. Herzing, A. A.; Kiely, C. J.; Carley, A. F.; Landon, P.; Hutchings, G. J., Identification of Active Gold Nanoclusters on Iron Oxide Supports for CO Oxidation. *Science* **2008**, *321* (5894), 1331-1335.
14. Yi, N.; Si, R.; Saltsburg, H.; Flytzani-Stephanopoulos, M., Steam reforming of methanol over ceria and gold-ceria nanoshapes. *Applied Catalysis B: Environmental* **2010**, *95* (1-2), 87-92.
15. Häkkinen, H.; Abbet, S.; Sanchez, A.; Heiz, U.; Landman, U., Structural, electronic, and impurity - doping effects in nanoscale chemistry: supported gold nanoclusters. *Angewandte Chemie International Edition* **2003**, *42* (11), 1297-1300.
16. Borman, V. D.; Pushkin, M. A.; Tronin, V. N.; Troyan, V. I., Evolution of the electronic properties of transition metal nanoclusters on graphite surface. *Journal of Experimental and Theoretical Physics* **2010**, *110* (6), 1005-1025.
17. Green, I. X.; Tang, W.; Neurock, M.; Yates, J. T., Spectroscopic Observation of Dual Catalytic Sites During Oxidation of CO on a Au/TiO₂ Catalyst. *Science* **2011**, *333* (6043), 736-739.

18. Haruta, M.; Daté, M., Advances in the catalysis of Au nanoparticles. *Applied Catalysis A: General* **2001**, *222* (1–2), 427-437.
19. Stakheev, A. Y.; Kustov, L. M., Effects of the support on the morphology and electronic properties of supported metal clusters: modern concepts and progress in 1990s. *Applied Catalysis A: General* **1999**, *188* (1–2), 3-35.
20. Tai, Y.; Yamaguchi, W.; Okada, M.; Ohashi, F.; Shimizu, K.-i.; Satsuma, A.; Tajiri, K.; Kageyama, H., Depletion of CO oxidation activity of supported Au catalysts prepared from thiol-capped Au nanoparticles by sulfates formed at Au–titania boundaries: Effects of heat treatment conditions on catalytic activity. *Journal of Catalysis* **2010**, *270* (2), 234-241.
21. Zhai, H.-J.; Miao, C.-Q.; Li, S.-D.; Wang, L.-S., On the Analogy of B–BO and B–Au Chemical Bonding in B₁₁O– and B₁₀Au– Clusters. *The Journal of Physical Chemistry A* **2010**, *114* (46), 12155-12161.
22. Ma, L.; v. Issendorff, B.; Aguado, A., Photoelectron spectroscopy of cold aluminum cluster anions: Comparison with density functional theory results. *The Journal of Chemical Physics* **2010**, *132* (10), 104303.
23. Lin, X.; Nilius, N.; Freund, H. J.; Walter, M.; Frondelius, P.; Honkala, K.; Häkkinen, H., Quantum Well States in Two-Dimensional Gold Clusters on MgO Thin Films. *Physical Review Letters* **2009**, *102* (20), 206801.
24. Lu, J.-L.; Gao, H.-J.; Shaikhutdinov, S.; Freund, H.-J., Gold supported on well-ordered ceria films: nucleation, growth and morphology in CO oxidation reaction. *Catalysis Letters* **2007**, *114* (1), 8-16.
25. Berlich, A.; Liu, Y. C.; Morgner, H., Evaporation of Ni and carbon containing species onto NiO/Ni as case study for metal support catalysts investigated by Metastable

- Induced Electron Spectroscopy (MIES). *Radiation Physics and Chemistry* **2005**, *74* (3–4), 201-209.
26. Andersson, G. G.; Golovko, V. B.; Alvino, J. F.; Bennett, T.; Wrede, O.; Mejia, S. M.; Al Qahtani, H. S.; Adnan, R.; Gunby, N.; Anderson, D. P.; Metha, G. F., Phosphine-stabilised Au₉ clusters interacting with titania and silica surfaces: The first evidence for the density of states signature of the support-immobilised cluster. *The Journal of Chemical Physics* **2014**, *141* (1), 014702.
27. Büttner, M.; Oelhafen, P., XPS study on the evaporation of gold submonolayers on carbon surfaces. *Surface Science* **2006**, *600* (5), 1170-1177.
28. Kitsudo, Y.; Iwamoto, A.; Matsumoto, H.; Mitsuhara, K.; Nishimura, T.; Takizawa, M.; Akita, T.; Maeda, Y.; Kido, Y., Final state effect for Au 4f line from gold-nanoparticles grown on oxides and HOPG supports. *Surface Science* **2009**, *603* (13), 2108-2114.
29. Lim, D.-C.; Hwang, C.-C.; Ganteför, G.; Kim, Y. D., Model catalysts of supported Au nanoparticles and mass-selected clusters. *Physical Chemistry Chemical Physics* **2010**, *12* (46), 15172-15180.
30. Chusuei, C. C.; Lai, X.; Davis, K.; Bowers, E.; Fackler, J. P.; Goodman, D., A nanoscale model catalyst preparation: Solution deposition of phosphine-stabilized gold clusters onto a planar TiO₂ (110) support. *Langmuir* **2001**, *17* (13), 4113-4117.
31. Anderson, D. P.; Alvino, J. F.; Gentleman, A.; Al Qahtani, H.; Thomsen, L.; Polson, M. I.; Metha, G. F.; Golovko, V. B.; Andersson, G. G., Chemically-synthesised, atomically-precise gold clusters deposited and activated on titania. *Physical Chemistry Chemical Physics* **2013**, *15* (11), 3917-3929.
32. Achar, S.; Puddephatt, R. J.; Scott, J. D., *Polyhedron* **1996**, *15*, 2363.

CHAPTER 7

33. Boyen, H.-G.; Ethirajan, A.; Kästle, G.; Weigl, F.; Ziemann, P.; Schmid, G.; Garnier, M.; Büttner, M.; Oelhafen, P., Alloy formation of supported gold nanoparticles at their transition from clusters to solids: Does size matter? *Physical review letters* **2005**, *94* (1), 016804.
34. Raja, R.; Golovko, V. B.; Thomas, J. M.; Berenguer-Murcia, A.; Zhou, W.; Xie, S.; Johnson, B. F., Highly efficient catalysts for the hydrogenation of nitro-substituted aromatics. *Chemical communications* **2005**, (15), 2026-2028.
35. Hungria, A. B.; Raja, R.; Adams, R. D.; Captain, B.; Thomas, J. M.; Midgley, P. A.; Golovko, V.; Johnson, B. F. G., Single-Step Conversion of Dimethyl Terephthalate into Cyclohexanedimethanol with Ru₅PtSn, a Trimetallic Nanoparticle Catalyst. *Angewandte Chemie International Edition* **2006**, *45* (29), 4782-4785.
36. Turner, M.; Golovko, V. B.; Vaughan, O. P. H.; Abdulkin, P.; Berenguer-Murcia, A.; Tikhov, M. S.; Johnson, B. F. G.; Lambert, R. M., Selective oxidation with dioxygen by gold nanoparticle catalysts derived from 55-atom clusters. *Nature* **2008**, *454* (7207), 981-983.
37. Chen, M.; Goodman, D. W., Catalytically active gold on ordered titania supports. *Chemical Society Reviews* **2008**, *37* (9), 1860-1870.
38. Haruta, M.; Yamada, N.; Kobayashi, T.; Iijima, S., Gold catalysts prepared by coprecipitation for low-temperature oxidation of hydrogen and of carbon monoxide. *Journal of Catalysis* **1989**, *115* (2), 301-309.
39. Bagheri, S.; Muhd Julkapli, N.; Bee Abd Hamid, S., Titanium Dioxide as a Catalyst Support in Heterogeneous Catalysis. *The Scientific World Journal* **2014**, *2014*, 21.
40. Anderson, D. P.; Adnan, R. H.; Alvino, J. F.; Shipper, O.; Donoeva, B.; Ruzicka, J.-Y.; Al Qahtani, H.; Harris, H. H.; Cowie, B.; Aitken, J. B.; Golovko, V. B.; Metha, G. F.; Andersson, G. G., Chemically synthesised atomically precise gold clusters

- deposited and activated on titania. Part II. *Physical Chemistry Chemical Physics* **2013**, *15* (35), 14806-14813.
41. Ruzicka, J.-Y.; Abu Bakar, F.; Hoeck, C.; Adnan, R.; McNicoll, C.; Kemmitt, T.; Cowie, B. C.; Metha, G. F.; Andersson, G. G.; Golovko, V. B., Toward Control of Gold Cluster Aggregation on TiO₂ via Surface Treatments. *The Journal of Physical Chemistry C* **2015**, *119* (43), 24465-24474.
42. Liu, Y.; Tsunoyama, H.; Akita, T.; Tsukuda, T., Preparation of ~1 nm Gold Clusters Confined within Mesoporous Silica and Microwave-Assisted Catalytic Application for Alcohol Oxidation. *The Journal of Physical Chemistry C* **2009**, *113* (31), 13457-13461.
43. Hantsche, H., High resolution XPS of organic polymers, the scienta ESCA300 database. By G. Beamson and D. Briggs, Wiley, Chichester 1992, 295 pp., hardcover, £ 65.00, ISBN 0 - 471 - 93592 - 1. *Advanced Materials* **1993**, *5* (10), 778-778.
44. Barth, G.; Linder, R.; Bryson, C., Advances in charge neutralization for XPS measurements of nonconducting materials. *Surface and Interface Analysis* **1988**, *11* (6 - 7), 307-311.
45. Moulder, J.; Stickle, W.; Sobol, P.; Bomben, K., Handbook of X-ray Photoelectron Spectroscopy. Eden Prairie: Physical Electronics. Inc: **1995**.
46. Al Qahtani, H. S.; Kimoto, K.; Bennett, T.; Alvino, J. F.; Andersson, G. G.; Metha, G. F.; Golovko, V. B.; Sasaki, T.; Nakayama, T., Atomically resolved structure of ligand-protected Au₉ clusters on TiO₂ nanosheets using aberration-corrected STEM. *The Journal of Chemical Physics* **2016**, *144* (11), 114703.

47. Asami, K., A precisely consistent energy calibration method for X-ray photoelectron spectroscopy. *Journal of Electron Spectroscopy and Related Phenomena* **1976**, 9 (5), 469-478.
48. Seah, M.; Smith, G.; Anthony, M., AES: Energy calibration of electron spectrometers. I—an absolute, traceable energy calibration and the provision of atomic reference line energies. *Surface and interface analysis* **1990**, 15 (5), 293-308.
49. Dückers, K.; Bonzel, H., Core and valence level spectroscopy with Y M ζ radiation: CO and K on (110) surfaces of Ir, Pt and Au. *Surface Science* **1989**, 213 (1), 25-48.
50. Thomas, T. D.; Weightman, P., Valence electronic structure of AuZn and AuMg alloys derived from a new way of analyzing Auger-parameter shifts. *Physical Review B* **1986**, 33 (8), 5406.
51. Lim, D. C.; Dietsche, R.; Ganteför, G.; Kim, Y. D., Chemical properties of size-selected Au clusters treated under ambient conditions. *Chemical Physics Letters* **2008**, 457 (4-6), 391-395.
52. Ono, L. K.; Roldan Cuenya, B., Formation and Thermal Stability of Au₂O₃ on Gold Nanoparticles: Size and Support Effects. *The Journal of Physical Chemistry C* **2008**, 112 (12), 4676-4686.
53. Park, S.-K.; Shin, H., Effect of HCl and H₂SO₄ Treatment of TiO₂ Powder on the Photosensitized Degradation of Aqueous Rhodamine B Under Visible Light. *Journal of nanoscience and nanotechnology* **2014**, 14 (10), 8122-8128.
54. Yang, Q.; Xie, C.; Xu, Z.; Gao, Z.; Du, Y., Synthesis of Highly Active Sulfate-Promoted Rutile Titania Nanoparticles with a Response to Visible Light. *The Journal of Physical Chemistry B* **2005**, 109 (12), 5554-5560.

CHAPTER 7

55. Mohapatra, P.; Moma, J.; Parida, K. M.; Jordaan, W. A.; Scurrrell, M. S., Dramatic promotion of gold/titania for CO oxidation by sulfate ions. *Chemical Communications* **2007**, (10), 1044-1046.
56. Hidalgo, M. C.; Maicu, M.; Navío, J. A.; Colón, G., Effect of Sulfate Pretreatment on Gold-Modified TiO₂ for Photocatalytic Applications. *The Journal of Physical Chemistry C* **2009**, *113* (29), 12840-12847.
57. Haruta, M., Spiers Memorial Lecture Role of perimeter interfaces in catalysis by gold nanoparticles. *Faraday Discussions* **2011**, *152* (0), 11-32.
58. Ruth, K.; Hayes, M.; Burch, R.; Tsubota, S.; Haruta, M., The effects of SO₂ on the oxidation of CO and propane on supported Pt and Au catalysts. *Applied Catalysis B: Environmental* **2000**, *24* (3–4), L133-L138.
59. Al Qahtani, H. S.; Metha, G. F.; Golovko, V. B.; Andersson, G. G.; Nakayama, T., Aggregation behavior of Ligands protected Au₉ Clusters on sputtered ALD TiO₂ Using AFM and XPS techniques. *Planned to submitted to ACS Applied Materilas and Interfaces* **2016**.

CHAPTER 8

Conclusion

CHAPTER 8

This thesis presents results of investigations of chemically stabilised Au₉ clusters deposited onto titania surfaces. Cluster size and dispersion on surfaces, as well as electronic properties, are important for understanding metal nanocluster properties deposited on surfaces. Deposited Au clusters and titania surfaces were studied using a variety of surface science techniques.

Aberration corrected HAADF-STEM with low electron-beam acceleration voltages was successfully applied in this study to image geometric structure of Au₉ clusters deposited onto titania nanosheets. Due to intrinsic fluxionality, the geometric structure of Au clusters and structural transitions between various alternative structures play an important role in catalytic properties.

It was observed in this study that supported Au₉ clusters show three different atomic configurations as observed by STEM. The configurations observed are a 3-dimensional (3D) structure, corresponding to the previously proposed Au₉ core of the clusters, and two pseudo-2-dimensional (pseudo-2D) structures, newly found by this work. These experimental configurations were correlated to cluster structures determined *via* DFT calculations to rationalize various Au₉ geometrical structures and the possibility of transition between those structures. The 3D structure is assigned to ligand-protected clusters, while pseudo-2D structures are attributed to low energy, de-ligated structures formed through interaction with the titania nanosheet substrate. XPS supports the interpretation of STEM, that clusters do not agglomerate after deposition onto titania nanosheets.

The structure of Au₉ clusters on titania nanosheet before and after annealing was investigated with AFM, STM and XPS and integrated into an overall interpretation. After the deposition process, Au₉ clusters were attached to the surface as individual clusters or in groups of clusters. STM showed that groups of clusters consisted, at least partially, of individual

CHAPTER 8

clusters which retained their individual electronic structure before and after annealing. The height of deposited species and dispersion was determined by AFM. A combination of AFM, STM and XPS showed the existence of individual and agglomerated clusters in groups of clusters after heat treatment.

Pre-treatment conditions for titania surfaces may prevent Au clusters from agglomeration. AFM was used to determine height and distribution of Au₉ clusters adsorbed onto a sputtered ALD titania surface. Sputtering of ALD titania substrates induced a number of Ti³⁺ defects favourable for adsorption of Au NCs. Both AFM and XPS showed that Au₉ clusters deposited on ALD titania are partially agglomerated after annealing.

Au₉ clusters were adsorbed onto ALD titania pre-treated with sulphuric acid and the surface analysed using MIES. MIES was applied to quantitatively determine the electronic structure of supported clusters. Experimental MIE spectra was fitted with three reference spectra based on the SVD algorithm. These spectra were assigned to Au clusters attached to the titania surface after removal of ligands (the uncertainty of this assignment was outlined in the respective paragraph), the hydrocarbon including phosphine ligands, and sulphuric acid on the substrate. The assignment of one spectra to Au clusters was not finally clarified.

Correlating spectroscopic and microscopic techniques was shown to be a powerful tool in the investigation of deposited Au clusters onto titania surfaces. It was demonstrated in this thesis that Au₉ clusters lost their attached ligands after the annealing process. Clusters cores formed groups of clusters including small clusters and aggregation clusters. AFM measurements show agglomeration through an increase in height of features assigned to Au clusters. STM results cannot measure overall size of groups as compared to AFM. However, STM was used to observe the fine structure of the top layer of a group which cannot be analysed using AFM. While STM was used to observe individual Au₉ clusters deposited on

CHAPTER 8

titania nanosheet, STM does not allow analysis of whether these individual clusters merged to form larger particles or retained their identity as electronically isolated Au₉ cluster cores. XPS showed that at least a fraction of individual clusters did not merge to form larger particles. AFM and STM techniques cannot be used to reveal information about the second layer of a group (i.e. the layer below the top layer), while XPS can inform about the deeper layer.

Titania nanosheet showed a larger amount of Au clusters compared with ALD titania surfaces. The electronic properties of titania nanosheets differ from those of ALD titania or titania nanoparticles due to reduced dimensionality of the nanosheets. Thus, it can be expected that the interaction of Au clusters with titania nanosheets is different to the interaction of Au clusters with other titania materials. Also, titania nanosheet is a preferable substrate in AFM and STM techniques where surface roughness plays a major role in measurements.

Surface pre-treatments were explored to increase the strength of Au cluster bond to the titania surface to prevent Au cluster aggregation. The pre-treated titania surfaces using different procedures induced a number of defects which successfully attracted Au NCs. The sputtering pre-treatment ALD condition revealed a larger amount of Au cluster attraction compared to oxygen plasma and sulphuric acid pre-treated ALD.

There is much scope for further research, such as using Au clusters of different sizes, changing pre-treatment conditions for titania surfaces or using different metal oxide surfaces. The results of this study very important to the surface science community and outcomes are potentially useful in improving understanding of key factors affecting catalytic activity of atomically precise support immobilised clusters.

Appendix

A- Cartesian coordinates of the Au₉ clusters shown in Figure 4.5: (i.e. structures (I), (III) and (IV)).

Au₉ core (Structure I, from ligated calculation)

79	1.415645000	2.425059000	0.314187000
79	-1.415645000	-2.425059000	0.314187000
79	2.435941000	-0.204913000	1.411833000
79	-2.435941000	0.204913000	1.411833000
79	-1.415645000	2.425059000	-0.314187000
79	1.415645000	-2.425059000	-0.314187000
79	-2.435941000	-0.204913000	-1.411833000
79	2.435941000	0.204913000	-1.411833000
79	0.000000000	0.000000000	0.000000000

Au₉ Structure III)

79	0.000000000	2.398319000	-0.469701000
79	0.000000000	0.000000000	3.797965000
79	0.000000000	-2.398319000	-0.469701000
79	0.000000000	-2.455944000	2.325479000
79	0.000000000	2.455944000	2.325479000
79	0.000000000	0.000000000	-2.101246000
79	0.000000000	0.000000000	0.988886000
79	0.000000000	2.516653000	-3.198580000
79	0.000000000	-2.516653000	-3.198580000

Au₉ structure IV)

79	0.000000000	2.946158000	0.569243000
79	0.000000000	-1.437714000	2.914487000
79	0.000000000	-1.374649000	-1.919087000
79	0.000000000	-2.946158000	0.569243000
79	0.000000000	1.437714000	2.914487000
79	0.000000000	1.374649000	-1.919087000
79	0.000000000	0.000000000	0.503601000
79	0.000000000	4.202963000	-1.816444000
79	0.000000000	-4.202963000	-1.816444000

Au₉ (transition state between III & IV with 1 imaginary frequency (15.80i))

79	-2.822095000	-0.421827000	0.000012000
79	0.073541000	3.477082000	-0.000340000
79	2.108510000	-0.957247000	0.000078000
79	2.320572000	1.916649000	-0.000136000
79	-2.616187000	2.318612000	0.000399000
79	-0.463199000	-2.114198000	0.000079000
79	-0.230444000	0.712895000	0.000085000
79	-3.015067000	-3.170114000	-0.000278000
79	4.644369000	-1.761852000	0.000101000